

Electronic Thesis and Dissertation Repository

---

7-21-2022 1:00 PM

## Regulation of MHC II Trafficking and Expression by Host and Viral Factors

Alex Lac, *The University of Western Ontario*

Supervisor: Heit, Bryan, *The University of Western Ontario*

A thesis submitted in partial fulfillment of the requirements for the Master of Science degree in Microbiology and Immunology

© Alex Lac 2022

Follow this and additional works at: <https://ir.lib.uwo.ca/etd>



Part of the [Immunity Commons](#), [Immunology of Infectious Disease Commons](#), [Virology Commons](#), and the [Viruses Commons](#)

---

### Recommended Citation

Lac, Alex, "Regulation of MHC II Trafficking and Expression by Host and Viral Factors" (2022). *Electronic Thesis and Dissertation Repository*. 8683.

<https://ir.lib.uwo.ca/etd/8683>

This Dissertation/Thesis is brought to you for free and open access by Scholarship@Western. It has been accepted for inclusion in Electronic Thesis and Dissertation Repository by an authorized administrator of Scholarship@Western. For more information, please contact [wlsadmin@uwo.ca](mailto:wlsadmin@uwo.ca).

## Abstract

Antigen presentation by major histocompatibility complex class II (MHC II) to the adaptive immune system is crucial for mounting sterilizing immune responses. This central role has made antigen presentation a target for antagonism by many pathogens. Notably, infections with severe acute respiratory syndrome coronavirus 2 (SARS-CoV-2) decrease MHC II expression in several immune cells. The mechanisms responsible for this suppression are unknown but involves either redirecting MHC II molecules away from the cell surface or inhibiting MHC II expression. To understand how pathogens manipulate intracellular MHC II trafficking, we first investigated the role of the Golgi trafficking regulator, ERC1, in this pathway, which we have previously confirmed is necessary for phagosome maturation. Immunofluorescence microscopy demonstrated that ERC1 facilitates the recruitment of MHC II to phagosomes, thereby enabling antigen loading and presentation. Interestingly, SARS-CoV-2 non-structural protein 5 (NSP5) interacts with histone deacetylase 2 (HDAC2)—a regulator of MHC II transcription—suggesting that SARS-CoV-2 may antagonize antigen presentation through epigenetic reprogramming. We hypothesize that SARS-CoV-2 NSP5 downregulates MHC II expression via interactions with HDAC2. RT-qPCR and dual luciferase analyses demonstrated that NSP5 expression was sufficient to downregulate MHC II in primary human dendritic cells and RAW 264.7 macrophages. HDAC2 knockdown alleviated this suppression, indicating that NSP5 utilizes host histone deacetylation machinery to antagonize MHC II transcription. Unexpectedly, point mutations that inactivate the catalytic site of NSP5 failed to revert this phenotype, suggesting that the proteolytic ability of NSP5 is not required for this suppression. This research may identify an important mechanism used by SARS-CoV-2 to evade adaptive immune responses and may indicate a potential use of HDAC2 inhibitors as therapeutics against coronavirus disease 19 (COVID-19).

## Summary for Lay Audience

Every day we constantly encounter germs that can damage our bodies and cause debilitating diseases should they continue to persist. Our immune system fights off against infections through several ways. Particularly, specialized immune cells called phagocytes can eat microbes and break these microbes down into small pieces called antigens that are displayed on an MHC II molecule to communicate with other immune cells. To hide from the immune system, bacteria and viruses try to impair this process, either by decreasing MHC II levels or preventing MHC II from reaching the organelle where antigens reside. Surprisingly, it is unclear how MHC II is delivered to the antigen-containing organelle; hence, it is unknown how pathogens block this process. We discovered a protein called ERC1 that acts like a magnet by attracting MHC II to the antigen-containing organelle and allowing antigens to be presented to other immune cells. Interestingly, the virus responsible for COVID-19—SARS-CoV-2—interacts with components involved in controlling MHC II expression, suggesting that this virus targets these proteins to block MHC II from displaying antigens. We found that one of the viral proteins expressed by SARS-CoV-2, NSP5, can target another protein called HDAC2 to decrease MHC II levels in various immune cell types. In addition, modifying cells such that they no longer express HDAC2 restored MHC II levels. Together, these experiments help us better understand the functions of our immune system and how pathogens can persist in our bodies, such is the case in COVID-19. Using this information, it may be possible to develop better treatments to combat against COVID-19 and finally put an end to the pandemic.

### Keywords

MHC II, SARS-CoV-2, COVID-19, antigen presentation, phagocytosis, vesicular trafficking, ERC1, NSP5, CIITA, HDAC2

## Co-Authorship Statement

The entirety of this thesis was authored by Alex Lac; however, some of the data presented in this thesis were generated by others:

1. The data generated in Figure 9 is unpublished data from experiments conducted by Brandon Dickson.
2. The data generated in Figure 13D is unpublished data from experiments conducted by Peter Guo.

## Acknowledgments

I would first like to express my gratitude to my supervisor, Dr. Bryan Heit, for his invaluable guidance throughout the duration of my graduate studies. It was your encouragement and support that motivated me to continue my research, and it was a humbling experience working in your incredible lab over the past few years.

I would also like to thank my advisory committee members, Dr. Jimmy Dikeakos and Dr. Lisa Cameron, for their continuous advice and guidance. The insightful discussions we've had together were major factors that led to the success of my research project.

Thank you to the wonderful friends and colleagues from the Heit lab who played a crucial role in fostering a supportive environment and for all the laughs we shared along the way: Dr. Charles Yin, Tarannum Tasnim, Austin Lam, Maria Abou Taka, David Zheng, Mara Rosoga, Catherine Jung, Peter Guo, Dr. Nima Taefehshokr, Amena Aktar, Minhyuk Mun, Kasia Wodz, Brandon Dickson, Oneeb Hassan, Alice Kim, and Kerolos Kolta. A special thanks to our indispensable lab technician, Angela Vrieze, for not only mentoring me throughout the entirety of my graduate studies but for also the countless conversations we've had that kept me going through the day

Lastly, I would like to express my gratitude towards my family and friends for their support. My sincerest gratitude to my parents, Xuong and Kim, for providing me the opportunity to study at Western University. To my girlfriend, Maleana, thank you for always being there for me and sticking with me to the very end.

# Table of Contents

Abstract.....	ii
Summary for Lay Audience.....	iii
Co-Authorship Statement.....	iv
Acknowledgments.....	v
Table of Contents.....	vi
List of Tables.....	x
List of Figures.....	xi
List of Appendices.....	xiii
List of Abbreviations.....	xiv
Chapter 1.....	1
INTRODUCTION.....	1
1.1 Antigen Presentation on MHC II.....	1
1.2 CIITA and HDAC2 are Major Regulators of MHC II Transcription.....	2
1.3 Proper MHC II Trafficking is Crucial for Antigen Presentation.....	6
1.4 Two Potential Vesicular Trafficking Pathways Dictate the Formation of the MIIC.....	7
1.4.1 Indirect Endolysosomal Trafficking Pathway.....	7
1.4.2 Direct Golgi-to-MIIC Trafficking Pathway.....	9
1.5 Role of Rab GTPases in Regulating MHC II Trafficking.....	12
1.6 ERC1 Potentially Regulates Expression and Trafficking of MHC II Through the Canonical TLR-Mediated NF $\kappa$ B Activation Pathway.....	13
1.7 Antigen Presentation and CD4 <sup>+</sup> T Cell Responses are Impaired in Patients with COVID-19.....	15
1.8 SARS-CoV-2 Structure and Genome.....	16
1.9 Infection of Dendritic Cells and Macrophages by SARS-CoV-2.....	16

1.10 SARS-CoV-2 Antagonizes Antigen Presentation Through an Unknown Mechanism .....	18
1.11 SARS-CoV-2 NSP5 Potentially Suppresses MHC II Expression .....	19
1.12 Hypothesis and Aims .....	20
Chapter 2 .....	21
2 Materials and Methods .....	21
2.1 Materials .....	21
2.2 Plasmids and Oligos .....	22
2.3 Culturing and Transfection of Cell Lines .....	23
2.4 Culturing and Transduction of Human Primary Dendritic Cells .....	25
2.5 Molecular Cloning .....	26
2.5.1 MHC II-HaloTag Cloning .....	27
2.5.2 Dual Luciferase Cloning .....	28
2.5.3 NSP5 Cloning .....	28
2.6 Immunofluorescence Microscopy .....	28
2.6.1 Immunostaining .....	28
2.6.2 Fluorescence Imaging .....	29
2.6.3 Image Analysis .....	30
2.7 MHC II-HaloTag Expression System .....	30
2.7.1 Preparation of IgG-Coated Phagocytic Targets .....	30
2.7.2 Phagocytosis Assay .....	30
2.8 Quantitative Reverse Transcription PCR (RT-qPCR) .....	31
2.8.1 RNA Preparation .....	31
2.8.2 cDNA Preparation and RT-qPCR .....	32
2.9 Dual Luciferase Assay .....	33
2.10 Western Blot .....	33

2.11	Generation of Phylogenetic Trees.....	34
2.12	Statistical Analysis.....	35
Chapter 3	.....	37
3	Results – Development of Tools to Detect MHC II Trafficking and Expression .....	37
3.1	Development of MHC II-HaloTag Construct.....	37
3.2	Monitoring Protein Trafficking Dynamics in Macrophages.....	41
3.3	ERC1 May Facilitate Early Phagosome Maturation.....	43
3.4	Optimizing RT-qPCR Experiments for Detecting Gene Expression.....	45
3.5	Validation of Dual Luciferase Assay .....	48
Chapter 4	.....	51
4	Results – Assessing the Effects of SARS-CoV-2 NSP5 on MHC II Expression .....	51
4.1	Introduction.....	51
4.2	Subcellular Localization of NSP5 Provides Clues to Host Function Impairments .....	51
4.3	NSP5 Downregulates CIITA and MHC II.....	54
4.4	NSP5 Inhibits MHC II and CIITA Promoter Activity .....	59
4.5	HDAC2 Knockdown Restores CIITA and MHC II Expression.....	61
4.6	Inactivating NSP5 Proteolytic Activity Has No Effect on CIITA and MHC II Expression.....	64
4.7	HDAC2 Expression is Unaltered by NSP5.....	67
4.8	NSP5-Mediated Modulation of HDAC2 May Be Shared Between SARS- CoV-2 and Other Related Bat Coronaviruses .....	69
Chapter 5	.....	73
5	Discussion .....	73
5.1	Hypotheses and Answers .....	73
5.2	Rationale of Thesis .....	74



5.3 TLR and FcγR Signaling Activates ERC1 to Regulate MHC II Trafficking .....	77
5.4 NSP5-HDAC2-CIITA-MHC II Axis .....	80
5.5 Limitations and Pitfalls .....	81
5.6 Future Work .....	83
5.7 Complementary Findings .....	85
5.8 HDAC2 Inhibitors as Potential Therapeutics Against COVID-19 .....	85
5.9 Conclusion .....	87
References .....	91
Appendices .....	125
Curriculum Vitae .....	133

## List of Tables

Table 1. Cloning primer sequences used in this study .....	36
Table 2. RT-qPCR primer sequences used in this study.....	46

## List of Figures

Figure 1. Regulation of MHC II transcription. ....	5
Figure 2. Putative vesicular trafficking pathways of MHC II. ....	11
Figure 3. Determining the optimal concentrations and incubations of HaloTag ligand and doxycycline to induce MHC II-HaloTag expression. ....	40
Figure 4. Time-lapse of Rab5 and Rab7 recruitment to phagosomes. ....	42
Figure 5. Recruitment of ERC1 and MHC II to phagosomes. ....	44
Figure 6. Representative RT-qPCR primer melt curve plots. ....	47
Figure 7. Dual luciferase analyses of alterations in CIITA pI and MHC II promoter activity by NSP5. ....	49
Figure 8. NSP5 is localized to host nuclei. ....	53
Figure 9. NSP5 reduces MHC II expression independent of altering membrane trafficking. ....	56
Figure 10. RT-qPCR quantification of RFX5, CIITA, and MHC II expression. ....	58
Figure 11. NSP5 inhibits CIITA pI and MHC II promoter activity but not CIITA pIV activity. ....	60
Figure 12. HDAC2 knockdown reverts the effects of NSP5 on CIITA and MHC II expression. ....	63
Figure 13. Analysis of NSP5 point mutations on CIITA pI and MHC II promoter activity. ....	66
Figure 14. Western blot analysis of HDAC2 cleavage. ....	68
Figure 15. Phylogenetic analyses of ancestral NSP5 and HDAC2. ....	72

Figure 16. Proposed model of NSP5-mediated downregulation of MHC II transcription.

..... 90

## List of Appendices

Appendix A. Vector maps of MHC II-HaloTag constructs used in this study. ....	125
Appendix B. Vector maps of luciferase reporter constructs used in this study. ....	127
Appendix C. Vector maps of NSP5 lentiviral vectors used in this study. ....	130

## List of Abbreviations

ACE2	angiotensin-converting enzyme 2
AP	adaptor protein
BSA	bovine serum albumin
CD74	invariant chain
CIITA	class II transactivator
CLIP	class II-associated invariant chain peptide
DC	dendritic cell
ER	endoplasmic reticulum
ERC1	ELKS1/Rab6-interacting protein/CAST family member 1
FLuc	firefly luciferase
FRET	Förster resonance energy transfer
HAT	histone acetyltransferase
HDAC	histone deacetylase
HLA	human leukocyte antigen
IFN	interferon
IFN $\gamma$ R	interferon gamma receptor
IKK	I $\kappa$ B kinase
LICOR	CLx Imaging System
MERS-CoV	Middle Eastern respiratory syndrome coronavirus
MFI	mean fluorescence intensity
MHC	major histocompatibility complex
MIIC	MHC II loading compartment
MOI	multiplicity of infection
NF $\kappa$ B	nuclear factor kappa B

NSP	non-structural protein
pAPC	professional antigen presenting cell
PBMC	peripheral blood mononuclear cell
PBS	phosphate-buffered saline
PCR	polymerase chain reaction
pI/pIII/pIV	promoter I/III/IV
PS/DVB	polystyrene/divinylbenzene
ROI	region of interest
RLuc	renilla luciferase
RT-qPCR	quantitative reverse transcription PCR
S	spike protein
SARS-CoV-2	severe acute respiratory syndrome coronavirus 2
TBS-T	tris-buffered saline with Tween
Tfh	T follicular helper
TLR	Toll-like receptor
TMPRSS2	transmembrane serine protease 2
UT	untransfected/untransduced
WGA	wheat germ agglutinin
WT	wildtype

# Chapter 1

## INTRODUCTION

### 1.1 Antigen Presentation on MHC II

Professional antigen presenting cells (pAPCs), such as macrophages and dendritic cells (DCs), are pivotal in alerting the adaptive immune system to the presence of invading pathogens. Specifically, pAPCs present pathogen-derived antigens to T cells to mount an adaptive immune response—a process heavily mediated by major histocompatibility complex (MHC) molecules<sup>1,2</sup>.

Two major classes of MHC molecules are expressed in human cells: MHC I is present on all nucleated cells and is required for presenting endogenous antigens to CD8<sup>+</sup> T cells, while MHC II is expressed by pAPCs and specific non-pAPCs, such as endothelial and epithelial cells, and is responsible for presenting exogenous peptides to CD4<sup>+</sup> T cells. MHC II is a cell-surface protein composed of polymorphic  $\alpha$  and  $\beta$  chains containing a transmembrane region and two extracellular immunoglobulin domains<sup>3</sup>. These chains are assembled by chaperones in the endoplasmic reticulum (ER) where they associate with the invariant chain (CD74) that prevents inappropriate loading of endogenous antigens and induction of autoimmune disorders<sup>4-7</sup>. The MHC II-CD74 complex traffics through the Golgi and into a Golgi-derived vesicle where it is subsequently transported to the phagosome, and CD74 is degraded into a short peptide, known as class II-associated invariant chain peptide (CLIP), which acts as a placeholder prior to peptide loading<sup>8</sup>. Here, HLA-DM mediates the removal and exchange of CLIP with a pathogen-derived peptide onto MHC II<sup>9</sup>. This MHC II-peptide complex is then exported to the cell surface



to be presented to a CD4<sup>+</sup> T cell to initiate adaptive immune responses against the target pathogen<sup>10</sup>.

While the importance of MHC II in antigen presentation is well established, it is critical to understand the mechanisms that regulate MHC II expression and trafficking to their necessary locations to ensure that adaptive immune responses are properly initiated. Antigen presentation on MHC II is dependent on two regulatory processes: MHC II transcription and MHC II trafficking.

## 1.2 CIITA and HDAC2 are Major Regulators of MHC II Transcription

Transcription of MHC II genes is controlled at several levels (**Figure 1**). Notably, a highly conserved cis-regulatory sequence (W-X1-X2-Y box) located directly upstream of the MHC II transcriptional start site plays an important role in this process<sup>11</sup>. These regulatory elements are bound by the transcription factors RFX5, CREB, and NF-Y, leading to the formation of a transcriptionally inactive, combinatorial DNA-protein complex. Binding of the class II transactivator (CIITA) protein to this complex forms the MHC II enhanceosome, activating MHC II expression<sup>12</sup>. An additional enhancer region is found several kilobases 5' to this region, with a similar W-X1-X2-Y box structure that may be required to initiate transcription of MHC II genes<sup>13</sup>.

CIITA is considered the master regulator of interferon gamma (IFN $\gamma$ )-induced transcription of MHC II genes, thereby playing a crucial role in generating adaptive immune responses against pathogens. Deficient levels of CIITA have been linked to

downregulation of MHC II, leading to severe autoimmune diseases such as type II bare lymphocyte syndrome<sup>14</sup>. CIITA-mediated MHC II transcription is dependent on IFN $\gamma$  receptor (IFN $\gamma$ R) binding to its target ligand, initiating a downstream signaling pathway that leads to phosphorylation and homodimerization of STAT1, enabling its entry into the nucleus. Nuclear STAT1 then activates IRF1, and together, they induce expression of CIITA. While not binding directly to the W-X1-X2-Y enhancer elements, CIITA functions by forming a transcriptionally active complex with transcription factors bound to those enhancer elements, where it coordinates the recruitment of additional regulatory proteins. Notably, enhanceosome-bound CIITA recruits multiple histone acetyltransferases (HATs), such as CBP and PCAF, to the MHC II promoter to activate transcription<sup>15,16</sup>. CIITA itself also possesses intrinsic acetyltransferase activity, allowing for direct induction of MHC II transcription<sup>17</sup>.

CIITA can also function as a negative regulator through recruitment of histone deacetylases (HDACs) that silence MHC II transcription. HDACs regulate many cellular processes through the removal of acetyl groups from N-terminal lysine residues on core histones, thereby playing a crucial role in repressing expression of multiple genes<sup>18,19</sup>. This reversible process is opposed by HATs that acetylate histones, thereby increasing the accessibility of chromatin by DNA-binding proteins and activating gene expression<sup>20</sup>. HDACs are classified into four distinct classes based on size and function, consisting of Class I, Class IIa, Class IIb, Class III, and Class IV. HDAC2—a Class I HDAC—is a transcriptional and functional regulator of CIITA and MHC II through various modifications<sup>21,22</sup>. Specifically, HDAC2 inhibits transcription of CIITA and MHC II through histone deacetylation on the promoter regions<sup>23,24</sup>. Likewise, chromatin

immunoprecipitation studies demonstrated that HDAC2 prevents recruitment of CIITA to RFX5, thereby repressing activation of MHC II transcription<sup>22</sup>. Lastly, CIITA is also marked for degradation by the proteasome through interactions with HDAC2. Treatment with HDAC2 inhibitors have been identified to ameliorate this downregulation of CIITA expression and activity<sup>24</sup>, suggesting a potential opportunity in targeting HDAC2 to restore MHC II and CIITA expression in patients suffering from impaired adaptive immune responses.

In addition to post-translational modifications, CIITA expression is regulated at the level of transcription in a cell type- and cytokine-dependent manner. Three different CIITA isoforms, each containing a unique first exon, can be generated depending on which promoter is used<sup>25</sup>. CIITA promoter I (pI) drives expression in myeloid cells such as DCs and macrophages stimulated with IFN $\gamma$ , pIII drives expression in lymphoid cells including B cells and human activated CD4<sup>+</sup> T cells, and pIV drives expression in IFN $\gamma$ -stimulated non-hematopoietic cells.

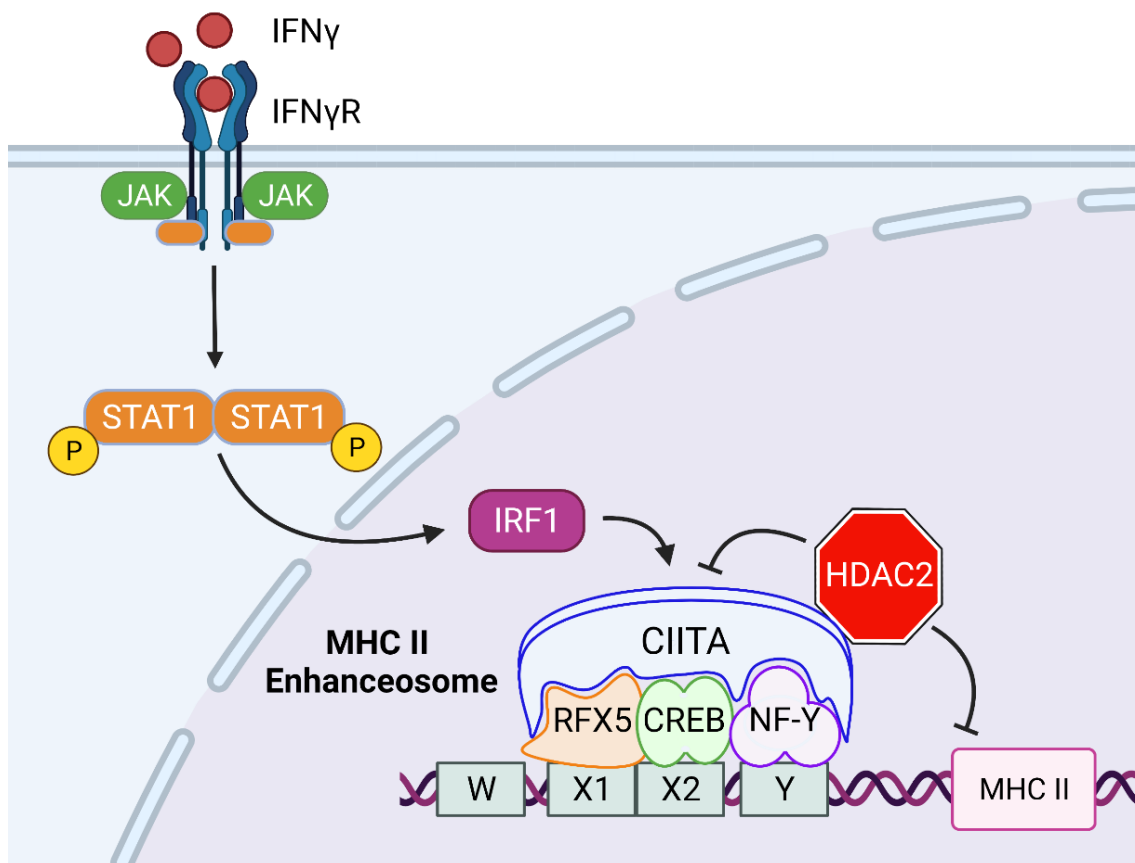


**Figure 1. Regulation of MHC II transcription.**

Transcription of MHC II genes is controlled through a highly conserved regulatory sequence (W-X1-X2-Y box) located directly upstream of the transcriptional start site. This module is bound by transcription factors RFX5, CREB, and NF-Y, forming a transcriptionally inactive DNA-protein complex. IFN $\gamma$  receptor activation initiates a signaling cascade that induces expression of CIITA, enabling its recruitment to the complex and activating MHC II transcription. HDAC2 serves as a negative regulator of CIITA and MHC II transcription through histone deacetylation at the promoters. Figure prepared in BioRender.

### 1.3 Proper MHC II Trafficking is Crucial for Antigen Presentation

Another form of MHC II regulation is the trafficking of this protein to an appropriate destination, such as the phagosome for antigen loading or to the cell surface for antigen presentation. While it is well established that many pathogens can obscure their detection by hijacking host cell machinery and manipulating intracellular MHC II trafficking, it has remained controversial for over twenty years how newly synthesized MHC II molecules are delivered to phagosomes<sup>8,26</sup>. As such, before exploring the mechanisms by which pathogens alter the vesicular trafficking pathways responsible for initiating antigen presentation, it is crucial to understand how MHC II is transported to the phagosome for proper peptide loading.

The peptide-loading process for MHC II is well understood, starting with pAPCs sampling the extracellular environment and encountering an extracellular pathogen which is recognized by surface receptors and engulfed through phagocytosis. Following engulfment, the internalized pathogen is fully contained within a plasma membrane-derived vacuole termed the phagosome. The phagosome undergoes a series of highly regulated biochemical modifications to efficiently degrade the internalized pathogen in a remodeling process called phagosome maturation. This process is characterized both by sequential fusion with early and late endosomes along with progressive acidification of the phagosomal lumen to drive the breakdown of phagocytic cargo. Phagosome maturation is driven by the sequential recruitment of the small GTPases Rab5 and Rab7 to the phagosome surface. Following closure of the phagocytic cup, Rab5 is recruited to the site of phagocytosis where it mediates the fusion between the phagosome and early

endosomes. Rab5 is subsequently replaced by Rab7, marking the transition to the late endosome which undergoes gradual acidification and fusion with lysosomes to form the phagolysosome<sup>27</sup>. Upon acquisition of lysosome-derived enzymes, internalized pathogens are killed and degraded into short antigenic peptides. Phagosome-derived Toll-like receptor (TLR) signaling then initiates the fusion between phagolysosomes with incoming MHC II-containing vesicles, thereby forming the MHC II loading compartment (MIIC) where peptide loading occurs<sup>28</sup>. This MHC II-peptide complex is subsequently exported to cell surface, allowing the peptide to be presented to CD4<sup>+</sup> T cells to initiate adaptive immune responses against the phagocytosed pathogen.

## 1.4 Two Potential Vesicular Trafficking Pathways Dictate the Formation of the MIIC

While the importance of antigen processing and presentation in generating sterilizing immune responses are well established, it remains controversial how newly synthesized MHC II molecules are transported from the Golgi to the MIIC, with two putative trafficking pathways speculated to be responsible for this delivery (**Figure 2**).

### 1.4.1 Indirect Endolysosomal Trafficking Pathway

The antigen presentation field favours a trafficking model where unloaded MHC II-CD74 complexes are released from the Golgi and exported to the cell surface via the constitutive secretion pathway, followed by re-internalization by clathrin-mediated endocytosis and delivery to the MIIC through endolysosomal trafficking<sup>29,30</sup>. This model

is based primarily on the detection of MHC II and CD74 on the plasma membranes of pAPCs, as well as high rates of surface MHC II endocytosis<sup>31-34</sup>. *In vitro* studies identified two dileucine-based signals in the CD74 cytoplasmic domain involved in directing MHC II molecules to the cell surface and to endocytic compartments<sup>35</sup>. Specifically, these signals bind to adaptor protein (AP) complexes, AP-1 and AP-2, which are components of clathrin coats involved in vesicle formation and cargo sorting<sup>36</sup>. While the mechanisms by which these proteins are involved in directing MHC II trafficking are unclear, RNA silencing of AP-2—a major regulator of transport between the plasma membrane and early endosomes—impairs the transport of CD74 to endosomal vesicles, committing CD74 to remain on the cell surface<sup>37</sup>. As AP-2 is solely associated with the plasma membrane, this finding supports the role of clathrin-mediated endocytosis in the indirect route of MHC II-CD74 trafficking<sup>38</sup>. While these findings suggest that MHC II utilizes an indirect endolysosomal trafficking pathway, there are several flaws with this model. Critically, unloaded cell-surface MHC II molecules have not been observed to traffic from the cell surface through Rab5- and Rab7-decorated endosomes, despite studies claiming passage through these compartments being a requisite step in the delivery of MHC II to MIICs<sup>39</sup>. Likewise, recent studies demonstrated that CD74 trafficking does not correspond directly with MHC II transport, with these two molecules being observed to passage through separate intracellular compartments upon LPS stimulation in mature DCs<sup>40</sup>. Specifically, CD74 is often detected on the cell surface in the absence of newly synthesized MHC II, and vice versa, suggesting that the presence of this complex on the cell surface is coincidental and may not be indicative of unloaded MHC II undergoing cellular export<sup>41-43</sup>. As such, despite

CD74 appearing on the cell surface and possessing AP-2-interacting motifs conducive of clathrin-mediated endocytosis, the evidence supporting the indirect endolysosomal route for MHC II trafficking are weak.

### 1.4.2 Direct Golgi-to-MIIC Trafficking Pathway

Given the aforementioned limitations, some groups have postulated that an alternative pathway may be responsible for trafficking MHC II to the MIIC. Specifically, MHC II may be transported by vesicles from the Golgi directly to the MIIC, independent of its exocytosis and re-internalization<sup>44,45</sup>. Indeed, some studies observed that MHC II and CD74 are transported directly from the trans-Golgi network towards the MIIC<sup>45-47</sup>. However, as with the studies proposing the indirect endolysosomal route, there is a lack of evidence demonstrating that MHC II transports through pathways known to deliver Golgi-derived proteins to intracellular organelles<sup>45</sup>. While not previously implicated in the delivery of MHC II to the MIIC, most organelles receive proteins directly from the Golgi through a Rab6-mediated Golgi export pathway<sup>48-50</sup>. This pathway was previously shown to deliver Golgi-derived cargo to other lysosome-derived organelles. For example, in melanocytes, Rab6 delivers melanin synthesis enzymes from the Golgi directly to lysosome-derived melanosomes, with the Rab6 effector protein ERC1 on melanosomes acting as a docking site for Rab6-bearing vesicles<sup>51</sup>. Published work by our lab used magnetic isolation and mass spectrometry to identify the presence of MHC II, Rab6, and components of the Rab6 docking complex, including ERC1, on the membranes of phagosomes from human primary macrophages<sup>52</sup>. Furthermore, ERC1 was observed to be recruited to phagosomes, and ERC1 knockdown using shRNA delayed the recruitment



of MHC II to the phagosome and abrogated the formation of MIICs (data not shown). As MIICs are also lysosome-derived organelles, these findings suggest that Rab6 and ERC1 are responsible for delivering MHC II to this compartment via a direct Golgi export pathway.

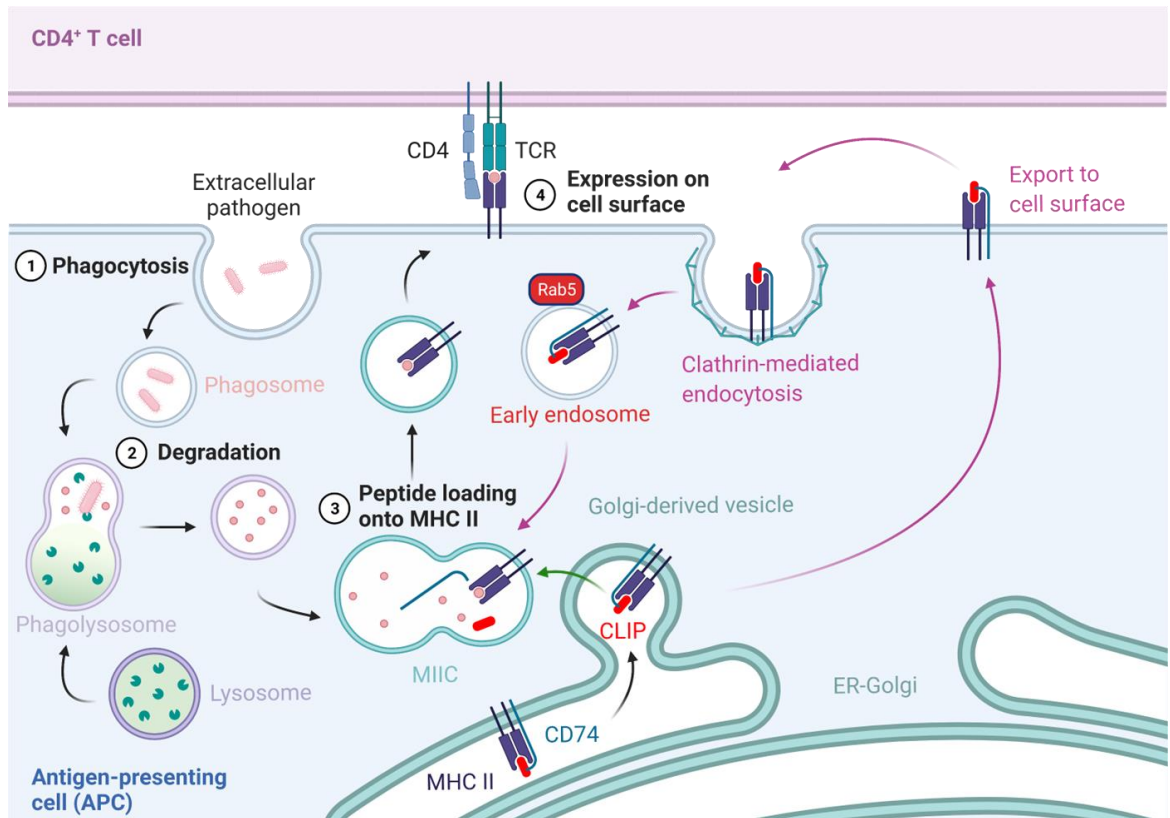


**Figure 2. Putative vesicular trafficking pathways of MHC II.**

Upon phagocytosis, newly synthesized MHC II molecules may be delivered from the Golgi to the site of antigen acquisition via two possible pathways: 1) initial export to the plasma membrane followed by clathrin-mediated endocytosis and endolysosomal trafficking to the MIIC (pink), or 2) direct Golgi-to-MIIC transport (green). Figure prepared in BioRender.

## 1.5 Role of Rab GTPases in Regulating MHC II Trafficking

Rab GTPases are monomeric proteins that function as master regulators of vesicular trafficking by directing the movement and fusion of vesicles with other cellular compartments<sup>53</sup>. While typically in its inactive state when bound by GDP, Rabs are activated by GTP exchange factors which mediate the exchange of GDP for GTP<sup>54</sup>. Once activated, Rabs regulate intracellular trafficking by enabling the budding and targeting of transport vesicles and their cargo from donor to specific acceptor compartments<sup>54,55</sup>. Rabs possess intrinsic GTPase activity that mediate their self-inactivation via removal of a terminal phosphate from their bound GTP, thus converting to an inactive GDP-bound state. This activity is induced by interactions with GTPase activating proteins<sup>56</sup>. Within the human genome, there are over 70 Rabs involved in the transport of specific intracellular compartments and vesicles, thereby providing specificity to cellular trafficking pathways<sup>55</sup>. As previously mentioned, Rabs and their effector proteins are likely involved in the vesicular trafficking of MHC II from the Golgi to MIICs. Currently, two vesicular trafficking pathways have been described to facilitate this process, each utilizing different Rab GTPases.

The indirect endolysosomal trafficking pathway would require a secretory or exocytic pathway to mediate the export of MHC II from the Golgi to the cell surface, as well as endosomal regulators that deliver surface MHC II to the MIIC. Three Rab GTPases have been described to regulate trafficking of secretory vesicles from the Golgi to the plasma membrane—Rab3a, Rab8, and Rab27<sup>57-59</sup>. While not reported to be involved in MHC II trafficking, these proteins modulate exocytosis by interacting directly with secretory vesicles and granules in multiple cell types, with Rab3a observed to localize proximal to

plasma membranes<sup>60</sup>. Rab5 is the most well-characterized regulator of endocytic trafficking, where it is primarily found in clathrin-coated endocytic vesicles and early endosomes, playing a role in receptor-mediated endocytosis and early endosome biogenesis<sup>61</sup>. Lastly, Rab7 is a regulator of the fusion of early endocytic vesicles with late endosomes and lysosomes<sup>62</sup>. Altogether, we speculate that should MHC II utilize the indirect endolysosomal route, it likely involves the sequential actions of exocytic trafficking regulators (e.g. Rab3) to initially export MHC II-CD74 to the cell surface, Rab5 to mediate endocytosis and formation of the early endosome, and Rab7 to facilitate endolysosomal trafficking to the MIIC. In contrast, an alternative pathway has been described wherein MHC II is directly transported from the Golgi to the MIIC. Rab6 is the major regulator of vesicular budding from the Golgi network in both anterograde and retrograde directions, and it has been implicated in the delivery of proteins directly to lysosome-derived organelles<sup>49,51,63</sup>. Rab6 was also observed to regulate the transport of secretory vesicles to ERC1-decorated plasma membranes, suggesting that it may be involved in the indirect endolysosomal trafficking pathway<sup>64</sup>. However, previous findings from our lab and the literature suggest that Rab6 and ERC1 are responsible for facilitating the direct Golgi-to-MIIC trafficking pathway.

## 1.6 ERC1 Potentially Regulates Expression and Trafficking of MHC II Through the Canonical TLR-Mediated NFκB Activation Pathway

ERC1 is a 128 kDa, multifaceted, globular, coiled-coil protein that is ubiquitously expressed in the cytosol<sup>65</sup>. It contains a coiled Rab-binding domain at its C-terminus that

mediates interactions with Rab6. ERC1 is central to the canonical nuclear factor kappa B (NF $\kappa$ B) activation pathway. Typically, inactive NF $\kappa$ B is sequestered in the cytosol through the masking of its nuclear localization signal by the inhibitor I $\kappa$ B $\alpha$ <sup>66</sup>. Release of NF $\kappa$ B requires phosphorylation of I $\kappa$ B $\alpha$  by the I $\kappa$ B kinase (IKK) complex, which is composed of three subunits: the kinase domain ( $\alpha$  and  $\beta$ ) and the regulatory domain ( $\gamma$ , NEMO)<sup>67</sup>. TLR signaling can initiate a signaling cascade that results in phosphorylation and activation of NEMO, subsequently leading to IKK-mediated phosphorylation of I $\kappa$ B $\alpha$  and nuclear translocation of NF $\kappa$ B<sup>68</sup>. NF $\kappa$ B family members then modulate the expression of several genes, including MHC II and other pro-inflammatory cytokines that can exacerbate inflammatory responses and tissue damage should their expression exceed normal levels<sup>69,70</sup>. As such, it is important that NF $\kappa$ B translocation and activation is tightly controlled. ERC1 is known to be activated downstream of TLR signaling and is a critical component of the IKK complex, where its absence has been linked to delayed phosphorylation of I $\kappa$ B $\alpha$  and, consequently, cytosolic sequestration of NF $\kappa$ B in its inactive state<sup>71</sup>. The exact mechanisms by which ERC1 controls phosphorylation of I $\kappa$ B $\alpha$  remain unclear, but studies have implicated ERC1 to function as a bridging molecule by facilitating the recruitment of NEMO to the  $\alpha$  and  $\beta$  subunits and enabling phosphorylation of the IKK complex by upstream kinases<sup>72</sup>.

As phagosomes bear functional TLRs, which are known to be activated by the detection of pathogen-derived molecules, it is suggested that phagocytosis can initiate a signaling cascade that releases ERC1 from the IKK complex, enabling its deposition onto the phagosome membrane. Based on previous findings from our lab, phagosome-bound ERC1 then facilitates the vesicular trafficking of Golgi-secreted proteins directly to the

phagosome through interactions with Rab6, thereby forming an MIIC upon delivery of MHC II.

## 1.7 Antigen Presentation and CD4<sup>+</sup> T Cell Responses are Impaired in Patients with COVID-19

Presentation of antigens on MHC II to CD4<sup>+</sup> T cells is a crucial step in initiating sterilizing immune responses against pathogens. This central role has made antigen presentation a prime target for antagonism by many pathogens to prevent successful generation of adaptive immunity, either by suppressing MHC II transcription or redirecting MHC II away from the cell surface. One such example is the virus responsible for causing coronavirus disease 2019 (COVID-19).

With the emergence of severe acute respiratory syndrome coronavirus 2 (SARS-CoV-2) in late 2019, the ongoing COVID-19 pandemic has garnered international attention and has taken the lives of over 6 million people worldwide, making infections with this deadly virus one of the leading causes of morbidity and mortality, overtaken only by heart diseases and cancer<sup>73</sup>. While human infections with coronaviruses is not unheard of, as we have seen regular zoonotic transmission of coronaviruses to humans over the past 20 years, including the original SARS-CoV outbreak in the early 2000s and repeated outbreaks of Middle Eastern respiratory syndrome coronavirus (MERS-CoV) starting in 2012, it remains poorly understood how infections with these likely bat-originated coronaviruses result in high lethality in humans<sup>74</sup>. Notably, patients with COVID-19 have been observed to suffer from T cell exhaustion and short-lived humoral immunity, with

reduced MHC II expression and antigen presentation to CD4<sup>+</sup> T cells speculated to be underlying causes. How SARS-CoV-2 downregulates MHC II remains to be elucidated.

## 1.8 SARS-CoV-2 Structure and Genome

Coronaviruses are members of the *Coronaviridae* family and are enveloped viruses with a positive-sense single-stranded RNA genome ranging from 26 to 32 kb in size<sup>75</sup>. SARS-CoV-2 is closely related to SARS-CoV and MERS-CoV, and it expresses 29 viral proteins, consisting of 16 non-structural proteins (NSP1-16), 4 structural proteins (Spike/S, Envelope/E, Matrix/M, Nucleocapsid/N), and 9 accessory factors (ORF3a-b, 6, 7a-b, 8, 9b-c, and 10). Many of these viral proteins are capable of interfering with host immune systems through various mechanisms<sup>76</sup>. Notably, ORF6 limits antiviral cytokine responses by preventing nuclear translocation of STAT1 and suppressing type I IFN signaling pathways, whereas ORF8 reduces activation of CD8<sup>+</sup> cytotoxic T cells by selectively directing MHC I molecules to lysosomes where they are degraded<sup>77,78</sup>.

## 1.9 Infection of Dendritic Cells and Macrophages by SARS-CoV-2

Coronaviruses infect human cells through interactions between envelope-anchored S glycoprotein with host angiotensin-converting enzyme 2 (ACE2) receptors. S-protein consists of two subunits: an ACE2 receptor-binding domain (S1) and a domain that drives viral and host cell membrane fusion (S2)<sup>79</sup>. Viral entry occurs upon host transmembrane serine protease 2 (TMPRSS2)-mediated cleavage of S-protein<sup>80,81</sup>.

SARS-CoV-2 may also enter host cells via clathrin-mediated endocytosis, allowing entry into endosomes, and subsequent fusion between viral and endolysosomal membranes upon cleavage of S protein by endosomal cysteine protease cathepsin L<sup>82,83</sup>.

While it is well established that the ACE2 receptor is required for coronavirus infection of human cells, SARS-CoV-2 can infect and activate lung-tissue resident DCs despite these cells lacking ACE2<sup>84-87</sup>. Several studies have implicated that S protein may interact with TLRs to active immune responses<sup>88-90</sup>. However, exposure of DCs to S protein and SARS-CoV-2 virus particles does not lead to TLR4 activation; rather, ACE2-expressing DCs were shown to be infected and activated by SARS-CoV-2 infections, suggesting that intracellular viral sensors are necessary for detecting and responding to SARS-CoV-2<sup>91</sup>. While this observation explains how DCs can be activated by SARS-CoV-2, it remains poorly understood how they can be infected in the first place. It is speculated that DCs uptake SARS-CoV-2 virions by engulfing infected ACE2-expressing cells to initiate antigen processing and presentation to CD4<sup>+</sup> T cells. However, once internalized, the acidic environment of the phagosome favours membrane fusion rather than delivery of viruses to the lysosome for degradation<sup>92-95</sup>. Ultimately, SARS-CoV-2 can escape the phagosomes of DCs and enter host cytosol, leading to viral replication and assembly<sup>87,96</sup>. As such, despite lacking ACE2 expression, DCs can be infected indirectly via engulfment of the virions themselves or of SARS-CoV-2-infected cells. Macrophages, on the other hand, express ACE2 and are therefore conducive to direct infections by SARS-CoV-2.



## 1.10 SARS-CoV-2 Antagonizes Antigen Presentation Through an Unknown Mechanism

It is well known that human coronaviruses can impair antigen presentation on MHC II. For example, infections with MERS-CoV—a closely related member to SARS-CoV-2—have been observed to downregulate MHC II and MHC I expression in pAPCs, thereby suppressing CD4<sup>+</sup> and CD8<sup>+</sup> T cell responses<sup>97,98</sup>. Additionally, patients with severe COVID-19 have decreased levels of MHC I and MHC II in several immune cells, including monocytes, DCs, and B cells, and *in vitro* infections with SARS-CoV-2 reduced surface MHC II expression in human macrophages<sup>99–101</sup>. Despite the importance of antigen presentation in initiating the defense responses necessary for controlling SARS-CoV-2 infections, it remains unknown how this virus can impair this process to escape immunosurveillance. While it was recently discovered that SARS-CoV-2 ORF6 may potentially reduce MHC I expression, the specific viral proteins responsible for suppressing MHC II expression have not been identified<sup>102</sup>.

A common strategy utilized by pathogens to prevent antigen presentation is redirecting MHC molecules away from the cell surface, thereby limiting the generation of CD4<sup>+</sup> T cell responses. For example, the HIV Nef prevents antigen presentation by trafficking MHC I molecules away from the cell surface and towards a Golgi-proximal organelle<sup>103</sup>. In addition to redirection of surface MHC molecules, pathogens may also suppress MHC II expression. For example, other human coronaviruses, such as MERS-CoV, have been shown to epigenetically reprogram the host transcriptional machineries in infected cells, thereby reducing MHC II levels<sup>97,104</sup>. Indeed, a recent interactome analysis of SARS-CoV-2 identified viral non-structural protein 5 (NSP5) as an interactor of HDAC2—an

epigenetic regulator of CIITA and MHC II transcription—albeit the effects of NSP5 on HDAC2 activity are unknown<sup>105</sup>. NSP13 was also identified to target multiple components of Golgi trafficking pathways, including ERC1, suggesting that SARS-CoV-2 may also block antigen presentation through manipulating the direct Golgi-to-phagosome trafficking route for MHC II, thus impairing MIIC formation. However, the focus of this thesis is the investigation of SARS-CoV-2 NSP5 in altering MHC II expression.

## 1.11 SARS-CoV-2 NSP5 Potentially Suppresses MHC II Expression

NSP5 is one of two cysteine proteases expressed by SARS-CoV-2. It plays a critical role in viral infection by proteolytically cleaving the SARS-CoV-2 polyprotein into individual NSPs, subsequently leading to viral replication and assembly<sup>106</sup>. Self-cleavage at the N- and C-terminals of NSP5 is also an important processing step for proper function. This central role in viral replication makes NSP5 an interesting and viable drug target, as malfunctions and deletions of NSP5 have been shown to decrease virus viability and reduce ensuing inflammatory responses<sup>107–109</sup>.

Outside of its role in viral replication, it is speculated that NSP5 from other coronaviruses can cleave host proteins to disrupt molecular pathways and host immune responses<sup>110</sup>. Recent studies implicated NSP5 as a multifaceted protein that functions in interfering with multiple antiviral response pathways to assist in viral propagation. For example, NSP5 impairs antiviral responses through multiple mechanisms, including antagonism of RIG-I and MAVS, as well as prevention of IRF3 nuclear translocation to suppress

expression of IFN-stimulated genes<sup>111</sup>. Likewise, NSP5 enhances expression of pro-inflammatory cytokines, including IL-6, IL-1B, TNF $\alpha$ , and IL-2, through activation of the NF $\kappa$ B pathway, possibly attributing to the excessive inflammatory responses and cytokine storms observed in patients with COVID-19<sup>112,113</sup>. Most intriguingly, NSP5 was recently identified to interact with HDAC2, suggesting a possibility to directly impair MHC II expression and prevent activation of CD4<sup>+</sup> T cells necessary to clear infections<sup>105</sup>.

## 1.12 Hypothesis and Aims

In this thesis, I addressed two hypotheses. Firstly, I hypothesized that MIICs are formed via a Rab6/ERC1-dependent trafficking pathway which directly transports MHC II from the Golgi to the phagosome. Secondly, I hypothesized that SARS-CoV-2 NSP5 downregulates MHC II expression via interactions with HDAC2.

Aim 1: Develop the tools necessary to detect MHC II trafficking and expression and determine how MHC II is delivered to phagosomes.

Aim 2: Assess the effects of SARS-CoV-2 NSP5 on MHC II expression and antigen presentation.

## Chapter 2

### 2 Materials and Methods

#### 2.1 Materials

HeLa cells were gifts from Dr. Stephen Barr (University of Western Ontario, London, Canada). HEK293T cells were gifts from Dr. Sergio Grinstein (Hospital for Sick Children, Toronto, Canada). RAW 264.7 and J774A.1 murine macrophages were purchased from ATCC (Manassas, Virginia). Roswell Park Memorial Institute (RPMI), Dulbecco's Modified Eagle Medium (DMEM), and Fetal Bovine Serum (FBS) were purchased from Wisent (Saint-Jean-Baptiste, Canada). Trypsin-EDTA and antibiotic/antimycotic were purchased from Corning (Manassas, Virginia). #1.5 thickness 8-mm round coverslips and 16 % paraformaldehyde (PFA) were purchased from Electron Microscopy Supplies (Hatfield, Pennsylvania). GenJet Plus, DNA isolation kits, and all lab plasticware were purchased from Frogga Bio (Concord, Canada). All laboratory chemicals were purchased from Bioshop Canada (Burlington, Canada). WGA-AlexaFluor 647, Hoechst, Permafluor mounting reagent, FuGene HD, and HALT protease/phosphatase inhibitors, were purchased from Thermo Fisher Canada (Mississauga, Canada). Phusion DNA polymerase, all restriction enzymes, HiFi Gibson Assembly Kit, Monarch Nucleic Acid Preparation Kit, and T4 DNA ligase were purchased from NEB Canada (Whitby, Canada). Retro-X Universal Packaging System was purchased from Takara Bio (San Jose, California). Recombinant human GM-CSF, IFN $\gamma$ , and IL-4 were purchased from Peprotech (Cranbury, New Jersey). iScript Select cDNA Synthesis Kit, SsoFast EvaGreen Supermix, Instagene, and all protein blotting reagents and gels were purchased from Bio-Rad Canada (Mississauga, Canada).

Lympholyte-poly was purchased from Cedarlane Laboratories (Burlington, Canada). Cell Proliferation Dye eFluor 670 was purchased from eBioscience (San Diego, California). Polybrene Infection Reagent and ivermectin were purchased from EMD Millipore Corp (Norwood, Ohio). Dual-Luciferase Reporter Assay System, and Janelia Fluor HaloTag Ligands 549 and 646 were purchased from Promega (Madison, Wisconsin). RNeasy Mini Kit was purchased from Qiagen (Germantown, Maryland). CD14 Positive Cell Selection Kit and anti-DYKDDDDK tag (L5) were purchased from BioLegend (San Diego, California). Polystyrene/divinylbenzene (PS/DVB) microsphere beads were purchased from Bangs Laboratories (Fishers, Indiana). Lipofectamine 3000 and Lipofectamine LTX transfection reagents were purchased from Life Technologies (Carlsbad, California). *Escherichia coli* DH5 $\alpha$  and ML35 strains were gifts from Drs. John McCormick and Susan Koval, respectively (Western University, London, Canada).

## 2.2 Plasmids and Oligos

GalT-mCherry, KDEL-GFP, Rab5-GFP, and Rab7-mCherry expression constructs were gifts from Dr. Sergio Grinstein (Hospital for Sick Children, Toronto, Canada). EGFP-Rab3A (Plasmid #49542), EGFP-Rab8 (Plasmid #49543), and EGFP-Rab27 (Plasmid #49605) expression constructs were purchased from Addgene (Watertown, Massachusetts). pLVX-IRES-zsGreen lentiviral vector and pCMV-zsGreen packaging vector were gifts from Dr. Jimmy Dikeakos (Western University, London, Canada). pGL4.20 [luc/Puro] was purchased from Promega (Madison, Wisconsin). pRetroX-Tet3G and pRetroX-TRE3G were purchased from Takara Bio (San Jose, California). The renilla

luciferase internal control vector pRL-TK was a gift from Dr. Rodney DeKoter (Western University, London, Canada). Accell SMARTpool non-targeting siRNA, HDAC2-targeting siRNA, siRNA delivery media, and siRNA buffer were purchased from Horizon Discovery (Cambridge, United Kingdom). All DNA primers, oligos, and synthesized genes were purchased from IDT (Coralville, Iowa), and the sequences for all primers used in this study can be found in **Tables 1-2**.

## 2.3 Culturing and Transfection of Cell Lines

HeLa cells, and RAW 264.7 and J774A.1 murine macrophages were maintained in DMEM supplemented with 10 % FBS. Cells were split at 80 % confluency by washing once with phosphate buffered saline (PBS: 0.9 % NaCl, 10 mM Na<sub>2</sub>HPO<sub>4</sub>, 2 mM KH<sub>2</sub>PO<sub>4</sub>, pH 7.4) followed by a 5 min incubation in trypsin-EDTA at 37 °C and resuspension in DMEM + 10 % FBS. For imaging, HeLa cells were seeded into 12-well tissue culture plates with #1.5 thickness 18 mm diameter coverslips, 1 mL of DMEM + 10 % FBS added, and 100 µL of cell suspension added dropwise to each well. After overnight incubation, cells were transfected with the desired DNA construct according to manufacturer's protocol. Briefly, for each well, two tubes of 38 µL serum-free DMEM were prepared. Then, 3 µL of GenJet Plus was added to one tube and 1 µg of DNA was added to the second tube. Diluted GenJet Plus reagent was added to the diluted DNA solution. Following a brief vortex, the mixture was incubated for 10-15 min at room temperature to allow the DNA:GenJet Plus complexes to form. Finally, the mixture was added dropwise to the desired well and incubated for 18-24 h at 37 °C. For ivermectin treatment, 25 µM of ivermectin or DMSO were added to cells for 90 min at 37 °C.

RAW 264.7 macrophages were transfected using Neon electroporation as per manufacturer's instructions. Briefly,  $1 \times 10^6$  cells/well were collected in 1.5 mL tubes and centrifuged at 400 xg for 5 min, followed by resuspension in 1 mL of PBS. Cells were centrifuged again at 400 xg for 5 min, and supernatant was removed afterwards. Each sample was then resuspended in 5  $\mu$ g of DNA and an appropriate volume of R buffer. Samples were then transferred to a Neon electroporation apparatus and shocked using the following conditions: 1680 V, 20 ms pulse width, and 1 pulse. Following transfection, cells were allowed to recover for 20 min in a new PCR tube. Cells were then transferred to a 12-well plate and incubated at 37 °C.

J774A.1 macrophages were transfected using the FuGene method.  $2.5 \times 10^5$  cells were seeded into 12-well tissue culture plates on #1.5 thickness 18 mm diameter coverslips with 1 mL of DMEM + 10 % FBS added. DNA was prepared according to manufacturer's instructions. Briefly, to each well to be transfected, 150  $\mu$ L of serum-free DMEM was added to a sterile 1.5 mL microfuge tube, to which a total of 3.3  $\mu$ g of the desired DNA construct(s) were added. After a brief vortex to mix the contents, 10  $\mu$ L of FuGene HD transfection reagent was added to the tube followed by mixing the DNA-reagent solution. The mixture was allowed to incubate for 15 mins at room temperature before being added dropwise to the desired well and incubated for 18-24 h at 37 °C to allow for cell recovery and transgene expression.

## 2.4 Culturing and Transduction of Human Primary Dendritic Cells

Primary human dendritic cells were prepared from monocytes isolated from whole blood isolated from healthy adult donors with ethics approval from the Office of Human Research Ethics at Western University Health Sciences Research Ethics Boards and performed in accordance with the guidelines of the Tri-Council policy statement on human research. Blood was collected through venipuncture into vacuum tubes coated with heparin, and monocytes were isolated using Lympholyte-poly separation media according to manufacturer's instructions. Briefly, approximately 4 mL of blood was layered over an equal volume of Lympholyte-poly and centrifuged for 25 min at 500  $\times$ g at 50 % acceleration and zero deceleration. The mononuclear cell layer was carefully removed using a transfer pipette to a clean 50 mL tube and resuspended in 50 mL of PBS and subsequently centrifuged for 6 min at 300  $\times$ g at full acceleration and deceleration.

Peripheral blood mononuclear cells (PBMCs) were resuspended in 200  $\mu$ L of warm RPMI for each well of a 12-well plate. Sterile, acid-washed glass coverslips (2 M HCl, overnight at 55  $^{\circ}$ C) were placed into 12-well plates and the PBMC suspension was transferred onto coverslips. Cells were incubated for 2 h at 37  $^{\circ}$ C + 5 % CO<sub>2</sub> to allow monocytes to adhere to glass. Coverslips were washed 3 $\times$  with PBS to remove non-adherent cells. Cells were maintained in culture with RPMI supplemented with 10 % FBS, L-glutamine and sodium bicarbonate, 10,000 U/mL penicillin, 10 mg/mL streptomycin, 25  $\mu$ g/ml amphotericin B, and buffered with 25 mM HEPES to pH 7.2. To generate dendritic cells, adherent monocytes were additionally supplemented with 1000 U/mL rhGM-CSF and 500 U/mL rhIL-4 for 48 h, with culture media replenished with



fresh complete RPMI supplemented with 1000 U/mL rhGM-CSF and 500 U/mL rhIL-4 for an additional 48 h.

Primary DCs were transduced with NSP5-expressing or empty pLVX-zsGreen lentiviral vectors. Briefly, cells were plated on 48-well tissue culture plates and infected at a multiplicity of infection (MOI) of 30, followed by centrifugation at 500 ×g for 90 min at 32 °C. Plates were then transferred to a 37 °C + 5 % CO<sub>2</sub> incubator for 8 h, at which point cells were supplemented with fresh warm media and allowed to incubate for an additional 72 h. For IFN $\gamma$  stimulation, 10 ng/mL of recombinant human IFN $\gamma$  was added for 24 h to induce MHC II expression. For siRNA treatment, 5 nmol of HDAC2- and non-targeting siRNA were resuspended in 50  $\mu$ L of 1x siRNA buffer (300 mM KCl, 30 mM HEPES-pH 7.5, 1.0 mM MgCl<sub>2</sub>) to obtain a 100  $\mu$ M stock solution. 2  $\mu$ M of siRNA resuspended in siRNA delivery media were added to the cells, followed by incubation at 37 °C + 5 % CO<sub>2</sub> for 72 h.

## 2.5 Molecular Cloning

Recombinant expression vectors were prepared through restriction enzyme digestion and subsequent ligation of appropriate insert sequences and vector backbones. Briefly, a DNA insert consisting of the consensus coding sequence of the gene of interest was amplified using standard PCR with primers designed to add flanking restriction enzyme sites compatible with the multiple cloning site of the vector backbone. A list of all PCR primers used for cloning can be found in **Table 1**. PCR reactions were run for 30 cycles with Phusion DNA polymerase according to manufacturer's instructions. Subsequently,

the insert and backbone were digested with appropriate restriction enzymes for 1 h at 37 °C and gel purified using 1% agarose gel and the Monarch Nucleic Acid Preparation Kit according to manufacturer's instructions. Purified cut insert and backbone were ligated at a ratio of 10:1 insert to backbone overnight at 16 °C with 20,000 U/mL T4 ligase. Ligated vectors were transformed into chemically competent *Escherichia coli* DH5 $\alpha$  cells by heat shock for 2 min at 42 °C. Transformed *E. coli* were plated on LB agar supplemented with the appropriate selective antibiotic and incubated overnight at 37 °C. Single colonies appearing following incubation were propagated in liquid LB media overnight at 37 °C and shaking at 200 RPM. Following overnight incubation, plasmids were harvested from cultures using the High-Speed Plasmid Mini Kit according to manufacturer's instructions. Correct insertion of insert into backbone was confirmed by Sanger sequencing at the Robarts Research Institute.

### 2.5.1 MHC II-HaloTag Cloning

A gene block comprised of HLA-DRB1 with a short GS linker to HaloTag and HLA-DRA was cloned into a pRetroX-TRE3G vector by Gibson assembly. CD74-MHC II-HaloTag was generated by amplifying two fragments of the original MHC II-HaloTag vector using PCR, followed by Gibson assembly to clone a CD74 gene block into the MHC II-HaloTag vector. Amplicons were then circularized with T4 DNA ligase. Vector maps for MHC II-HaloTag cloning are available on **Appendix A**.

## 2.5.2 Dual Luciferase Cloning

MHC II and CIITA (pI and pIV) promoters were amplified from human DNA via PCR using primers from **Table 1**. After amplification, promoters were cloned into pGL4.2 luciferase reporter vectors by Gibson assembly, and amplicons were circularized with T4 DNA ligase. Vector maps for dual luciferase cloning are available on **Appendix B**.

## 2.5.3 NSP5 Cloning

Briefly, FLAG-tagged NSP5 was cloned into an EcoRI-digested pLVX-puro lentiviral vector, and untagged NSP5 was cloned into a pLVX-zsGreen lentiviral vector by Gibson assembly. Point mutants were generated by amplifying the entirety of the original NSP5-FLAG vector with phosphorylated primers that incorporate the point mutation in the first base pair of the forward primer, while deletion mutants were generated by amplifying the vector from either side of the desired deletion with phosphorylated primers. Following amplification, the parental plasmid was removed by DpnI digestion, and the amplicons were circularized with T4 DNA ligase. Vector maps for NSP5 cloning are available on **Appendix C**.

## 2.6 Immunofluorescence Microscopy

### 2.6.1 Immunostaining

Cells to be stained were grown on 18 mm, #1.5 thickness round coverslips placed into the wells of a 12-well tissue culture plate. If necessary, cells were stained with wheat germ agglutinin (WGA) for 10 min at 10 °C and rinsed 3× with PBS. Otherwise, cells were

equilibrated to room temperature to prevent membrane turnover and subsequently washed 1× with PBS. Cells were fixed with 4 % PFA for 20 min at room temperature and subsequently washed with PBS to remove excess PFA. Fixed cells were blocked and permeabilized with blocking buffer (0.1 % Triton X-100, 2.5 % bovine serum albumin (BSA)) in PBS. Blocking buffer was removed, and primary antibody in 2.5 % BSA was added to cells and allowed to incubate for 1 h at room temperature. Cells were washed 3× 10 min. Secondary antibodies in 2.5 % BSA was added to cells and allowed to incubate for 1 h at room temperature. Cells were washed 3 × 10 min and incubated in 1:10000 Hoechst in PBS for 5 min. Cell-containing coverslips were mounted onto glass slides using Permafluor mounting reagent and stored at 4 °C until imaging.

## 2.6.2 Fluorescence Imaging

Microscopy was used to visualize cell morphology and perform quantification of fluorescence intensity. In all cases, at least three technical replicates were analyzed. For measurement of fluorescence within individual cells, a minimum of 30 cells were quantified. To minimize observer bias, random fields of view were captured whenever possible. Imaging of stained cells was performed using a Leica DMI6000B epifluorescence microscope equipped with a photometrics Evolve-512 delta EM-CCD camera (Teledyne Photometrics), and a Sedat Quad filter set (Chroma) operated by Leica LAS-X software. If necessary, z-sections were captured for phagocytosis assays and colocalization experiments across the entire depth of the phagocyte separated by at least 0.25 μm between stacks.

### 2.6.3 Image Analysis

All image analyses were performed using the FIJI distribution of ImageJ, unless otherwise stated<sup>114,115</sup>. Measurements of fluorescence intensity was performed by forming a selection around the region of interest (ROI) and using the “Measure” feature to obtain the area and integrated density of the ROI. Background fluorescence was measured using a region free of any cells or other features and was subtracted from the integrated density of each ROI.

## 2.7 MHC II-HaloTag Expression System

### 2.7.1 Preparation of IgG-Coated Phagocytic Targets

Whole IgG-coated beads were prepared according to our lab’s published methods<sup>116</sup>. Briefly, 10  $\mu$ L of 3.17  $\mu$ m PS/DVB microsphere beads were mixed with 1 mL of PBS in a 1.5 mL microfuge tube, followed by centrifugation at 5000  $\times$ g for 1 min. Supernatant was removed and beads were resuspended in 100  $\mu$ L of PBS and 10  $\mu$ L of whole rat IgG. Tubes were rotated for 90 min at room temperature. Afterwards, beads were washed twice and resuspended with 100  $\mu$ L of PBS.

### 2.7.2 Phagocytosis Assay

Phagocytosis assays were carried out according to our lab’s previously published methods<sup>116</sup>. J774A.1 macrophages were grown on #1.5 thickness 18 mm round glass coverslips on a 12-well plate. Following overnight incubation, cells were transfected with Rab5-GFP and Rab7-mCherry according to Section 2.3.

For live cell imaging, cells were transferred to a heated and CO<sub>2</sub>-perfused Leiden chamber, filled with an appropriate volume of warm media, attached to the piezoelectric stage of a Leica DMI6000B epifluorescence microscope. 10 µL of suspended IgG-coated beads were added into the Leiden chamber and mixed carefully using a pipette. Images were captured at 4-min intervals up to a duration of 2 h. Between 5-10 cells of interest were marked using the Mark and Find feature of the Leica LAS-X software.

For fixed cell imaging, cells were allowed to equilibrate to room temperature to prevent premature target uptake. The desired number of phagocytic targets were added into each well, and the mixture was centrifuged for 1 min at 500 g to force contact between phagocytes and phagocytic targets. Plates were then incubated at various time points at 37 °C, followed by fixation using 4 % PFA and staining with Hoechst. If necessary, cells were stained with the appropriate primary and species-specific secondary antibodies according to Section 2.6.1. Finally, cell-containing coverslips were mounted onto glass slides and imaged using an epifluorescence microscope. A minimum of 30 macrophages were counted for each condition.

## 2.8 Quantitative Reverse Transcription PCR (RT-qPCR)

### 2.8.1 RNA Preparation

Total RNA was isolated from THP-1 cells or primary DCs using RNeasy Mini Kit (Bio-Rad) according to manufacturer's instructions. Cells were harvested as a pellet and homogenized in 350 µL of Buffer RLT. An equal volume of 70 % ethanol was added to cell lysate. Samples were transferred to an RNeasy Mini spin column placed in a 2 mL

collection tube and centrifuged for 15 s at 8000 ×g. 700 μL of Buffer RW1 was added to the spin column, and samples were centrifuged for 15 s at 8000 ×g. 500 μL of Buffer RPE was added to the spin column, and samples were centrifuged for 15 s at 8000 ×g. This step was repeated once more after flowthrough was discarded. Spin columns were transferred to a new 1.5 mL collection tube, and 50 μL of RNase-free water was added. Samples were centrifuged for 1 min at 8000 ×g to elute the RNA. Total RNA concentration and quality were measured using a NanoDrop 1000 Spectrophotometer prior to cDNA preparation.

### 2.8.2 cDNA Preparation and RT-qPCR

cDNA was generated from total RNA using the iScript Select cDNA Synthesis Kit (Bio-Rad) according to manufacturer's instructions, with an equal amount of starting RNA and equal mix of the oligo(dT)<sub>20</sub> primer mixes. RT-qPCR was performed using the SsoFast EvaGreen Supermix with an equal amount of starting cDNA. All RT-qPCR primers used in this thesis can be found in **Table 2**. RT-qPCR reactions were run on a QuantStudio 3 Real-Time PCR System (Thermo Fisher) for 40 amplification cycles. Relative expression of genes of interest was calculated using the following  $\Delta\Delta C_t$  method with GAPDH serving as the reference gene:

$$\text{Relative expression} = 2^{-\Delta\Delta C_t}$$

## 2.9 Dual Luciferase Assay

Dual luciferase assays were performed using a Dual-Luciferase Reporter Assay System according to manufacturer's instructions to measure MHC II and CIITA promoter activity in response to NSP5 expression. RAW 264.7 macrophages and HeLa cells were co-transfected with NSP5-FLAG, the internal renilla luciferase control vector pRL-TK, and either a pGL4.20-MHC II, pGL4.20-CIITA pI, or pGL4.20-CIITA pIV firefly luciferase reporter vector using the Neon electroporation method according to Section 2.3. At 72 h post-transfection, cells were lysed using passive lysis buffer for 15 min, with agitation. Lysed cells were transferred to a 1.5 mL Eppendorf tube and centrifuged at max speed for 1 min. Equal volumes of supernatant (50  $\mu$ L) were transferred to a 96-well white plate in duplicates. 25  $\mu$ L of Luciferase Assay Reagent II (LAR II) was added to each well, and Firefly luciferase (FLuc) expression was measured using a Cytation 5 luminometer. 50  $\mu$ L of Stop and Glo 1X reagent was added to quench the LAR II, and Renilla luciferase (RLuc) expression was measured. Promoter activity was calculated using the following equation:

$$\text{Promoter activity} = \frac{FLuc}{RLuc}$$

## 2.10 Western Blot

Western blotting was employed to detect proteins of interest in cultured cells.  $1 \times 10^6$  HeLa cells were cultured and transfected with appropriate DNA. Cells were washed in PBS and incubated for 72 h to allow protein detection prior to lysis. Cellular lysis was



performed using RIPA (150 mM NaCl, 1% Triton X-100, 0.5% sodium deoxycholate, 0.1% SDS, and 50 mM pH 8.0 Tris-HCl). Appropriate lysis buffer containing 1:100 v/v mammalian protease and phosphatase inhibitors were added to cells, followed by scraping cells into suspension. Lysate was immediately transferred to a clean 1.5 mL tube and boiled for 5 min. Denatured cell lysates were run on a 10 % SDS-PAGE gel for 60 min at 120 V or until the leading edge of the lysates have nearly reached the bottom of the gel. Proteins were transferred to a nitrocellulose membrane overnight at 40 V at 4 °C. Following transfer, membranes were washed 1× with Tris-buffered saline + 0.1% Tween (TBS-T) prior to processing. Membranes were blocked with 5% BSA blocking buffer in TBS-T for a minimum of 2 h at room temperature with gentle agitation. Primary antibodies were added to blocking buffer at an appropriate concentration and allowed to incubate for 1 h at room temperature. Membranes were washed 3 × with TBS-T and incubated in blocking buffer with an appropriate concentration of infrared dye-conjugated secondary antibodies added. Membranes were allowed to incubate for 1 h at room temperature with gentle agitation. Subsequently, membranes were washed 3 × with TBS-T and imaged on an Odyssey CLx Imaging System (LI-COR).

## 2.11 Generation of Phylogenetic Trees

Amino acid sequences of HDAC2 from various vertebrate species were retrieved from the NCBI BLASTp database. Amino acid sequences of NSP5 across four coronavirus genera were retrieved in a similar manner. Amino acid alignments of HDAC2 and NSP5 sequences were imported into MEGA11, and coding sequence alignments were generated with MUSCLE using default parameters<sup>117</sup>. Pairwise distances were calculated using a

Poisson model assuming uniform rates across sites, and maximum likelihood trees were generated using a 500-iteration bootstrapping approach. Phylogenetic trees were then generated to explore the evolutionary relationship of each protein across multiple species.

## 2.12 Statistical Analysis

All statistical analyses were performed on GraphPad Prism 9 software. Comparisons between two means/medians made use of a Mann-Whitney test, while comparisons between multiple means made use of a Kruskal-Wallis test.

**Table 1. Cloning primer sequences used in this study**

<b>Primer</b>	<b>Sequence</b>
<i>Dual luciferase cloning primers</i>	
CIITA pI	F: 5'-AGCTCGCTAGCCTCGAGGATGATATTGGCAGCTGGCACCA-3' R: 5'-CGCCGAGGCCAGATCTTGATCAGCTCAGAAGCACACAGCC-3'
CIITA pIV	F: 5'-AGCTCGCTAGCCTCGAGGATTGCCACTTCTGATAAAGCACGTGG-3' R: 5'-CGCCGAGGCCAGATCTTGATGGCAGCTCGTCCGCTGGTCA-3'
MHC II Promoter	F: 5'-AGCTCGCTAGCCTCGAGGATTCCGTGATTGACTAACAGTC-3' R: 5'-CGCCGAGGCCAGATCTTGATGAATAAAAGAAAAGAGAATGTGGG-3'
Luciferase Split	5'-AACTGGCCGGTACCTGAGC-3' 5'-AGGCCAGAGAAATGTTCTGGCAC-3'
<i>MHC II-HaloTag cloning primers</i>	
CD74	F: 5'-TCTTATACTTGGATCCATCGATACGCGTG-3' R: 5'-CTCCAGGGAACTTCAGACACACCA-3'
MHC II	F: 5'-AACACTTTTGTCTTATACTTGGATCCATCGATACG-3' R: 5'-CTCCAGGGAACTTCAGACACACCA-3'
pRetroX-Tre3G Split	F: 5'-TCGACCCTAGAGAACCATCAGATGTTC-3' R: 5'-GAAACATCTGATGGTTCTCTAGGGTCGA-3'
MHC II Polycistronic	F: 5'-ATGGTGTGTCTGAAGTTCCTGG-3' R: 5'-GCACGCGTATCGATGGATCC-3'
<i>NSP5 cloning primers</i>	
NSP5-FLAG	F: 5'-CCGACTCTACTAGAGGATCTATTTCCGGT-3' R: 5'-CGGCCGCTCTAGAAGTCTCTCG-3'
NSP5 <sup>H41A</sup>	F: 5'- CTGTGATCTGCACCTCTGAAGACATGC -3' R: 5'- CTCTTGGACAGTAAACTACGTCATCAAGCCA -3'
NSP5 <sup>C145S</sup>	F: 5'- CTGGTAGTGTTGGTTTTAACATAGATTATGACTGTGT-3' R: 5'- ATGAACCATTAAGGAATGAACCCTTAATAGTGAAATTG -3'
NSP5 <sup>Δ1-192</sup>	F: 5'- GCAGCTGGTACGGACACAACACTATTAC-3' R: 5'- CATGAATTCACCGGAAATAGATCCTCTAGTAGAG-3'
NSP5 <sup>Δ199-306</sup>	F: 5'- GCATCACCGGTAGACTACAAGGACC-3' R: 5'- TGTGTCCGTACCAGCTGCTTG-3'

## Chapter 3

### 3 Results – Development of Tools to Detect MHC II Trafficking and Expression

#### 3.1 Development of MHC II-HaloTag Construct

To enable studies of MHC II trafficking, I first needed to design a technique to enable the observation of MHC II movement in live cells, and in a manner that would allow its expression to be controlled. Moreover, a method was required which would allow for MHC II trafficking to be monitored shortly after its synthesis in the ER through to its delivery to the MIIC. Fluorescent MHC II reporter transgenes were not viable options as they are constitutively expressed, and the maturation time of most fluorescent proteins lack the speed (>30 min) to enable visualization of newly synthesized MHC II molecules<sup>118</sup>. Further complicating matters is the need to express the alpha (HLA-DRA) and beta (HLA-DRB) chains of MHC II, along with CD74, to ensure proper formation of the MHC II-CD74 complex. As such, I generated a doxycycline-inducible expression system comprised of a CD74-HLA-DRB-HaloTag-HLA-DRA fusion protein containing T2A self-cleaving peptide motifs between each protein, ensuring this protein will be cleaved into individual CD74, HLA-DRB-HaloTag, and HLA-DRA proteins during translation at a 1:1 stoichiometry. This reporter construct is normally turned off; however, with the addition of a second regulatory Tet3G vector and doxycycline, I can induce expression of Tet3G which subsequently binds to response elements on the promoter of the MHC II-HaloTag construct, thereby allowing for inducible expression of MHC II. The MHC II reporter itself is fused to a HaloTag that can be labeled with fluorescent ligands, allowing for visualization of MHC II synthesis and trafficking on a fluorescence

microscope, with labeling occurring within minutes of HaloTag ligand addition, thereby enabling the ability to monitor protein trafficking immediately after translation into the ER<sup>119</sup>.

This system was validated by co-transfecting HEK 293T cells with the MHC II-HaloTag reporter and Tet3G regulatory constructs, followed by staining of MHC II and immunofluorescence microscopy to confirm that fluorescently labeled HaloTag is indicative of MHC II expression (**Figure 3A**). This system was further optimized by determining the optimal doses for doxycycline and HaloTag ligand that would provide a detectable MHC II signal under a fluorescence microscope. Serial dilutions of the fluorescent HaloTag ligand demonstrated that a 40 nM dose maximized signal without adding background or wasting reagent (**Figure 3B**). Furthermore, dose response experiments were performed using serial dilutions of doxycycline prior to HaloTag labeling, where I determined that 500 ng of doxycycline is an ideal concentration to induce expression of MHC II-HaloTag without apparent expression artifacts, such as the formation of large intracellular inclusions of the fluorescent protein (**Figure 3C**). In a parallel experiment, I determined that the optimal time that induced the highest expression of MHC II-HaloTag is 30 min post-treatment with doxycycline (**Figure 3D**). Altogether, these experiments provided the framework and conditions required for monitoring MHC II trafficking in more relevant cell types, such as macrophages and DCs, in future experiments.

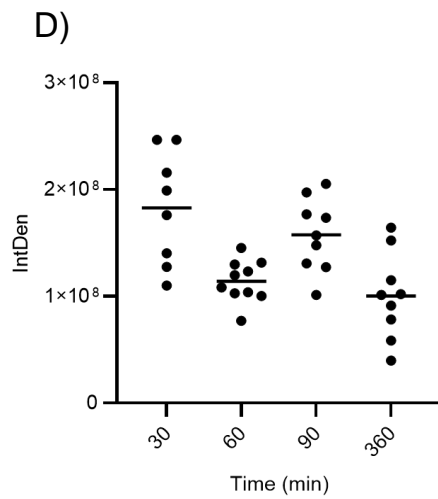
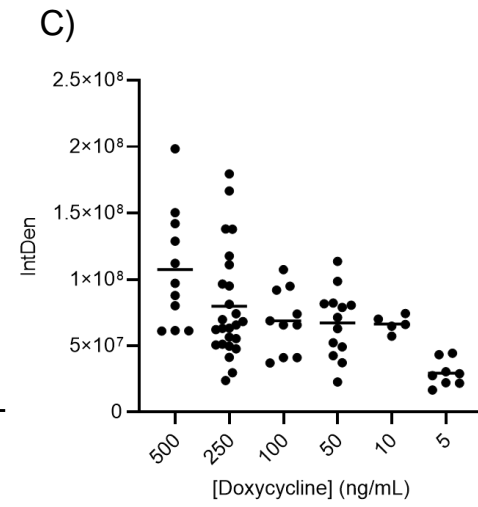
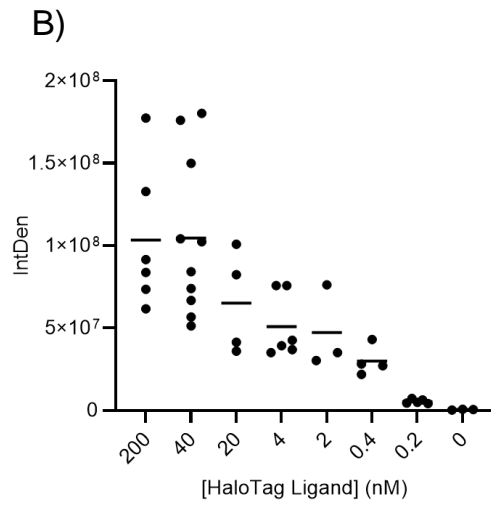
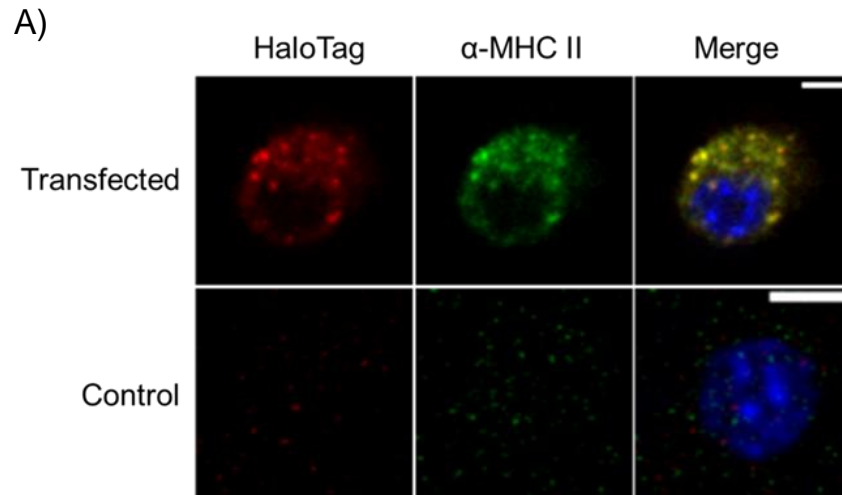


**Figure 3. Determining the optimal concentrations and incubations of HaloTag ligand and doxycycline to induce MHC II-HaloTag expression.**

HEK 293T cells were co-transfected with Tet3G and MHC II-HaloTag constructs. **A)** Validation of doxycycline-inducible MHC II-HaloTag system via immunofluorescence microscopy showing near-perfect overlap of the HaloTagged MHC II (red) and immunostaining of MHC II (green). **B)** Cells were labeled with various concentrations of HaloTag ligands following overnight incubation of 500 ng/mL doxycycline. **C)** Cells were stimulated overnight with various concentrations of doxycycline, followed by labeling with 40 nM of HaloTag ligand. **D)** Cells were stimulated with doxycycline at various time points, followed by HaloTag labeling. Z-stacks were captured using immunofluorescence microscopy, with image analyses to quantify integrated density (IntDen) of MHC II-HaloTag. Data are presented as mean intensity of total MHC II-HaloTag expressed in cells for each condition and was obtained from one independent experiment (n = 1). Scale bar is 10  $\mu$ m.

## 3.2 Monitoring Protein Trafficking Dynamics in Macrophages

IgG-opsionized beads were used as pathogen mimics to perform phagocytosis assays in J774A.1 macrophages co-expressing Rab5-GFP and Rab7-mCherry. While these beads cannot be degraded by macrophages, their large size allows for detection by DIC microscopy and enables accurate detection and quantification of fluorescent markers recruited to phagosomes, thereby making them an ideal phagocytic target for the purposes of this thesis. To demonstrate the utility of this model, I demonstrated the immediate recruitment of Rab5 to the site of phagocytosis, followed by its replacement by Rab7, visualized with this model system (**Figure 4**). This optimized assay can now be used to quantify the recruitment of MHC II to phagosomes by expressing the inducible MHC II trafficking reporter, described above, in this model system.



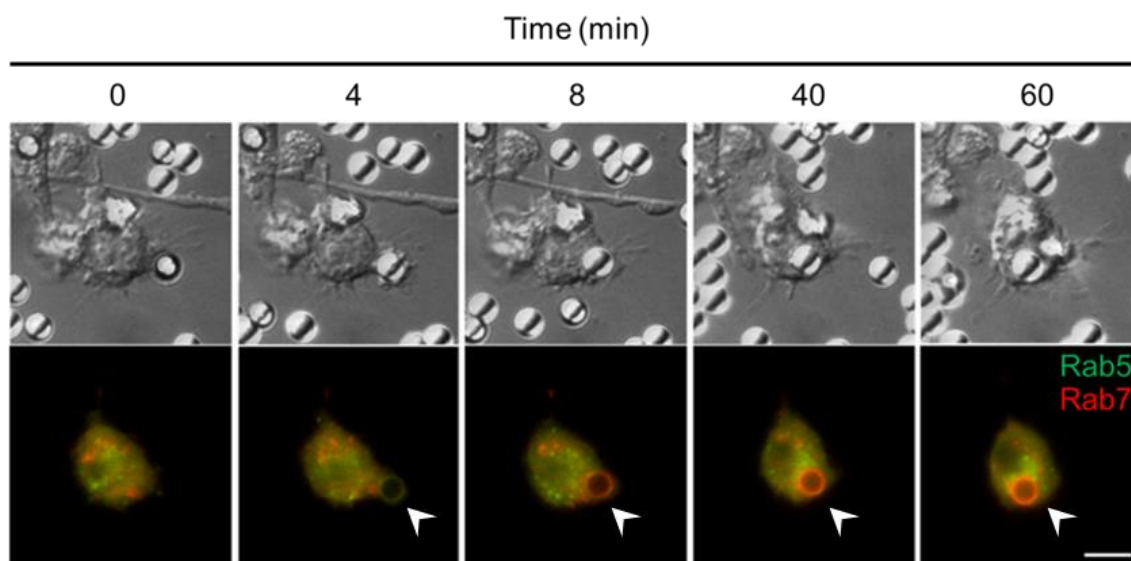


**Figure 4. Time-lapse of Rab5 and Rab7 recruitment to phagosomes.**

RAW 264.7 macrophages were co-transfected with Rab5-GFP (green) and Rab7-mCherry (red), and live cell fluorescence microscopy was performed to track the localization of Rab5 and Rab7 to phagosomes formed after the engulfment of IgG-coated PS/DVB beads. Images were captured with a 100 $\times$  objective at 4-minute intervals obtained from 2 independent experiments. Rab5 can be observed on the phagosome early following phagosome formation (4 min), followed by replacement by Rab7 shortly thereafter (>8 min). Data is presented where 0 min is the timepoint when the bead is first fully engulfed by the macrophage. Arrows demark formation of the phagosome. Data are representative of three independent experiments ( $n = 3$ ). Scale bar is 10  $\mu\text{m}$ .

### 3.3 ERC1 May Facilitate Early Phagosome Maturation

Unpublished work from our lab previously showed that knocking down ERC1 abrogated the delivery of MHC II to phagosomes, suggesting that ERC1 is required for mediating this trafficking pathway. In other cells, ERC1 acts as a docking site for Golgi-derived vesicles on lysosome-derived organelles. Should ERC1 serve a similar purpose in pAPCs, it should be observed being deposited on phagosomal membranes, thereby allowing for the recruitment of MHC II-bearing vesicles originated in the Golgi. To probe this possibility, RAW 264.7 macrophages expressing MHC II-HaloTag were treated with doxycycline and fluorescent HaloTag ligands to induce expression of and label MHC II molecules, respectively. Phagocytosis assays using fluorescent IgG-coated beads were performed, and the cells were fixed at various time points, followed by immunostaining of ERC1 to track the recruitment of ERC1 and newly synthesized MHC II molecules on phagosomes. ERC1 was immediately recruited to phagosomes (30 min to 1 h), followed shortly by the recruitment of MHC II towards ERC1<sup>+</sup> phagosomes (2 h to 4 h). At later timepoints (6 h), ERC1 gradually dissipated while MHC II persisted on phagosomal membranes (**Figure 5**). These results suggest that ERC1 may be involved in early MIIC maturation through the initial recruitment of MHC II to phagosomes.

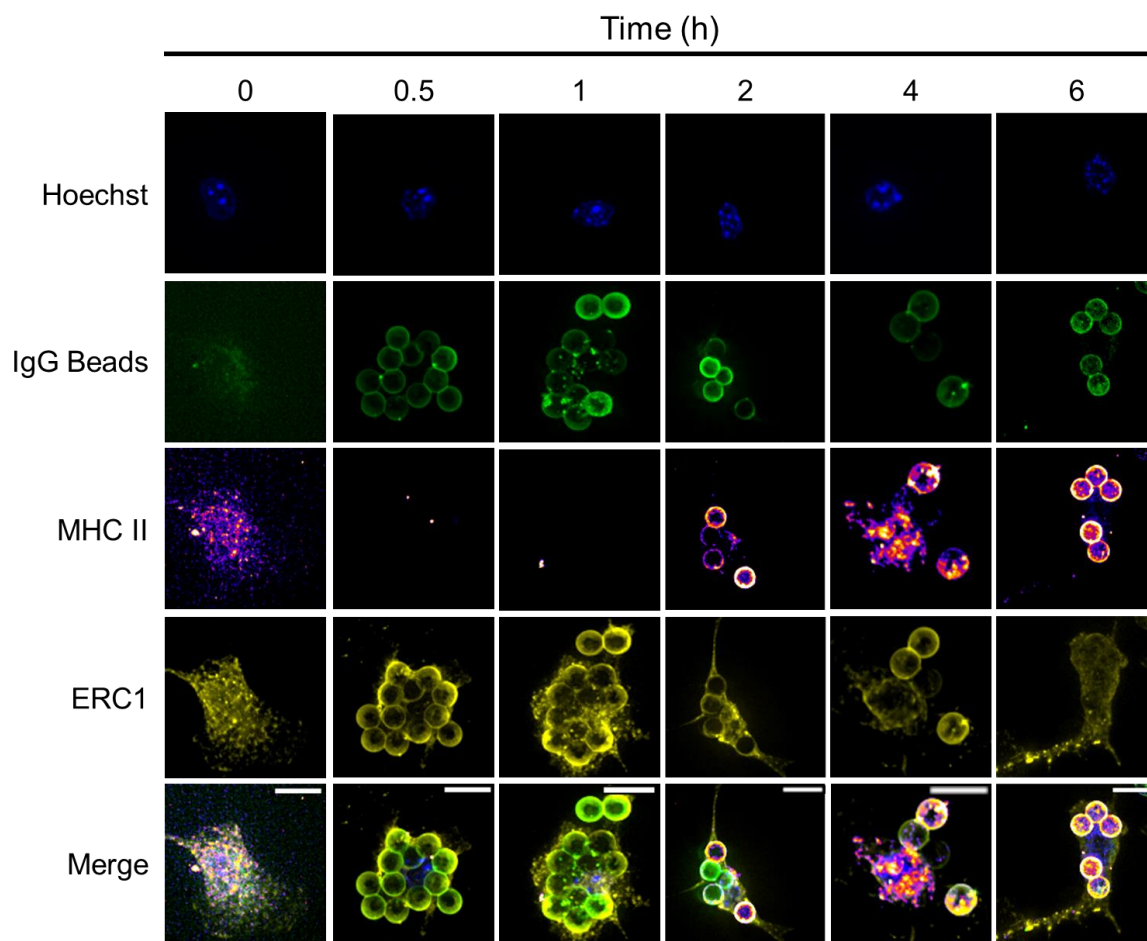


**Figure 5. Recruitment of ERC1 and MHC II to phagosomes.**

Mouse macrophage cell line RAW 264.7 cells expressing MHC II-CD74-HaloTag were treated with doxycycline for 1 h, followed by HaloTag labeling and addition of IgG-coated phagocytic targets (green). Phagocytosis assays were performed at various time points and ERC1 was stained (yellow). Z-stacks were captured using immunofluorescence microscopy and deconvolved in Leica Application Suite X using an iterative blinded deconvolution algorithm. Data are presented as maximum intensity, where 0 min represents the timepoint IgG-coated beads were initially added to macrophage-containing wells. Data is representative of one independent experiment ( $n = 1$ ). Scale bar is 10  $\mu\text{m}$ .

### 3.4 Optimizing RT-qPCR Experiments for Detecting Gene Expression

In addition to intracellular trafficking, MHC II can also be regulated at the level of expression. As such, I needed to develop a method to detect MHC II expression in human primary cells and cell lines. To ensure that we were specifically measuring mRNA levels of our genes of interest, RT-qPCR primer efficiency tests were performed. Briefly, total RNA was extracted from  $1 \times 10^6$  THP-1 cells followed by synthesizing 50 ng cDNA. RT-qPCR was then performed using serial dilutions of cDNA for each primer set to determine whether primers fall within 90-110% efficiency and were suitable for usage in future experiments when I test the effects of SARS-CoV-2 NSP5 on expression of genes in primary human DCs (**Table 2**). In addition, melt curve analyses were performed for primer pairs of each gene of interest to ensure a single, specific RT-qPCR product was produced. Representative melt curves for each gene are shown in **Figure 6**.

**Table 2. RT-qPCR primer sequences used in this study.**

<b>Gene</b>	<b>Sequence</b>	<b>Melting Temperature (°C)</b>	<b>Primer Efficiency (%)</b>
<i>RT-qPCR primers</i>			
CIITA	F: 5'- CTGAAGGATGTGGAAGACCTGGGAAAG-3'	62.5	100.7
	R: 5'- ACCCTCGTCCCCGATCTTGTTCTCACTC-3'	64.5	
MHC II	F: 5'-CGAGTTCTATCTGAATCCTG-3'	55.7	100.9
	R: 5'-GTTCTGCTGCATTGCTTTTGC-3	56.1	
RFX5	F: 5'-TCCTTCAGTTCCATCGTTGAG-3'	54.5	103.0
	R: 5'-TTCAGCTGTCCTCTTGACACC-3'	56.9	
GAPDH	F: 5'-TCAAGGCTGAGAACGGGAAG-3'	57.0	97.3
	R: 5'-CGCCCCACTTGATTTTGGAG-3'	56.7	

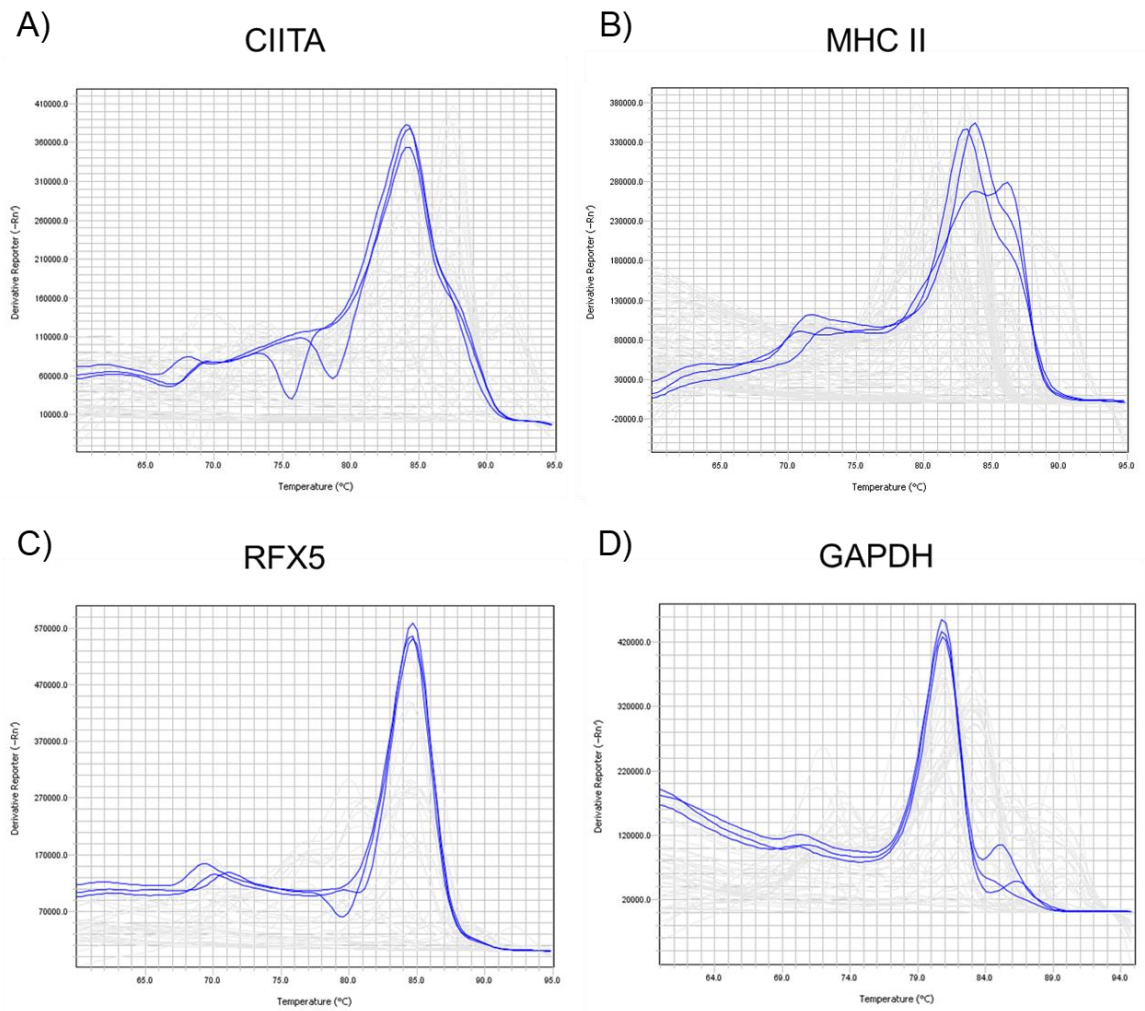


**Figure 6. Representative RT-qPCR primer melt curve plots.**

RNA was extracted from  $1 \times 10^6$  THP-1 monocytes, followed by cDNA synthesis. **A-D)** Serial dilutions of cDNA were used to perform RT-qPCR experiments for 40 amplification cycles to measure the efficiency of primers to detect CIITA (A), MHC II (B), RFX5 (C), and GAPDH (D) mRNA. Melt curve analyses were performed to evaluate the ability of primer pairs to produce single, specific RT-qPCR products for each gene. Data are representative of one independent experiment ( $n = 1$ ).

### 3.5 Validation of Dual Luciferase Assay

To measure the activity of the MHC II and CIITA promoters, dual luciferase vectors were generated containing ~200 bases upstream of the MHC II promoter, CIITA pI, or CIITA pIV cloned into a pGL4 firefly luciferase vector, such that FLuc expression was under control of the cloned promoter. This vector was co-transfected with a pRL-TK regulatory vector that constitutively expresses RLuc, thereby acting as a transfection control. These vectors were validated by seeding  $3 \times 10^5$  HeLa cells onto 12-well tissue culture plates, followed by a 3-day transfection using pGL4 reporter constructs for CIITA pI and MHC II, as well as a promoter-less pGL4 construct to measure any leakiness in the constructs. pRL-TK constructs were also co-expressed in these cells to account for differences in transfection efficiencies between samples. We initially examined whether any differences in CIITA pI and MHC II promoter activity would be observed in response to NSP5 expression. No significant differences in MHC II and CIITA promoter activities were observed between mock-transfected versus NSP5-expressing HeLa cells, as was expected as these cells do not express the transcription factors required for either CIITA (**Figure 7A**) or MHC II (**Figure 7B**) transcription. Through these experiments, I optimized the DNA amount, lysate amount, reagent volume, and incubation times for efficient measurements of FLuc and RLuc luminescence in future experiments using more relevant cell lines.

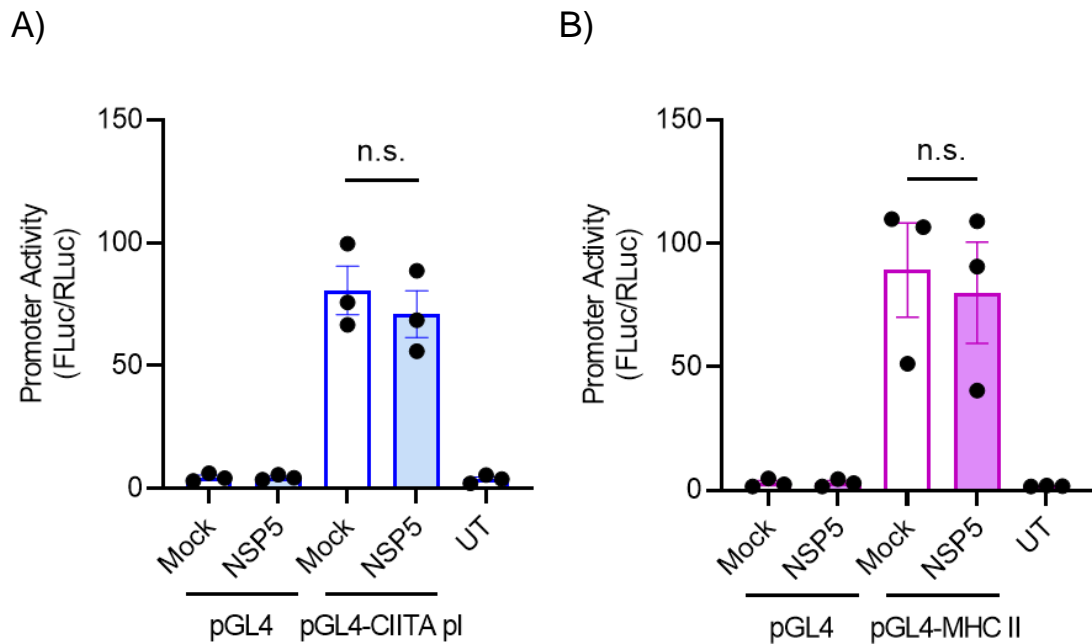


**Figure 7. Dual luciferase analyses of alterations in CIITA pI and MHC II promoter activity by NSP5.**

HeLa cells were co-transfected with NSP5-FLAG and dual luciferase reporter constructs for CIITA pI (pGL4-CIITA pI) or MHC II (pGL4-MHC II), followed by cell harvesting at 72 h post-transfection using passive lysis buffer. Equal volume of protein was used to measure firefly luciferase (FLuc) and renilla luciferase (RLuc) luminescence readings. **A-B)** Promoter activity was calculated by dividing FLuc by RLuc to obtain relative measurements of CIITA pI (A) and MHC II (B) promoter activity in NSP5-expressing versus mock-transfected cells. Data represent mean  $\pm$  SEM obtained from three independent experiments ( $n = 3$ ). Mann-Whitney test, n.s., not significant. UT = untransfected. pGL4 = promoter-less vector control.



Ultimately, these developed tools provide the ability to track MHC II expression and, for the first time, the ability to directly monitor MHC II trafficking in live pAPCs. The MHC II trafficking tools will be co-expressed along with fluorescent markers of the exocytic (Rab3a, Rab8, and Rab27), endocytic (Rab5 and Rab7), recycling (Rab11 and Arf6), and Golgi (Rab6) trafficking pathways, with live-cell imaging of the phagocytosis model allowing for visualization of MHC II as it is transported from the ER/Golgi to phagosomes. Unfortunately, due to the COVID-19 pandemic, I was unable to pursue these experiments further, but I was able to leverage some of these tools to understand how SARS-CoV-2 manipulates antigen presentation on MHC II.

## Chapter 4

### 4 Results – Assessing the Effects of SARS-CoV-2 NSP5 on MHC II Expression

#### 4.1 Introduction

Previous studies have demonstrated that severe infections with SARS-CoV-2 downregulated MHC II expression in pAPCs, and *in vitro* infections in macrophages reduced levels of MHC II surface expression<sup>100,101</sup>. The mechanisms for this suppression remain unknown; however, it may involve epigenetic reprogramming of MHC II expression or manipulation of MHC II trafficking—common mechanisms utilized by pathogens to inhibit antigen presentation and adaptive immune responses. Recent interactome analyses have identified SARS-CoV-2 NSP5 to interact with host HDAC2—an epigenetic regulator of MHC II expression. To gain an idea of how NSP5 may impair host cell responses, our lab generated untagged and FLAG-tagged expression vectors for NSP5.

#### 4.2 Subcellular Localization of NSP5 Provides Clues to Host Function Impairments

I first determined the subcellular localization of NSP5 relative to various organelles using immunofluorescence microscopy of HeLa cells co-transfected with NSP5-FLAG, the Golgi marker GalT-mCherry, the ER marker KDEL-GFP, and stained with anti-FLAG and Hoechst to demark the nucleus. I demonstrated that NSP5 was present in the cytosol, localizing strongly to the nucleus, weakly to the ER, and showing no localization to the Golgi (**Figure 8A**). This strong nuclear localization suggests that NSP5 may possess a

potential function in altering molecular pathways and host responses within the nucleus<sup>120,121</sup>.

To confirm whether NSP5 is indeed localized to the nucleus, HeLa cells expressing FLAG-tagged NSP5 were treated with the nuclear import inhibitor ivermectin. Significant reductions in the fraction of nuclear NSP5 was observed when compared to DMSO-treated cells (**Figures 8B-C**). These results suggested that NSP5 utilizes an importin-mediated trafficking pathway or hijacks a host protein to enter nuclei. Unpublished data from a colleague in the lab showed that NSP5 colocalized with HDAC2 in the nucleus, consistent with previous reports identifying interactions between HDAC2 and NSP5. HDAC2 is a nuclear protein known to function as a regulator of expression of multiple genes through deacetylating histones. The presence of NSP5 on the nucleus suggests that it may interact with HDAC2 to dysregulate target gene expression. Specifically, it is speculated that NSP5 downregulates MHC II and its upstream transcriptional regulators through an HDAC2-mediated mechanism.

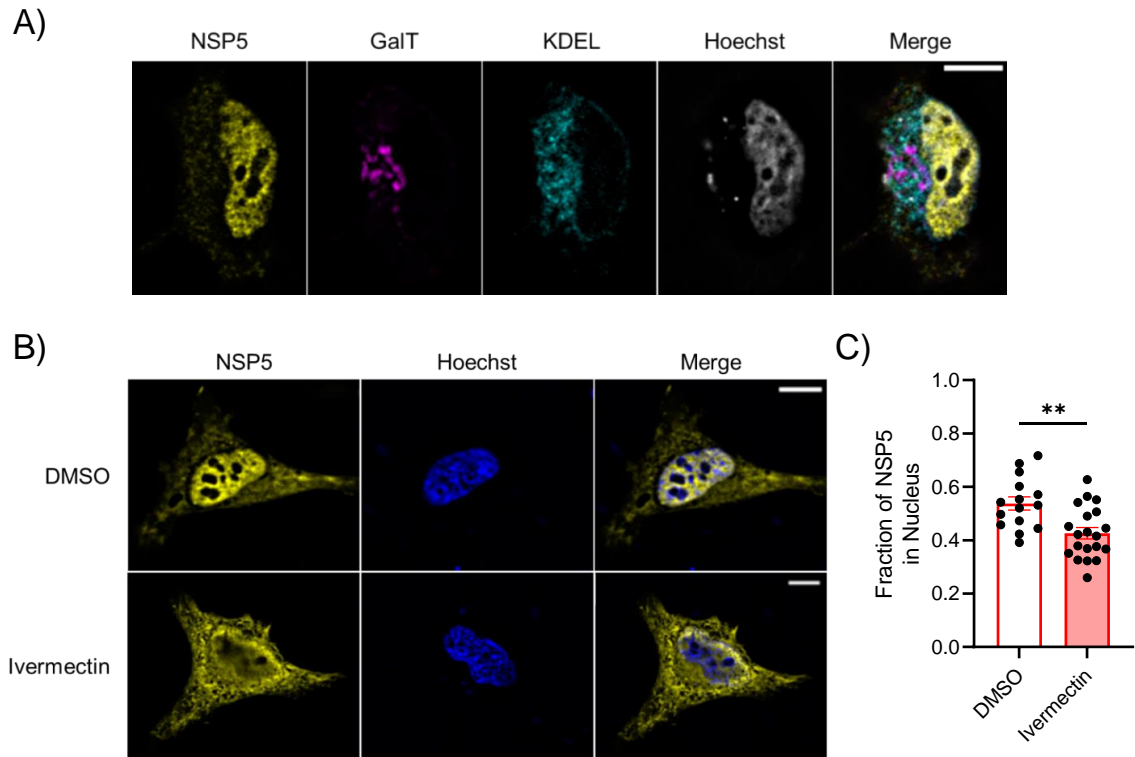


**Figure 8. NSP5 is localized to host nuclei.**

**A)** Visualization of NSP5 subcellular localization. HeLa cells were co-transfected with NSP5-FLAG (yellow), GaIT (magenta), and KDEL (cyan), followed by staining with anti-FLAG and Hoechst (grey). Immunofluorescence imaging was performed to observe the localization of NSP5 relative to fluorescent markers of subcellular organelles. **B)** Representative immunofluorescence microscopy images of NSP5 localization in DMSO- versus ivermectin-treated cells. HeLa cells expressing NSP5-FLAG were treated with 25  $\mu\text{M}$  of ivermectin or DMSO for 90 min, followed by staining with anti-FLAG and immunofluorescence microscopy to observe nuclear localization of NSP5. **C)** Quantification of NSP5 nuclear fraction between DMSO- and ivermectin-treated cells. Data are presented as mean  $\pm$  SEM and are representative of three independent experiments ( $n = 3$ ). Mann-Whitney test, \*\*,  $p < 0.01$ . Scale bar is 10  $\mu\text{m}$ .

### 4.3 NSP5 Downregulates CIITA and MHC II

To investigate whether NSP5 has the capacity to suppress MHC II expression, RAW 264.7 murine macrophages were transduced with empty or NSP5-expressing pLVX-zsGreen lentiviral vectors. Following transduction, plasma membranes were stained using wheat germ agglutinin (WGA), and immunofluorescence microscopy compared differences in MHC II expression in these two samples (**Figures 9A-B**). Analysis of transduced zsGreen<sup>+</sup> cells demonstrated that expression of MHC II was significantly reduced in NSP5-expressing cells (**Figure 9C**). To probe the possibility that this reduction in MHC II expression is due to NSP5-mediated alterations in MHC II trafficking, the proportion of surface MHC II versus cytosolic MHC II was measured based on colocalization with WGA. We observed no significant differences between surface MHC II levels in both samples (**Figure 9D**), suggesting that NSP5 downregulates MHC II independent of mis-trafficking molecules away from the cell surface.

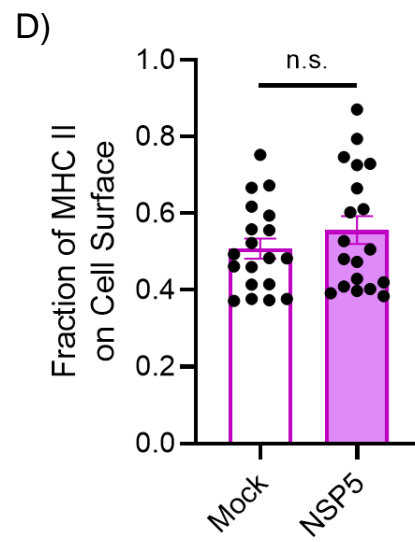
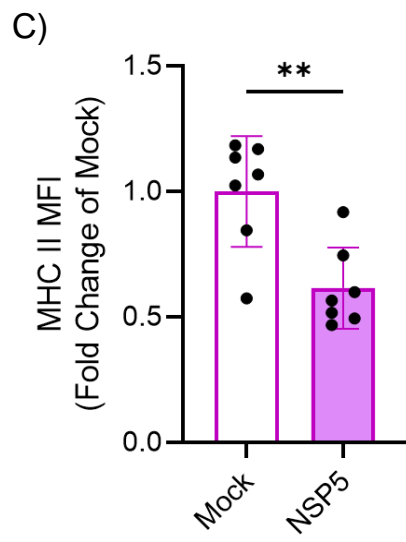
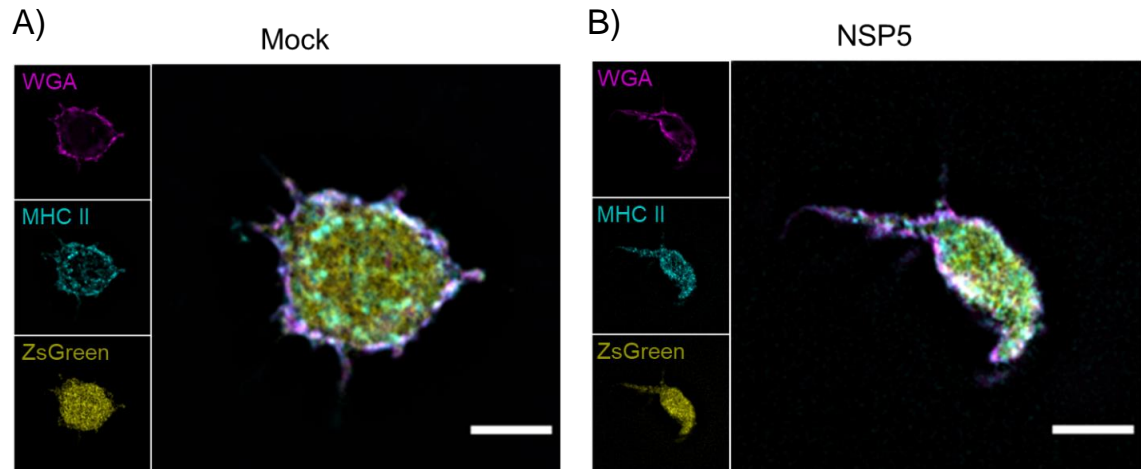


**Figure 9. NSP5 reduces MHC II expression independent of altering membrane trafficking.**

RAW 264.7 macrophages were transduced with empty (Mock) or NSP5-expressing (NSP5) lentiviral vectors for 72 h and stained with anti-MHC II and the plasma membrane marker wheat germ agglutinin (WGA). **A-B**) Immunofluorescence microscopy was performed to detect MHC II expression and localization in mock infected (A) versus NSP5-expressing (B) macrophages. **C**) Quantification of mean fluorescence intensity (MFI) of MHC II in mock infected versus NSP5-expressing cells. Data is normalized to mock samples. **D**) Quantification of the fraction of surface MHC II between mock infected versus NSP5-expressing cells. WGA was used to demark plasma membranes and determine the proportion of MHC II on the cell surface relative to the cytosol. Images were captured on an epifluorescence microscope at 100 × magnification and deconvolved in Leica Application Suite X using an iterative blinded deconvolution algorithm. Data are presented as mean ± SEM and are representative of three independent experiments (n = 3). Mann-Whitney test, \*\*,  $p < 0.01$ ; n.s., not significant. Scale bar is 10 μm. Data courtesy of Brandon Dickson.

In addition to mis-trafficking MHC II molecules, some pathogens limit antigen presentation by suppressing MHC II expression. I sought to measure the mRNA levels of MHC II, CIITA, and RFX5 in NSP5-expressing primary human DCs, as expression of these genes were observed to be downregulated in patients with COVID-19. Briefly, primary DCs were transduced with empty or NSP5-expressing pLVX-zsGreen lentiviral vectors, followed by IFN $\gamma$  stimulation to induce CIITA and MHC II expression. Cells were then sorted based on expression of zsGreen via fluorescence activated cell sorting (FACS) to ensure measurements of gene expression were conducted in transduced cells only. Following RNA isolation and cDNA synthesis, CIITA and MHC II mRNA levels were measured using RT-qPCR, with expression of these genes significantly reduced in NSP5-expressing cells (**Figure 10**), suggesting that NSP5 expression is sufficient to suppress CIITA and MHC II expression. This reduction was not observed in RFX5, with no significance differences in mRNA levels between NSP5- and empty vector-transduced cells, suggesting that the antagonistic effect of NSP5 on CIITA and MHC II transcription is not caused via global suppression of gene expression but, instead, involves selective targeting of the CIITA and MHC II genes.



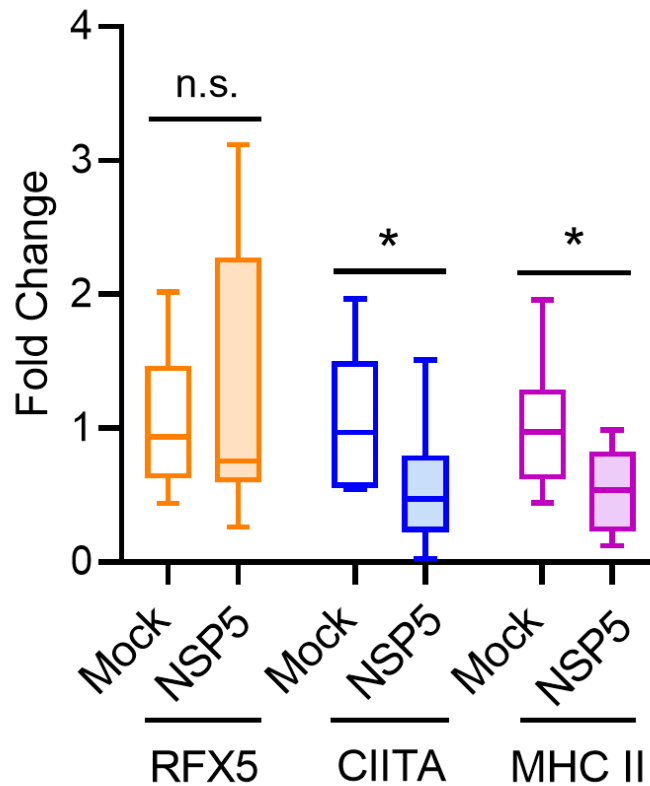


**Figure 10. RT-qPCR quantification of RFX5, CIITA, and MHC II expression.**

Human primary dendritic cells were infected with empty zsGreen (Mock) or NSP5-zsGreen (NSP5) lentiviral vectors for 72 h and treated with IFN $\gamma$  for 24 h. zsGreen<sup>+</sup> cells were sorted via FACS followed by RNA extraction and cDNA synthesis. RFX5 (orange), CIITA (blue), and MHC II (pink) mRNA levels were quantified by RT-qPCR reactions performed for 40 amplification cycles using a constant amount of cDNA (50 ng). Data are presented on a box-and-whisker plot, with the median, maximum, minimum, and quartiles shown. Data are relative to GAPDH mRNA expression and normalized to mock (empty vector-transduced) samples. Data are obtained from four independent experiments (n = 4). Mann-Whitney test, \*, p < 0.05; n.s., not significant.

## 4.4 NSP5 Inhibits MHC II and CIITA Promoter Activity

While RT-qPCR analysis confirmed downregulation of MHC II and CIITA by NSP5, the mechanisms by which NSP5 suppresses these genes remain unknown. To address this question, I investigated whether NSP5 inhibits the activity of MHC II and CIITA promoters. RAW 264.7 macrophages were co-transfected with NSP5, a FLuc construct controlled by an MHC II or CIITA promoter, and a regulatory pRL-TK vector expressing constitutive RLuc. Macrophages were then lysed and harvested, and a dual luciferase assay was performed to measure the effects of NSP5 on MHC II and CIITA promoter activities. Measurements of FLuc and RLuc luminescence levels demonstrated that both CIITA pI (**Figure 11A**) and MHC II (**Figure 11B**) promoter activities were significantly inhibited in NSP5-expressing macrophages compared to macrophages transfected with an empty lentiviral vector. In contrast, CIITA pIV—the promoter expressed by non-hematopoietic cells—was minimally active in these cells, and NSP5 had no measurable impact on activity of this promoter (**Figure 11C**). These data indicate that the altered MHC II expression mediated by NSP5 occurs through inhibition at the level of CIITA promoter I activity specifically.

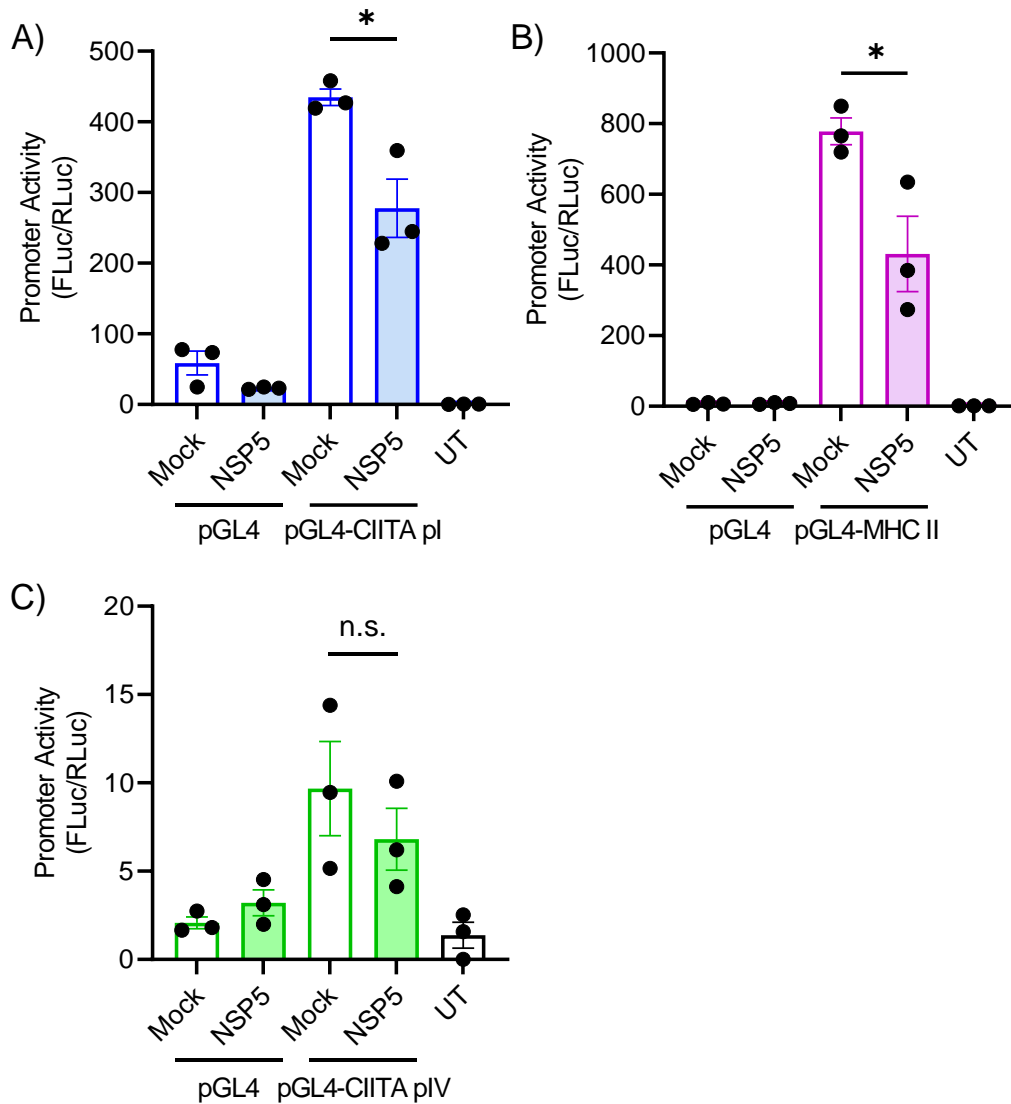


**Figure 11. NSP5 inhibits CIITA pI and MHC II promoter activity but not CIITA pIV activity.**

**A-C)** Promoter activity was quantified in RAW 264.7 macrophages co-transfected with NSP5-FLAG and dual luciferase reporter constructs of the CIITA pI (A), MHC II (B), or CIITA pIV (C) promoters. Promoter activity is relative to RLuc. Data are representative of mean  $\pm$  SEM obtained from three independent experiments ( $n = 3$ ), with duplicate samples analyzed in each experiment. Mann-Whitney test, \*,  $p < 0.05$ ; n.s., not significant. UT = untransfected. pGL4 = promoter-less vector control.

## 4.5 HDAC2 Knockdown Restores CIITA and MHC II Expression

While I demonstrated that expression of NSP5 is sufficient to downregulate MHC II and CIITA expression at the levels of both mRNA and promoter activity, it remains unknown how NSP5 manipulates this pathway. Previous studies identified interactions between SARS-CoV-2 NSP5 and human HDAC2, which is known to repress CIITA and MHC II expression via deacetylation of the histone tails. To elucidate the role of NSP5 in this pathway, HDAC2 was knocked down in NSP5-expressing DCs using siRNA to assess the resulting effects on MHC II and CIITA expression. Western blot was performed to confirm knockdown of HDAC2 (**Figure 12A**). RT-qPCR analysis demonstrated that when compared to cells treated with non-targeting siRNA, HDAC2 knockdown restored expression of CIITA (**Figure 12B**) and MHC II (**Figure 12C**) in human DCs despite the presence of NSP5. To further investigate the effects of NSP5 on MHC II and CIITA transcription, a dual luciferase assay was performed to measure differences in promoter activity of these genes in NSP5<sup>+</sup>/HDAC2<sup>-</sup> RAW 264.7 macrophages. While knocking down HDAC2 rescued CIITA pI activity by almost 2-fold (**Figure 12D**), this effect was not observed on the MHC II promoter regardless of whether HDAC2 is present or absent (**Figure 12E**). It is unclear why there is a disparity between MHC II promoter activity and mRNA levels in the presence of NSP5, but this discordance may be due to the absence of distal regulatory sites in the MHC II promoter that are known to be required for de-silencing of the MHC II loci<sup>13</sup>. Altogether, these results suggest that downregulation of MHC II and CIITA can be reverted by preventing NSP5 from targeting HDAC2.

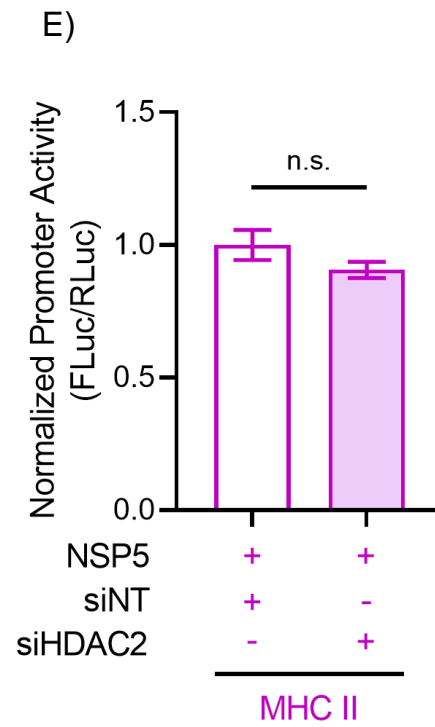
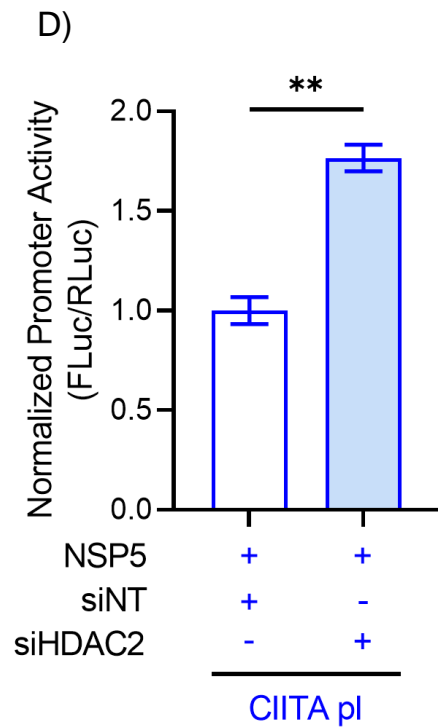
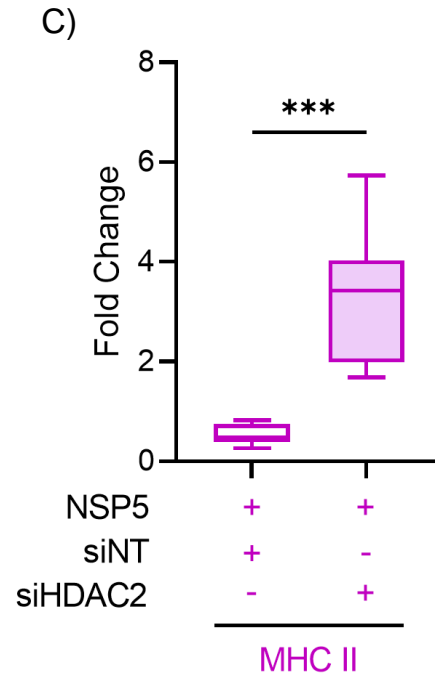
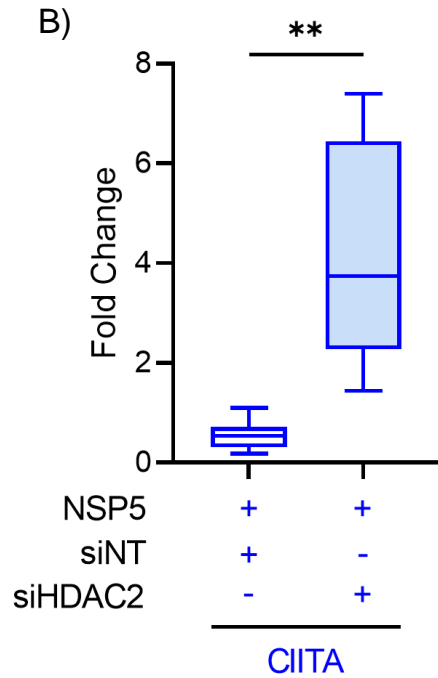
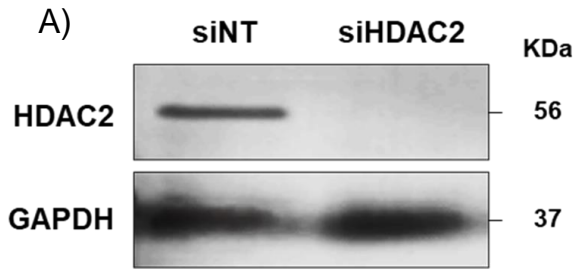


**Figure 12. HDAC2 knockdown reverts the effects of NSP5 on CIITA and MHC II expression.**

**A)** Detection of HDAC2 knockdown. Human primary DCs were treated with HDAC2-targeting siRNA (siHDAC2) or non-targeting siRNA (siNT) for 96 h. Western blot analysis was performed to confirm HDAC2 knockdown in siHDAC2-treated cells. GAPDH was used as a housekeeping gene to confirm equal loading. **B-C)** RT-qPCR quantification of CIITA (**B**) and MHC II (**C**) expression in HDAC2 knockdown human primary DCs. Cells were infected with lentiviral vectors expressing NSP5-zsGreen for 72 h, followed by treatment with IFN $\gamma$  and siRNA for 24 h and 96 h, respectively. mRNA levels were quantified by RT-qPCR reactions performed for 40 amplification cycles using a constant amount of cDNA (50 ng) and are relative to GAPDH mRNA expression. Data are presented on a box-and-whisker plot outlining the median, maximum, minimum, and quartiles. **D-E)** Dual luciferase analysis of CIITA pI (**D**) and MHC II (**E**) promoter activity in HDAC2-deficient macrophages. Promoter activity was quantified in HDAC2-knockdown RAW 264.7 macrophages co-transfected with NSP5-FLAG and dual luciferase reporter constructs of the CIITA pI or MHC II promoters. Promoter activity is relative to RLuc and normalized to siNT. Data are representative of mean  $\pm$  SEM obtained from a minimum of three independent experiments. Mann-Whitney test, \*\*,  $p < 0.01$ ; \*\*\*,  $p < 0.001$ ; n.s., not significant.

## 4.6 Inactivating NSP5 Proteolytic Activity Has No Effect on CIITA and MHC II Expression

NSP5 is comprised of three domains: a catalytic domain comprised of two globular domains (A and B) which form a catalytic dimer at the core of which are the catalytic residues H41 and C145, and a C-terminal domain (B') which functions to stabilize interactions between the catalytic site and target peptides. We generated deletion mutants of the catalytic A/B and B' domains, as well as point mutations of these two critical residues (H41A and C145S) to probe whether the catalytic function of NSP5 is responsible for altering HDAC2 activity and suppressing MHC II and CIITA expression (**Figure 13A**). While the point mutants expressed well, minimal expression of the deletion mutants was observed, precluding further analysis of these mutants.

RAW 264.7 macrophages expressing dual luciferase reporter constructs for MHC II and CIITA pI were transfected with either wildtype (WT) NSP5 or with the NSP5 point mutants, and then promoter activity was measured. Unexpectedly, inactivation of the catalytic sites had no observable effect on the expression of CIITA (**Figure 13B**) and MHC II (**Figure 13C**).

Previous computational studies predicted that NSP5 may proteolytically cleave HDAC2 near its nuclear localization signal, thereby preventing its nuclear translocation and function. We showed via immunofluorescence microscopy analysis that the catalytically inactive NSP5 mutants failed to alter the localization of HDAC2 when compared to WT NSP5 (**Figure 13D**). These results suggest that NSP5 suppresses CIITA and MHC II expression independent of its proteolytic function or manipulation of HDAC2 localization.

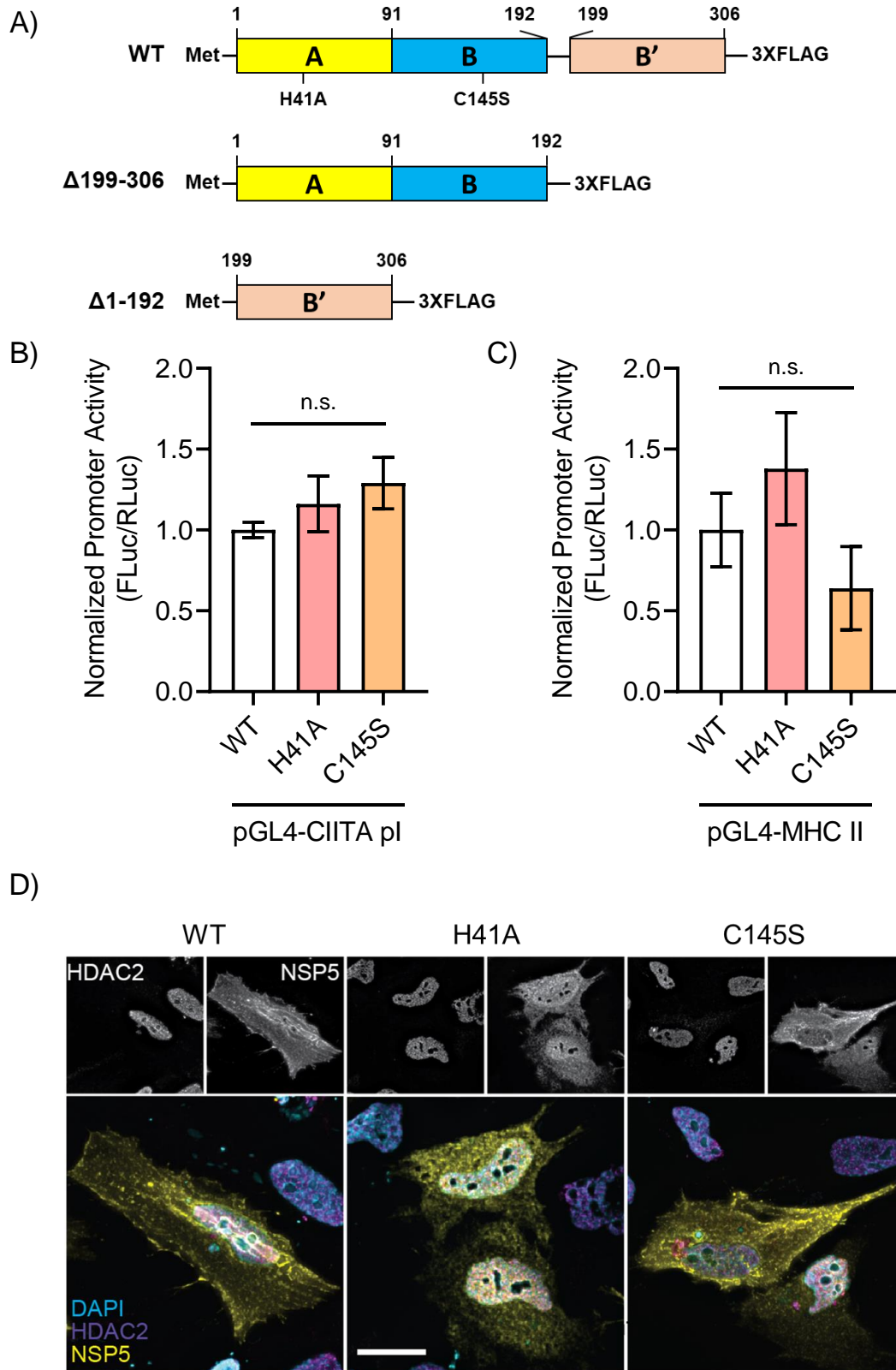




**Figure 13. Analysis of NSP5 point mutations on CIITA pI and MHC II promoter activity.**

**A)** Overview of NSP5 mutations. Wildtype (WT), deletion mutations of the N- ( $\Delta 1-192$ ) and C-terminal ( $\Delta 199-306$ ), and point mutations (H41A, C145S) on the catalytic site of NSP5 were generated to assess their effects on CIITA and MHC II expression. **B-C)** Dual luciferase analysis of CIITA pI (B) and MHC II (C) promoter activity in RAW 264.7 macrophages transfected with NSP5<sup>WT</sup>, NSP5<sup>H41A</sup>, or NSP5<sup>C145S</sup>. Promoter activity is relative to RLuc and normalized to WT. **D)** Immunofluorescence microscopy analysis of NSP5 mutants' subcellular localization. Z-stacks were captured on an epifluorescence microscopy at 100 $\times$  magnification and deconvolved in Leica Application Suite X using an iterative blinded deconvolution algorithm. Data are representative of three independent experiments (n = 3). Kruskal-Wallis test, n.s., not significant. Scale bar is 10  $\mu$ m. Panel D is courtesy of Peter Guo.

## 4.7 HDAC2 Expression is Unaltered by NSP5

While it has not been established that HDAC2 can be activated via cleavage, other HDACs have been shown to be cleaved at the C-terminus, leading to their activation and localization to the nucleus where they can silence expression of target genes<sup>122,123</sup>. As NSP5 primarily functions as a cysteine protease via cleavage of the SARS-CoV-2 polyprotein shortly after viral entry and translation in the host cytosol, NSP5 was speculated to alter HDAC2 activity via cleavage. While previous results showed that inactivating the proteolytic function of NSP5 did not restore MHC II and CIITA expression, western blot analyses were performed to probe the possibility that HDAC2 is proteolytically processed in the presence of NSP5. Should NSP5 cleave HDAC2 at the predicted location, HDAC2 would undergo a ~10 kDa decrease in its apparent mass or, alternatively, may be targeted for proteasomal degradation and, thus, decreasing its abundance. I did not observe the appearance of a lower-mass band indicative of HDAC2 cleavage nor were there any differences in HDAC2 expression between mock-transfected and NSP5-expressing cells (**Figure 14**). Therefore, these results confirmed that the effect of NSP5 on the MHC II transcriptional machinery is independent of HDAC2 cleavage but may involve other post-translational modifications or altered protein targeting that modulate HDAC2 enzymatic activity at the CIITA and MHC II promoters.

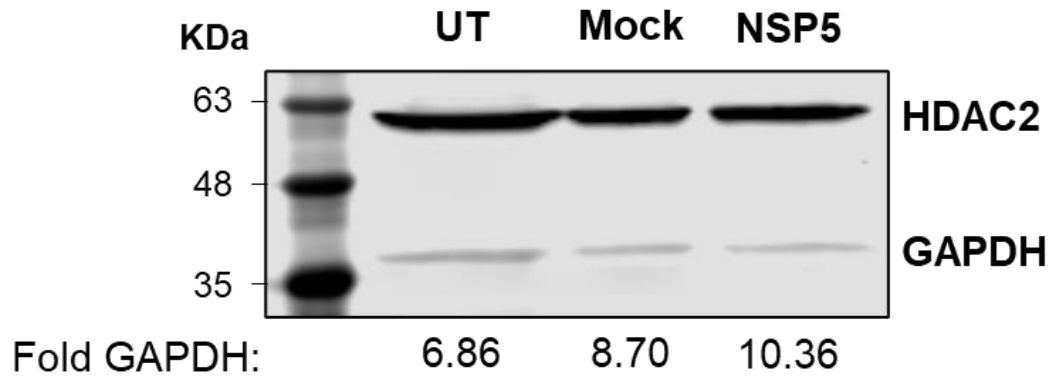


**Figure 14. Western blot analysis of HDAC2 cleavage.**

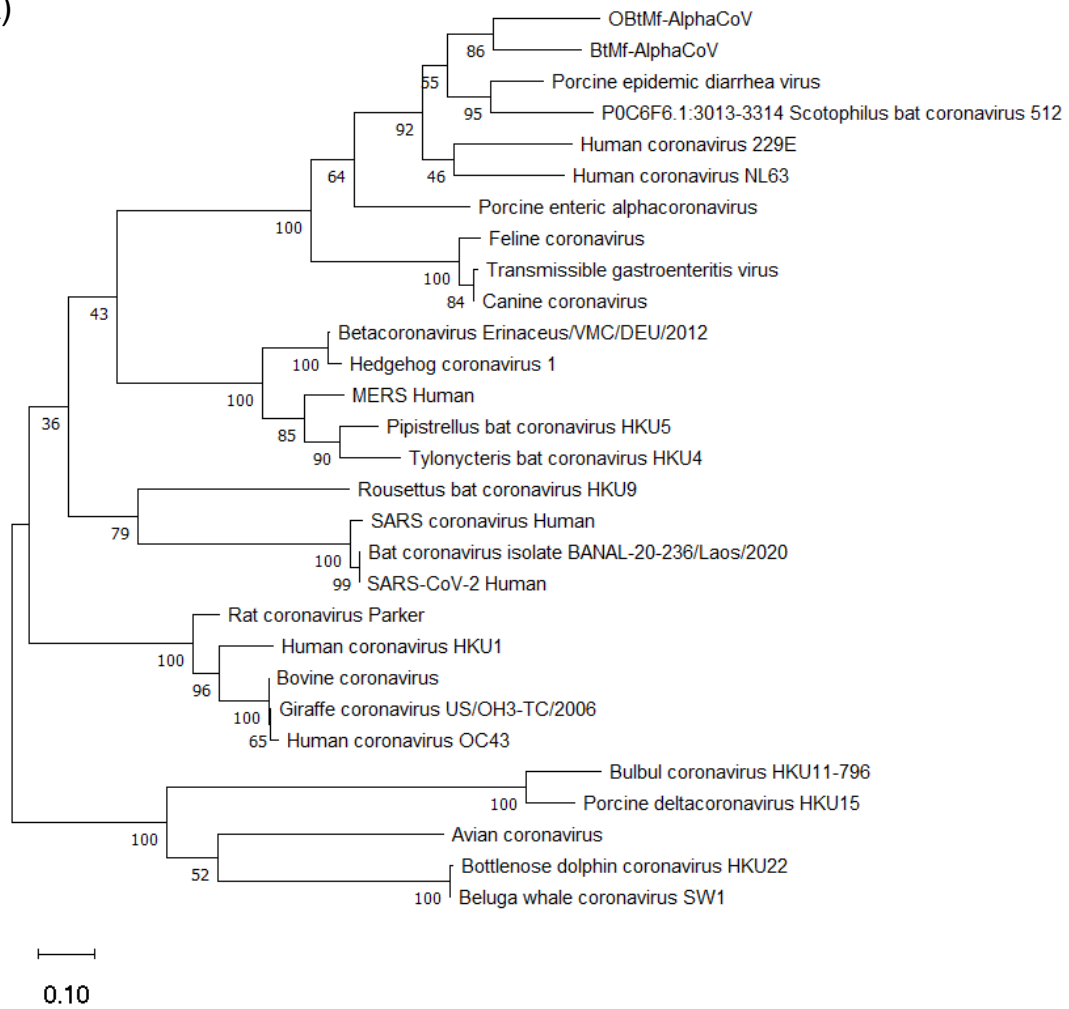
HeLa cells were transfected with empty (Mock) or NSP5-expressing (NSP5) lentiviral vectors, or were left untransfected (UT), for 72 h followed by lysis. Protein lysates were added to 10 % acrylamide gel at an equal volume. Western blot analysis compared differences in HDAC2 expression between samples. GAPDH was used as a housekeeping gene to normalize protein loading.

## 4.8 NSP5-Mediated Modulation of HDAC2 May Be Shared Between SARS-CoV-2 and Other Related Bat Coronaviruses

While our findings suggest that SARS-CoV-2 has the capacity to impair immune responses in humans through NSP5-mediated downregulation of MHC II expression, it remains poorly understood why a virus that likely originated in bats would have this specific effect on HDAC2 in human pAPCs. There are two possible explanations for this phenomenon: either HDAC2 is sufficiently conserved between humans and bats to preserve the NSP5 activity between species, or alternatively, NSP5 itself is highly conserved across *coronaviridae*, thereby mediating similar phenomena across host species. To address these possibilities, a phylogenetic tree was generated using protein sequences of NSP5 expressed by coronaviruses representative of the four major *coronaviridae* clades, including members known to infect bats and humans. NSP5 protein sequences are identical not only between SARS-CoV-2 and the original SARS-CoV but also with the bat coronavirus isolate, BANAL-20-236, which was recently identified as a potential link to the progenitor bat coronavirus prior to zoonotic transmission in humans (**Figure 15A**)<sup>74</sup>. Otherwise, NSP5 was highly diverse across the *coronaviridae* family. Likewise, a second phylogenetic tree was generated using protein sequences of HDAC2 from multiple species. HDAC2 was found to be extremely conserved across vertebrates, with less than 1 % protein sequence differences observed between species, including across multiple bat species (**Figure 15B**). Ultimately, although SARS-CoV-2 likely originated in bats, the high conservation of HDAC2 between bats and humans suggests that SARS-CoV-2 and its bat progenitor virus may utilize a similar mechanism involving NSP5 to impair adaptive immune responses. Unfortunately, bats are inherently tolerant to

viral infections compared to humans, allowing for them to act as viral reservoirs and transmit viruses without straining their immune systems<sup>124</sup>.

A)





## Chapter 5

### 5 Discussion

#### 5.1 Hypotheses and Answers

In this thesis, I tested the hypothesis that phagosome-derived TLR signaling activates ERC1 to facilitate the delivery of newly synthesized MHC II molecules via a direct Golgi-to-MIIC trafficking pathway. While it remains unclear which trafficking pathway is responsible for delivering MHC II to phagosomes, immunofluorescence microscopy and phagocytosis assays utilizing the inducible MHC II-HaloTag reporter demonstrated that ERC1 is likely involved in this process based on the recruitment of MHC II to ERC1-bearing phagosomes shortly after phagocytosis.

I also tested the hypothesis that SARS-CoV-2 NSP5 suppresses MHC II expression via interactions with HDAC2. Critically, I determined that NSP5 is capable of suppressing MHC II expression, and this suppression is mediated by HDAC2-dependent inhibition of CIITA and MHC II transcription. RT-qPCR and dual luciferase analyses of human primary DCs and cell-line macrophages showed that the presence of NSP5 reduced MHC II and CIITA expression at the level of mRNA and promoter activity. Additionally, RNA silencing of HDAC2 reverted expression of MHC II and CIITA despite the presence of NSP5, suggesting that HDAC2 is a necessary component for SARS-CoV-2-mediated antagonism of this pathway. While HDAC2 is not directly involved in the IFN $\gamma$  signaling pathway, it is a major regulator of several components of the MHC II antigen presentation pathway, specifically by repressing CIITA and MHC II expression. Our findings implicate NSP5 as a biological activator of HDAC2 to downregulate CIITA and



MHC II, leading to impaired adaptive immune responses in infected individuals. Critically, I identified HDAC2 as a potential target for preventing SARS-CoV-2 infections from overwhelming patients' immune system, as its inhibition may outright block viral access to the MHC II transcriptional machinery, thereby restoring host immune responses.

## 5.2 Rationale of Thesis

The investigation into MHC II trafficking pathways was based on several key findings. Firstly, our lab previously discovered the presence of ERC1 and Rab6 on phagosomal membranes of macrophages. Based on the literature, these proteins are major regulators of Golgi export pathways and have been shown to facilitate the delivery of Golgi-derived vesicles to target organelles in other cell types<sup>51,125</sup>. Lastly, unpublished data from our lab demonstrated that knocking down ERC1 with shRNA abrogates the delivery of MHC II to MIICs. Based on these findings, we postulated that ERC1 is involved in delivering MHC II directly to MIICs through an uncharacterized trafficking pathway. Should we observe this phenomenon, it would resolve the 2-decade-old controversy surrounding the pathways responsible for intracellular MHC II trafficking. Investigating the components required for delivering MHC II to its designated location, either the phagosome or cell surface, is important not only from a mechanistic perspective but is also crucial for understanding how pathogens can evade host immunosurveillance. Many pathogens can prevent the generation of adaptive immune responses by redirecting MHC II molecules away from the cell surface. By identifying the regulators involved in transporting MHC II

for antigen presentation, we can target these components and prevent pathogens from hijacking molecular pathways and ensure that immune responses are mounted.

SARS-CoV-2 is one such pathogen capable of dysregulating CD4<sup>+</sup> T cell-mediated responses despite these adaptive immune cells' role in controlling infections. While macrophages and DCs are capable of being infected by SARS-CoV-2, these infections are generally non-productive and do not drive production of pro-inflammatory cytokines<sup>126</sup>. However, the resultant effects of these infections on these innate immune cells may still have profound immunological impacts in patients. Normally, macrophages and DCs play a major role in presenting pathogen-derived peptides on MHC II to CD4<sup>+</sup> T cells, leading to CD4<sup>+</sup> T cell activation that initiates effector functions to reduce viral spread. For example, activated CD4<sup>+</sup> T cells can differentiate into T follicular helper (Tfh) cells that play a protective role by activating B cells to produce neutralizing antibodies against foreign SARS-CoV-2 antigens<sup>125,126</sup>. However, Tfh cell differentiation and germinal centers have been observed to be diminished in patients with severe COVID-19, attributing to short-lived and reduced humoral responses. Likewise, the Th1 responses crucial for mediating cell-mediated responses are depleted while Th2 responses are overreactive in COVID-19 patients, potentially leading to non-productive T cell activation and exhaustion<sup>127,128</sup>. Consequently, these non-functional T cell responses enable the virus to propagate in our airways and continually infect cells. SARS-CoV-2 proteins, such as ORF6 and ORF8, can then further inhibit antiviral responses and mediate non-productive secretion of proinflammatory cytokines<sup>77,78</sup>. This combination of reduced viral clearance by effector T cells and antibodies along with excessive production of pro-inflammatory cytokines can exacerbate inflammatory responses,

ultimately leading to the hallmark cytokine storm and multiorgan failure associated with COVID-19<sup>129</sup>.

How SARS-CoV-2 facilitates these host defense defects remains unknown, but we speculate that downregulation of MHC II in infected pAPCs is an underlying factor. Many studies demonstrated that infections with SARS-CoV-2 reduced MHC II levels in COVID-19 patients' pAPCs, suggesting that virulence factors expressed by SARS-CoV-2 may be responsible for mediating this immunoevasion<sup>78,102,130</sup>. Blocking MHC II access to the surface is a common strategy utilized by pathogens to escape host immune responses. While multiple pathogens utilize different virulence factors to target and inhibit the MHC II antigen presentation pathway, these mechanisms all revolve around either one of two strategies. The first strategy is the redirection of MHC II trafficking away from the cell surface. For example, HSV type 1 glycoprotein B hijacks the MHC II trafficking pathway by binding to and confining MHC II molecules to subcellular vesicles, thereby preventing their association with exogenous peptides<sup>131,132</sup>. Likewise, infections with *Salmonella Typhimurium* abrogates antigen presentation of DCs by inducing polyubiquitination of MHC II, thereby promoting the internalization and degradation of surface MHC II molecules through endosomal proteases<sup>133,134</sup>. The second strategy pathogens use to block antigen presentation is the antagonism of MHC II transcription. For example, infections with *Leishmania donovani* selectively inhibits transcription of MHC II genes through a cyclic AMP-dependent manner<sup>135</sup>. Moreover, Epstein-Barr virus transactivator protein Zta represses CIITA pIII activity in infected B cells, resulting in reduced MHC II expression<sup>136</sup>.

Our investigation into how SARS-CoV-2 suppresses antigen presentation is based on a key finding from the literature identifying NSP5 to interact with HDAC2, implicating a potential mechanism by which SARS-CoV-2 blocks MHC II expression. We proposed that SARS-CoV-2 utilizes NSP5 to antagonize the MHC II transcriptional machinery. I demonstrated that the presence of NSP5 decreased levels of MHC II transcription and that HDAC2 knockdown reverted this suppressed phenotype. Furthermore, immunofluorescence microscopy showed no reductions in the proportion of surface MHC II levels in NSP5-expressing cells compared to mock-infected cells, precluding the possibility that the decreased levels of MHC II is via NSP5-mediated manipulation of vesicular trafficking pathways to prevent MHC II from reaching the cell surface.

### 5.3 TLR and FcγR Signaling Activates ERC1 to Regulate MHC II Trafficking

While the controversy surrounding MHC II trafficking to phagosomes has existed for over two decades, our findings suggest that ERC1 is a major regulator of this process. Previous data showed that ERC1 is recruited to phagosomes during early stages of maturation preceding the recruitment of MHC II, and ERC1 silencing abrogates the formation of MIICs in macrophages. In this thesis, I demonstrated that newly synthesized MHC II is recruited directly to ERC1-bearing phagosomes, further supporting the role of ERC1 in mediating this trafficking pathway.

Previous studies into MHC II trafficking were limited, in the sense that they lacked the molecular tools required to visualize the intracellular movement of MHC II. In fact, most prior studies relied on either immunofluorescence microscopy of fixed cells, or on broad-

spectrum inhibitors of the trafficking pathways, thereby incurring several limitations<sup>137,138</sup>. Interpretation of fixed-cell images can be highly biased based on the timepoints where cells are fixed and analyzed. For example, some of the studies taking this approach looked at long timepoints following induction of MHC II signaling (6 hours or longer)—long enough for mature MHC II to both reach the cell surface and be re-internalized as part of normal membrane protein recycling<sup>137,139</sup>. A more recent study has shown that a significant portion of endocytosed MHC II molecules are targeted for degradation rather than transported to the MIIC<sup>140</sup>. Likewise, inhibitor-based studies can be difficult to interpret. For example, endocytosis inhibitors will not only impair the endocytosis of MHC II but also of small antigens, with some even interfering with phagocytosis<sup>32,37,141–143</sup>. Thus, in these studies, alterations in the formation of the MIIC may result from a failure to engulf antigens rather than from selective blocking of the endocytic route of MHC II delivery. By developing a live-cell-compatible MHC II trafficking reporter, we will be able to visualize the trafficking process as it occurs. Moreover, as this system is inducible, MHC II expression can be decoupled from other stimuli and from the use of inhibitors, therefore avoiding some of the issues faced by prior studies.

While it was initially predicted that TLR signaling would activate ERC1 to facilitate the delivery of MHC II to phagosomes, our data showed that ERC1 is recruited to phagosomes through FcγR-mediated phagocytosis of IgG-coated beads, suggesting that the potential effect of ERC1 on MHC II trafficking is independent of the canonical TLR-mediated NFκB activation pathway. However, while it has not been established whether FcγR-mediated phagocytosis can induce NFκB activation, a previous study has shown

that treatment with IgG-coated beads reduced levels of I $\kappa$ B $\alpha$  and reduced cytosolic sequestration of NF $\kappa$ B in bone marrow-derived macrophages<sup>144</sup>. Indeed, Fc $\gamma$ R signaling can activate mitogen-activated protein kinases, which in turn can activate NF $\kappa$ B via Syk kinase<sup>145</sup>. Likewise, stimulation of Fc $\gamma$ R in THP-1 macrophages using human IgG was observed to be sufficient to degrade I $\kappa$ B $\alpha$  and activate NF $\kappa$ B<sup>146</sup>. Our data are consistent with these findings, as we demonstrated that ERC1 is recruited to phagosomes when using either IgG-coated beads or fluorescently labeled bacteria. Ultimately, these results suggest that both Fc $\gamma$ R-mediated and TLR-mediated signaling are capable of activating ERC1, allowing for ERC1 to modulate the trafficking of newly synthesized MHC II molecules to MIICs.

In addition to regulating the delivery of MHC II to the MIIC, ERC1 may also be involved in regulating MHC II expression. While IFN $\gamma$  is required for inducing expression of MHC II, NF $\kappa$ B activation is required for maximal MHC II expression downstream of TLR4 and TLR9, with NF $\kappa$ B potentially driving CIITA-independent transcription of MHC II genes in macrophages<sup>69,147</sup>. Given the central role of ERC1 in regulating NF $\kappa$ B activation via assembly of the IKK complex, it is quite possible that knockdown of ERC1 will not only impair MHC II delivery to the MIIC but may also reduce or eliminate MHC II expression in response to phagocytosed pathogens. The RT-qPCR and dual luciferase assays developed in this thesis will enable us to study this pathway in depth, while the inducible MHC II-HaloTag reporter will allow us to study the effects of ERC1 knockdown on MHC II trafficking without imparting any effects on endogenous MHC II.

## 5.4 NSP5-HDAC2-CIITA-MHC II Axis

In this thesis, I identified a novel function of SARS-CoV-2 NSP5 outside of its role in viral replication, wherein it alters host immune responses by inhibiting MHC II and CIITA transcription. How NSP5 antagonizes expression of these genes is still up to debate, but we have shown that HDAC2 is likely involved in this process, as it is a known epigenetic regulator of MHC II and CIITA. While it is well established that HDACs regulate a vast repertoire of cellular activities through eukaryotic gene regulation, it remains poorly understood how these proteins themselves are regulated. For example, while HDAC3 and HDAC4 are known to be cleaved at the C-terminal, the effect of this post-translational modification is unclear. One study observed that caspase-dependent cleavage degrades HDAC4, while another study implicates HDAC4 activity is increased upon cleavage by the same caspases<sup>123,148</sup>. Likewise, while both HDAC1 and HDAC4 are known to undergo SUMOylation that potentiates their biological activity, it is unclear how their stability and expression is modulated<sup>149–151</sup>. Finally, there are no reports of HDAC2 cleavage being linked to increased activity.

In fact, NSP5 is predicted to have a cleavage site on HDAC2 that would prevent its nuclear transport and ability to attenuate inflammatory responses<sup>105,110</sup>. Other computational studies predict that blocking HDAC2 nuclear localization is cleavage-independent but initiates inflammatory responses by preventing HDAC2-mediated cytosolic sequestration of NF $\kappa$ B—a major regulator of transcription of multiple proinflammatory genes, including MHC II<sup>107</sup>. Intriguingly, our findings contrast with both prediction models, as we showed that HDAC2 does not undergo proteolytic processing in the presence of NSP5. Likewise, we observed no differences in HDAC2

nuclear localization in cells expressing wildtype NSP5 or NSP5 point mutants in which the catalytic sites are functionally inactivated. Currently, it remains unclear how the cysteine protease NSP5 modulates HDAC2 activity independent of proteolytic modifications. Previous studies have reported that coronaviruses, including MERS-CoV and SARS-CoV, can alter histone modifications and activate or repress expression of targeted genes, albeit the specific viral components have yet to be identified<sup>152</sup>. However, phylogenetic analyses demonstrated that NSP5 sequences are identical in SARS-CoV and SARS-CoV-2, and moderately conserved in MERS-CoV. Consistently, our findings showed that SARS-CoV-2 NSP5 selectively downregulates MHC II and CIITA, suggesting that NSP5 may be potentiating HDAC2-mediated histone modification independent of its proteolytic activity.

## 5.5 Limitations and Pitfalls

One major pitfall of our vesicular trafficking experiments is that surface MHC II may enter an alternative pathway, such as a receptor recycling pathway, and from there be directed to the phagosome. As such, we may not be able to fully characterize the trafficking pathway utilized by MHC II to reach the phagosome using our current fluorescent markers to probe indirect endocytic or direct Golgi trafficking pathways. Should we observe that MHC II is not transported via either of these pathways, further studies will use fluorescent markers of recycling pathways, such as Rab11 or Arf6 to probe this possibility. While unlikely, delivery of MHC II from other organelles can be assessed through the expression of organelle-specific markers, such as LC3-GFP to demark autophagosomes. A more likely pitfall is that multiple pathways may be involved



in the delivery of MHC II to phagosomes. By performing pulse-chase experiments with our inducible MHC II-HaloTag reporter, we can perform high-temporal resolution imaging of MHC II trafficking that will allow us to determine which pathways deliver MHC II molecules to phagosomes at different timepoints following induction of MHC II expression.

An intriguing finding from our investigation into the effects of NSP5 on MHC II expression was that knocking down HDAC2 failed to restore MHC II promoter activity, suggesting that HDAC2 may not be involved in NSP5-mediated antagonism of the MHC II transcriptional machinery. However, this seemingly inconsistent finding may be attributed to the limitations of our dual luciferase MHC II reporter construct. While it is well established that RFX5 and CIITA assemble on the MHC II enhanceosome by binding to the promoter-proximal W-X1-X2-Y regulatory elements, novel regulatory elements containing inverted W-X1-X2-Y motifs have been identified to be positioned several kilobases from the transcriptional start site<sup>153</sup>. These promoter-distal regulatory elements are also bound by RFX5 and CIITA, leading to histone acetylation *in vivo*<sup>13</sup>, suggesting that MHC II transcription is regulated through a mechanism more complex than originally thought, involving a combination of both promoter-proximal and promoter-distal regulatory elements. Consistent with this model, we saw restoration of MHC II mRNA levels from the endogenous promoter in NSP5-expressing cells treated with an HDAC2-depleting siRNA, while an equivalent restoration of MHC II promoter activity was not observed in our dual luciferase MHC II reporter construct which only possesses the promoter-proximal W-X1-X2-Y regulatory elements but not the promoter-distal regions. In addition, because measurements of promoter activity were based on

dual luciferase reporter vectors, there is a possibility of incomplete or altered histone recruitment and, therefore, a difference in HDAC2 activity on these vectors, which may account for the differences observed between genomic versus vector-based expression levels of MHC II.

## 5.6 Future Work

While I was unable to investigate the roles of the endosomal trafficking regulators Rab5 and Rab7 in the indirect endolysosomal trafficking pathway, I have optimized the toolset and framework that will allow us to study this mechanism. Particularly, time-lapse microscopy and phagocytosis assays can be utilized in conjunction with our inducible MHC II-HaloTag expression system to explore how different regulators are involved in the trafficking of MHC II to phagosomes. To explore the roles of ERC1 in the canonical NF $\kappa$ B activation pathway, RT-qPCR and dual luciferase assays can be utilized to quantify the effects of ERC1 knockdown on NF $\kappa$ B and MHC II expression. Lastly, ERC1 has been identified as an interactor of SARS-CoV-2 NSP13. As we have observed that ERC1 is involved in regulating the delivery of MHC II to MIICs, it would be interesting to further investigate whether NSP13 may antagonize this trafficking pathway as an immunoevasion strategy.

An important consideration of this thesis was to study how NSP5-mediated suppression of MHC II can impact antigen presentation and CD4<sup>+</sup> T cell activation. It would be intriguing to explore whether NSP5 is responsible for the impaired cell-mediated and humoral immune responses observed in patients with COVID-19. Further study could

address this possibility through a T cell activation assay. Specifically, PBMCs can be stimulated with a recombinant SARS-CoV-2 spike protein and stained with a CD4 surface antibody dye to obtain a pool of spike antigen-specific CD4<sup>+</sup> T cells. We can then co-culture these T cells with NSP5-expressing DCs and induce antigen presentation using the same recombinant spike protein, wherein flow cytometry will assess differences in CD4<sup>+</sup> T cell proliferation and activation using cell proliferation dyes or antibodies of surface T cell activation markers, including CD25 and CD71<sup>154,155</sup>. Should we observe reduced proliferative capabilities or reduced expression of surface T cell activation markers, it would provide strong indications that NSP5 is responsible for the diminished immune responses in patients with COVID-19. In addition, while we observed no evidence suggestive of HDAC2 cleavage in the presence of NSP5, it is plausible that western blot analyses may not be sensitive enough to detect small cleavage sites. Other HDACs have been shown to be proteolytically cleaved at the C-terminus, resulting in their activation. One potential experiment to overcome this issue would be to generate an HDAC2 reporter construct tagged with different monomeric fluorescent protein biosensors (e.g. mVenus and mTurquoise2) on either ends of the gene, and then co-expressing NSP5 with this construct in primary human DCs. We could exploit these fluorescent protein biosensors by performing a Förster resonance energy transfer (FRET) analysis to determine whether HDAC2 is cleaved in the presence of NSP5 based on the disappearance of the FRET signal on either biosensor<sup>156</sup>. Should we observe a loss of FRET signal, it would confirm whether HDAC2 activity is modulated by NSP5-mediated cleavage, and further approaches such as high-resolution mass spectrometry or Edman

degradation of the immunoprecipitated fragments can be used to identify the location of the cleavage site(s)<sup>156</sup>.

## 5.7 Complementary Findings

While direct measurements of MHC II protein expression in response to NSP5 expression were not heavily explored in this thesis, preliminary flow cytometry analysis performed in our lab showed identical trends in which surface MHC II is downregulated in NSP5-expressing DCs (data not shown), complementary to findings obtained via immunofluorescence microscopy, RT-qPCR, and dual luciferase analyses. A recently published study identified similar findings, demonstrating that SARS-CoV-2 ORF6 downregulates MHC I in infected cells<sup>102</sup>. While ORF6 directly inhibits the expression and function of the Class I transactivator protein, our findings implicate NSP5 as an indirect inhibitor of CIITA transcription through enhancing HDAC2-mediated deacetylation at the promoter. Interestingly, it appears that the IFN $\gamma$  signaling pathway is targeted at multiple steps by SARS-CoV-2, resulting in downregulation of MHC I and MHC II via ORF6 and NSP5, respectively, and potentially impairing antigen presentation to adaptive immune cells.

## 5.8 HDAC2 Inhibitors as Potential Therapeutics Against COVID-19

With the advent of vaccines being developed over the past couple of years, we have a strong preventative measure to limit SARS-CoV-2 spread across the world. Novel

vaccines have been developed that utilize lipid nanoparticles that encapsulate mRNA encoding the full-length SARS-CoV-2 S protein, such that delivery of this mRNA vaccine will allow cells to express this viral protein without the requirement of infections with viral particles<sup>157,158</sup>. S protein-expressing cells may then present SARS-CoV-2 antigens in the contexts of MHC II and MHC I to CD4<sup>+</sup> and CD8<sup>+</sup> T cells, respectively, thereby mounting potent immune responses against future infections of SARS-CoV-2 by activating antigen-specific memory T cells and generating S protein-specific antibodies<sup>159,160</sup>.

While prophylactic approaches may be the most effective strategies to prevent infections, they are less helpful in patients already suffering from COVID-19. Clinical studies are currently testing novel immunotherapeutic drugs or repurposing existing drugs to treat patients with COVID-19. Our findings potentially identified a novel target to improve COVID-19 prognosis. Specifically, we demonstrated that SARS-CoV-2 NSP5 targets HDAC2 to antagonize MHC II expression in primary human pAPCs, with knockdown of HDAC2 reverting this suppression. Our findings suggest that targeting NSP5 and HDAC2 may be effective therapeutic approaches against COVID-19. Targeting NSP5 may not only prevent viral replication but may also improve host immune responses and diminish inflammation. Currently, Pfizer is developing an NSP5 enzymatic inhibitor as a treatment against COVID-19<sup>161,162</sup>. While helpful in preventing SARS-CoV-2 replication and attenuating inflammatory responses, our data suggests that the proteolytic activity of NSP5 is not required for impairing adaptive immune responses, therefore it is unclear if this therapeutic agent would reverse the suppression of MHC II expression or reverse other NSP5-HDAC2 mediated events. It can be argued that an HDAC2 inhibitor may be

a more effective therapeutic agent against COVID-19. Critically, targeting host proteins rather than viral proteins would reduce the likelihood of SARS-CoV-2 evolving resistance to the treatment. Additionally, inhibiting HDAC2 can prevent SARS-CoV-2 access to the MHC II transcriptional machinery and restore reduced levels of CIITA and MHC II, thereby increasing T cell-mediated responses to eliminate the pathogen. In other diseases, including cancers and neurological disorders, treatment with HDAC inhibitors such as Trichostatin A and Panobinostat have been shown to increase expression of MHC II and co-stimulatory molecules through upregulating CIITA and ameliorating CIITA recruitment to RFX5, leading to an increased capacity to activate T cell responses<sup>22,163-165</sup>. Finally, HDAC2 inhibitors may have additional beneficial effects for patients with COVID-19, as these drugs have been shown to limit viral entry via reduced ACE2 expression, and they have been proposed to reduce both lung fibrosis and intensity of the cytokine storm<sup>148,166-168</sup>.

## 5.9 Conclusion

Understanding the signaling and vesicular trafficking pathways that dictate antigen presentation on MHC II is an important step in understanding how different pathogens, including SARS-CoV-2, can infect and manipulate host immune responses. By studying the components responsible for regulating these pathways, we can explore how we can protect ourselves and improve our survival against these pathogens. While it remains unclear how MHC II is transported from the Golgi to the MIIC, our data suggests that Rab6 and ERC1 may be facilitating this process via the canonical Golgi export pathway. Ultimately, our findings may identify a novel trafficking pathway for MHC II that will

provide deeper insights into the development of CD4<sup>+</sup> T cell-mediated responses against a multitude of pathogens that hijack components of MHC II regulatory processes to escape host immune responses. Specifically, understanding how SARS-CoV-2 modulates antigen presentation is an essential first step to developing effective vaccines and therapeutics against COVID-19. This thesis provides mechanistic insight into SARS-CoV-2-mediated immunoevasion through antagonizing the MHC II antigen presentation pathway. Furthermore, our data indicate that SARS-CoV-2 may suppress adaptive immune responses via targeting HDAC2—a major regulator of IFN $\gamma$ - and CIITA-dependent MHC II expression (**Figures 16A-B**). Altogether, the findings from this study may have potentially identified HDAC2 as a novel drug target in our combat against this deadly disease.

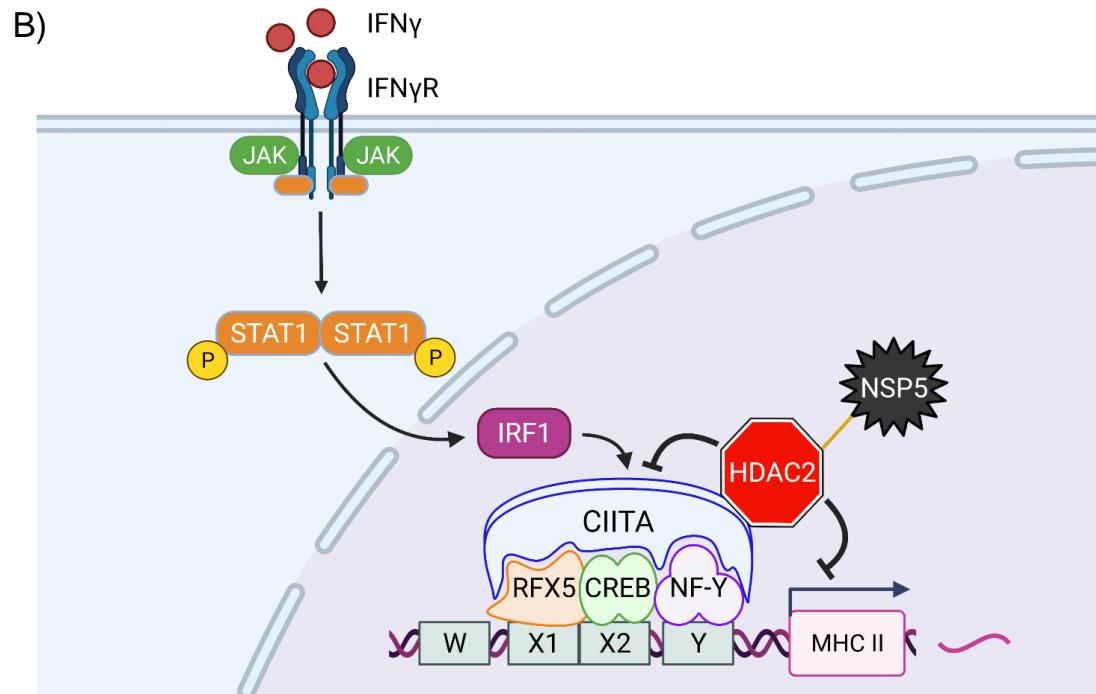
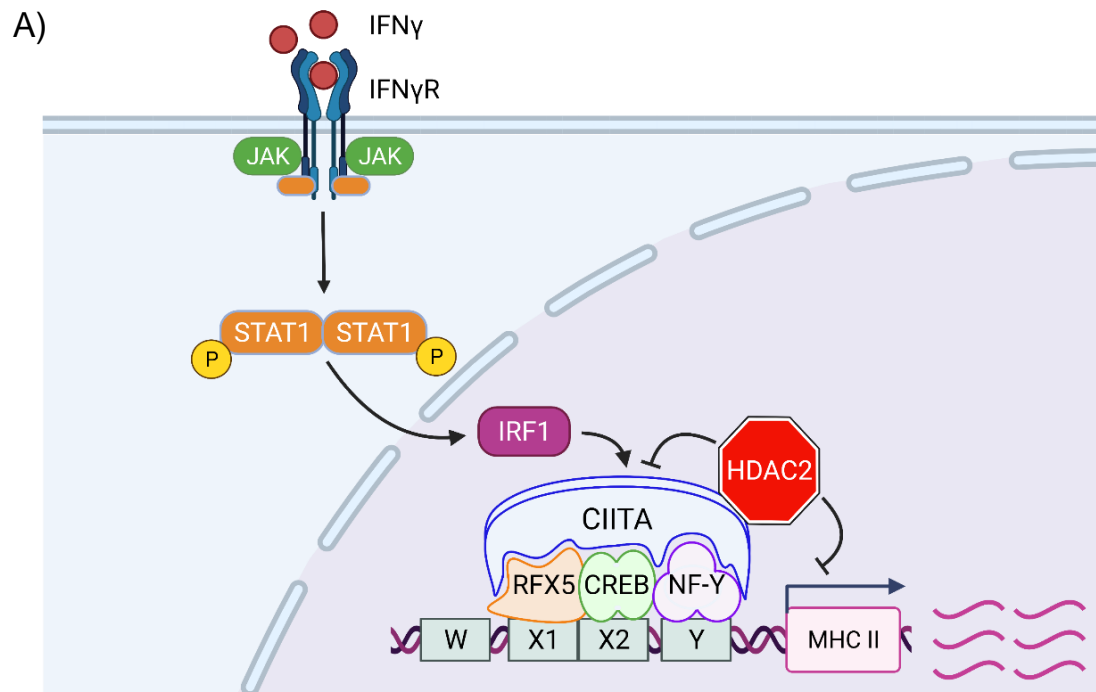




**Figure 16. Proposed model of NSP5-mediated downregulation of MHC II transcription.**

**A)** Normal MHC II transcription. IFN $\gamma$ -induced transcription of MHC II genes is mediated by CIITA binding to the promoter-proximal MHC II enhanceosome—consisting of RFX5, CREB, and NF-Y. HDAC2 represses transcription of CIITA and MHC II through deacetylating these genes' promoters. **B)** SARS-CoV-2-controlled MHC II transcription. SARS-CoV-2 NSP5 interacts with HDAC2 and increases its enzymatic activity, resulting in hyper-deacetylation of the CIITA and MHC II promoter, severely suppressing transcription of these genes. Figure prepared in BioRender.

## References

1. Roche, P. A., & Furuta, K. (2015). The ins and outs of MHC class II-mediated antigen processing and presentation. *Nature Reviews Immunology*, *15*(4), 203–216.  
<https://doi.org/10.1038/nri3818>
2. Frei, R., Steinle, J., Birchler, T., Loeliger, S., Roduit, C., Steinhoff, D., Seibl, R., Büchner, K., Seger, R., Reith, W., & Lauener, R. P. (2010). MHC Class II Molecules Enhance Toll-Like Receptor Mediated Innate Immune Responses. *PLoS ONE*, *5*(1), e8808. <https://doi.org/10.1371/journal.pone.0008808>
3. Brown, J. H., Jardetzky, T. S., Gorga, J. C., Stern, L. J., Urban, R. G., Strominger, J. L., & Wiley, D. C. (1993). Three-dimensional structure of the human class II histocompatibility antigen HLA-DR1. *Nature*, *364*(6432), 33–39.  
<https://doi.org/10.1038/364033a0>
4. Marks, M. S., Blum, J. S., & Cresswell, P. (1990). Invariant chain trimers are sequestered in the rough endoplasmic reticulum in the absence of association with HLA class II antigens. *Journal of Cell Biology*, *111*(3), 839–855.  
<https://doi.org/10.1083/jcb.111.3.839>
5. Roche, P. A., & Cresswell, P. (1990). Invariant chain association with HLA-DR molecules inhibits immunogenic peptide binding. *Nature*, *345*(6276), 615–618.  
<https://doi.org/10.1038/345615a0>

6. Elliott, E. A., Drake, J. R., Amigorena, S., Elsemore, J., Webster, P., Mellman, I., & Flavell, R. A. (1994). The Invariant Chain Is Required for Intracellular Transport and Function of Major Histocompatibility Complex Class II Molecules. *Journal of Experimental Medicine*, *179*, 681–694.
7. Bikoff, E. K., Huang, L.-Y., Episkopou, V., Meerwijk, J. van, Germain, R. N., & Robertson, E. J. (1993). Defective major histocompatibility complex class II assembly, transport, peptide acquisition, and CD4<sup>+</sup> T cell selection in mice lacking invariant chain expression. *Journal of Experimental Medicine*, *177*(6), 1699–1712.
8. Hiltbold, E. M., & Roche, P. A. (2002). Trafficking of MHC class II molecules in the late secretory pathway. *Current Opinion in Immunology*, *14*(1), 30–35.  
[https://doi.org/10.1016/S0952-7915\(01\)00295-3](https://doi.org/10.1016/S0952-7915(01)00295-3)
9. Schulze, M.-S. E., & Wucherpfennig, K. W. (2012). The mechanism of HLA-DM induced peptide exchange in the MHC class II antigen presentation pathway. *Current Opinion in Immunology*, *24*(1), 105–111.  
<https://doi.org/10.1016/j.coi.2011.11.004>
10. Gay, D., Maddon, P., Sekaly, R., Talle, M. A., Godfrey, M., Long, E., Goldstein, G., Chess, L., Axel, R., Kappler, J., & Marrack, P. (1987). Functional interaction between human T-cell protein CD4 and the major histocompatibility complex HLA-DR antigen. *Nature*, *328*(6131), 626–629. <https://doi.org/10.1038/328626a0>

11. Waldburger, J.-M., Masternak, K., Muhlethaler-Mottet, A., Villard, J., Peretti, M., Landmann, S., & Reith, W. (2008). Lessons from the bare lymphocyte syndrome: Molecular mechanisms regulating MHC class II expression. *Immunological Reviews*, *178*(1), 148–165. <https://doi.org/10.1034/j.1600-065X.2000.17813.x>
12. Masternak, K., & Reith, W. (2002). Promoter-specific functions of CIITA and the MHC class II enhanceosome in transcriptional activation. *EMBO Journal*, *21*(6), 1379–1388.
13. Krawczyk, M., Peyraud, N., Rybtsova, N., Masternak, K., Bucher, P., Barras, E., & Reith, W. (2004). Long Distance Control of MHC Class II Expression by Multiple Distal Enhancers Regulated by Regulatory Factor X Complex and CIITA. *The Journal of Immunology*, *173*(10), 6200–6210. <https://doi.org/10.4049/jimmunol.173.10.6200>
14. Mahanta, S. K., Scholl, T., Yang, F.-C., & Strominger, J. L. (1997). Transactivation by CIITA, the type II bare lymphocyte syndrome-associated factor, requires participation of multiple regions of the TATA box binding protein. *Proceedings of the National Academy of Sciences*, *94*(12), 6324–6329. <https://doi.org/10.1073/pnas.94.12.6324>
15. Beresford, G. W., & Boss, J. M. (2001). CIITA coordinates multiple histone acetylation modifications at the HLA-DRA promoter. *Nature Immunology*, *2*(7), 652–657. <https://doi.org/10.1038/89810>

16. Spilianakis, C., Papamatheakis, J., & Kretsovali, A. (2000). Acetylation by PCAF Enhances CIITA Nuclear Accumulation and Transactivation of Major Histocompatibility Complex Class II Genes. *Molecular and Cellular Biology*, 20(22), 8489–8498. <https://doi.org/10.1128/MCB.20.22.8489-8498.2000>
17. Raval, A., Howcroft, T. K., Weissman, J. D., Kirshner, S., Zhu, X.-S., Yokoyama, K., Ting, J., & Singer, D. S. (2001). Transcriptional Coactivator, CIITA, Is an Acetyltransferase that Bypasses a Promoter Requirement for TAFII250. *Molecular Cell*, 7(1), 105–115. [https://doi.org/10.1016/S1097-2765\(01\)00159-9](https://doi.org/10.1016/S1097-2765(01)00159-9)
18. Chen, H. P., Zhao, Y. T., & Zhao, T. C. (2016). *Histone Deacetylases and Mechanisms of Regulation of Gene Expression (Histone deacetylases in cancer)*. 17.
19. Gujral, P., Mahajan, V., Lissaman, A. C., & Ponnampalam, A. P. (2020). Histone acetylation and the role of histone deacetylases in normal cyclic endometrium. *Reproductive Biology and Endocrinology*, 18(1), 84. <https://doi.org/10.1186/s12958-020-00637-5>
20. Görisch, S. M., Wachsmuth, M., Tóth, K. F., Lichter, P., & Rippe, K. (2005). Histone acetylation increases chromatin accessibility. *Journal of Cell Science*, 118(24), 5825–5834. <https://doi.org/10.1242/jcs.02689>
21. Sun, W.-J., Zhou, X., Zheng, J.-H., Lu, M.-D., Nie, J.-Y., Yang, X.-J., & Zheng, Z.-Q. (2012). Histone acetyltransferases and deacetylases: Molecular and clinical

- implications to gastrointestinal carcinogenesis: Figure 1. *Acta Biochimica et Biophysica Sinica*, 44(1), 80–91. <https://doi.org/10.1093/abbs/gmr113>
22. Kong, X., Fang, M., Li, P., Fang, F., & Xu, Y. (2009). HDAC2 deacetylates class II transactivator and suppresses its activity in macrophages and smooth muscle cells. *Journal of Molecular and Cellular Cardiology*, 46(3), 292–299. <https://doi.org/10.1016/j.yjmcc.2008.10.023>
23. Chou, S.-D., Khan, A. N. H., Magner, W. J., & Tomasi, T. B. (2005). Histone acetylation regulates the cell type specific CIITA promoters, MHC class II expression and antigen presentation in tumor cells. *International Immunology*, 17(11), 1483–1494. <https://doi.org/10.1093/intimm/dxh326>
24. Gialitakis, M. (2006). Coordinated changes of histone modifications and HDAC mobilization regulate the induction of MHC class II genes by Trichostatin A. *Nucleic Acids Research*, 34(3), 765–772. <https://doi.org/10.1093/nar/gkj462>
25. Zinzow-Kramer, W. M., Long, A. B., Youngblood, B. A., Rosenthal, K. M., Butler, R., Mohammed, A.-U.-R., Skountzou, I., Ahmed, R., Evavold, B. D., & Boss, J. M. (2012). CIITA promoter I CARD-deficient mice express functional MHC class II genes in myeloid and lymphoid compartments. *Genes & Immunity*, 13(4), 299–310. <https://doi.org/10.1038/gene.2011.86>
26. Rocha, N., & Neefjes, J. (2008). MHC class II molecules on the move for successful antigen presentation. *The EMBO Journal*, 27(1), 1–5. <https://doi.org/10.1038/sj.emboj.7601945>

27. Vieira, O. V., Bucci, C., Harrison, R. E., Trimble, W. S., Lanzetti, L., Gruenberg, J., Schreiber, A. D., Stahl, P. D., & Grinstein, S. (2003). Modulation of Rab5 and Rab7 Recruitment to Phagosomes by Phosphatidylinositol 3-Kinase. *Molecular and Cellular Biology*, 23(7), 2501–2514. <https://doi.org/10.1128/MCB.23.7.2501-2514.2003>
28. Blander, J. M., & Medzhitov, R. (2004). Regulation of Phagosome Maturation by Signals from Toll-Like Receptors. *Science*, 304(5673), 1014–1018. <https://doi.org/10.1126/science.1096158>
29. Palade, G. (1975). Intracellular Aspects of the Process of Protein Synthesis. *Science*, 189(4200), 347–358. <https://doi.org/10.1126/science.1096303>
30. Rothman, J. E. (1994). Mechanisms of intracellular protein transport. *Nature*, 372(6501), 55–63. <https://doi.org/10.1038/372055a0>
31. Roche, P. A., Teletski, C. L., Stang, E., Bakke, O., & Long, E. O. (1993). Cell surface HLA-DR-invariant chain complexes are targeted to endosomes by rapid internalization. *Proceedings of the National Academy of Sciences*, 90(18), 8581–8585. <https://doi.org/10.1073/pnas.90.18.8581>
32. Wraight, C. J., van Endert, P., Möller, P., Lipp, J., Ling, N. R., MacLennan, I. C., Koch, N., & Moldenhauer, G. (1990). Human major histocompatibility complex class II invariant chain is expressed on the cell surface. *Journal of Biological Chemistry*, 265(10), 5787–5792. [https://doi.org/10.1016/S0021-9258\(19\)39432-3](https://doi.org/10.1016/S0021-9258(19)39432-3)

33. Karakikes, I., Morrison, I. E., O'Toole, P., Metodieva, G., Navarrete, C. V., Gomez, J., Miranda-Sayago, J. M., Cherry, R. J., Metodiev, M., & Fernandez, N. (2012). Interaction of HLA-DR and CD74 at the cell surface of antigen-presenting cells by single particle image analysis. *Federation of American Societies of Experimental Biology*, 26(12), 4886–4896. <https://doi.org/10.1096/fj.12-211466>
34. Hernández-Pérez, S., Vainio, M., Kuokkanen, E., Sustar, V., Petrov, P., Försten, S., Paavola, V., Rajala, J., Awoniyi, L. O., Sarapulov, A. V., Vihinen, H., Jokitalo, E., Bruckbauer, A., & Mattila, P. K. (2019). B cells rapidly target antigen and surface-derived MHCII into peripheral degradative compartments. *Journal of Cell Science*, jcs.235192. <https://doi.org/10.1242/jcs.235192>
35. Kongsvik, T. L., Höning, S., Bakke, O., & Rodionov, D. G. (2002). Mechanism of Interaction between Leucine-based Sorting Signals from the Invariant Chain and Clathrin-associated Adaptor Protein Complexes AP1 and AP2. *Journal of Biological Chemistry*, 277(19), 16484–16488. <https://doi.org/10.1074/jbc.M201583200>
36. Martzoukou, O., Amillis, S., Zervakou, A., Christoforidis, S., & Dhallinas, G. (2017). The AP-2 complex has a specialized clathrin-independent role in apical endocytosis and polar growth in fungi. *ELife*, 6, e20083. <https://doi.org/10.7554/eLife.20083>
37. McCormick, P. J., Martina, J. A., & Bonifacino, J. S. (2005). Involvement of clathrin and AP-2 in the trafficking of MHC class II molecules to antigen-processing



- compartments. *Proceedings of the National Academy of Sciences*, 102(22), 7910–7915. <https://doi.org/10.1073/pnas.0502206102>
38. Kelly, B. T., Graham, S. C., Liska, N., Dannhauser, P. N., Höning, S., Ungewickell, E. J., & Owen, D. J. (2014). AP2 controls clathrin polymerization with a membrane-activated switch. *Science*, 345(6195), 459–463. <https://doi.org/10.1126/science.1254836>
39. Moldenhauer, Henne, Karhausen, & Möller. (1999). Surface-expressed invariant chain (CD74) is required for internalization of human leucocyte antigen-DR molecules to early endosomal compartments. *Immunology*, 96(3), 473–484. <https://doi.org/10.1046/j.1365-2567.1999.00676.x>
40. Pérez-Montesinos, G., López-Ortega, O., Piedra-Reyes, J., Bonifaz, L. C., & Moreno, J. (2017). Dynamic Changes in the Intracellular Association of Selected Rab Small GTPases with MHC Class II and DM during Dendritic Cell Maturation. *Frontiers in Immunology*, 8. <https://doi.org/10.3389/fimmu.2017.00340>
41. Henne, C., Schwenk, F., & Koch, N. (1995). Surface expression of the invariant chain (CD74) is independent of concomitant expression of major histocompatibility complex class II antigens. *Immunology*, 84(2), 177–182.
42. Wilson, K. M., & PAWELEcT, G. (1993). Cell-surface expression of human histocompatibility leucocyte antigen (HLA) class II-associated invariant chain (CD74) does not always correlate with cell-surface expression of HLA class II molecules. *Immunology*, 79(2), 331–335.

43. Sekaly, R. P., Tonnelie, C., Strubin, M., Mach, B., & Long, E. O. (1986). Cell surface expression of class II histocompatibility antigens occurs in the absence of the invariant chain. *Journal of Experimental Medicine*, *164*(5), 1490–1504.  
<https://doi.org/10.1084/jem.164.5.1490>
44. Morton, P. A., Zacheis, M. A., Giacoletto, K. S., Manning, J. A., & Schwartz, B. D. (1995). Delivery of Nascent MHC Class II-Invariant Chain Complexes to Lysosomal Compartments and Proteolysis of Invariant Chain by Cysteine Proteases Precedes Peptide Binding in B-Lymphoblastoid Cells. *The Journal of Immunology*, *154*(1), 137–150.
45. Benaroch, P., & Yilla, M. (1995). How MHC class II molecules reach the endocytic pathway. *EMBO Journal*, *14*(1), 37–49. <https://doi.org/10.1002/j.1460-2075.1995.tb06973.x>
46. Warmerdam, P. A., Long, E. O., & Roche, P. A. (1996). Isoforms of the invariant chain regulate transport of MHC class II molecules to antigen processing compartments. *Journal of Cell Biology*, *133*(2), 281–291.  
<https://doi.org/10.1083/jcb.133.2.281>
47. Liu, S.-H., Marks, M. S., & Brodsky, F. M. (1998). A Dominant-negative Clathrin Mutant Differentially Affects Trafficking of Molecules with Distinct Sorting Motifs in the Class II Major Histocompatibility Complex (MHC) Pathway. *Journal of Cell Biology*, *140*(5), 1023–1037.  
<https://doi.org/10.1083/jcb.140.5.1023>

48. Januschke, J., Nicolas, E., Compagnon, J., Formstecher, E., Goud, B., & Guichet, A. (2007). Rab6 and the secretory pathway affect oocyte polarity in *Drosophila*. *Development*, *134*(19), 3419–3425. <https://doi.org/10.1242/dev.008078>
49. Iwanami, N., Nakamura, Y., Satoh, T., Liu, Z., & Satoh, A. K. (2016). Rab6 Is Required for Multiple Apical Transport Pathways but Not the Basolateral Transport Pathway in *Drosophila* Photoreceptors. *PLOS Genetics*, *12*(2), e1005828. <https://doi.org/10.1371/journal.pgen.1005828>
50. Ito, Y., & Boutté, Y. (2020). Differentiation of Trafficking Pathways at Golgi Entry Core Compartments and Post-Golgi Subdomains. *Frontiers in Plant Science*, *11*, 609516. <https://doi.org/10.3389/fpls.2020.609516>
51. Patwardhan, A., Bardin, S., Miserey-Lenkei, S., Larue, L., Goud, B., Raposo, G., & Delevoe, C. (2017). Routing of the RAB6 secretory pathway towards the lysosome related organelle of melanocytes. *Nature Communications*, *8*(1), 15835. <https://doi.org/10.1038/ncomms15835>
52. Yin, C., Kim, Y., Argintaru, D., & Heit, B. (2016). Rab17 mediates differential antigen sorting following efferocytosis and phagocytosis. *Cell Death & Disease*, *7*(12), e2529–e2529. <https://doi.org/10.1038/cddis.2016.431>
53. Martiniere, A., & Moreau, P. (2020). Complex roles of Rabs and SNAREs in the secretory pathway and plant development: A never-ending story. *Journal of Microscopy*, *280*(2), 140–157. <https://doi.org/10.1111/jmi.12952>

54. Cabrera, M., & Ungermann, C. (2013). Guanine Nucleotide Exchange Factors (GEFs) Have a Critical but Not Exclusive Role in Organelle Localization of Rab GTPases. *Journal of Biological Chemistry*, 288(40), 28704–28712. <https://doi.org/10.1074/jbc.M113.488213>
55. Langemeyer, L., Nunes Bastos, R., Cai, Y., Itzen, A., Reinisch, K. M., & Barr, F. A. (2014). Diversity and plasticity in Rab GTPase nucleotide release mechanism has consequences for Rab activation and inactivation. *ELife*, 3, e01623. <https://doi.org/10.7554/eLife.01623>
56. He, H., Huang, J., Wu, S., Jiang, S., Liang, L., Liu, Y., Liu, W., Xie, L., Tao, Y., Jiang, Y., & Cong, L. (2021). The roles of GTPase-activating proteins in regulated cell death and tumor immunity. *Journal of Hematology & Oncology*, 14(1), 171. <https://doi.org/10.1186/s13045-021-01184-1>
57. van Weering, J. R. T., Toonen, R. F., & Verhage, M. (2007). The Role of Rab3a in Secretory Vesicle Docking Requires Association/Dissociation of Guanidine Phosphates and Munc18-1. *PLoS ONE*, 2(7), e616. <https://doi.org/10.1371/journal.pone.0000616>
58. Henry, L., & Sheff, D. R. (2008). Rab8 Regulates Basolateral Secretory, But Not Recycling, Traffic at the Recycling Endosome. *Molecular Biology of the Cell*, 19(5), 2059–2068. <https://doi.org/10.1091/mbc.e07-09-0902>
59. Ostrowski, M., Carmo, N. B., Krumeich, S., Fanget, I., Raposo, G., Savina, A., Moita, C. F., Schauer, K., Hume, A. N., Freitas, R. P., Goud, B., Benaroch, P.,

- Hacohen, N., Fukuda, M., Desnos, C., Seabra, M. C., Darchen, F., Amigorena, S., Moita, L. F., & Thery, C. (2010). Rab27a and Rab27b control different steps of the exosome secretion pathway. *Nature Cell Biology*, *12*(1), 19–30.  
<https://doi.org/10.1038/ncb2000>
60. Vázquez-Martínez, R., & Malagón, M. M. (2011). Rab Proteins and the Secretory Pathway: The Case of Rab18 in Neuroendocrine Cells. *Frontiers in Endocrinology*, *2*. <https://doi.org/10.3389/fendo.2011.00001>
61. Jovic, M., Sharma, M., Rahajeng, J., & Caplan, S. (2010). *The early endosome: A busy sorting station for proteins at the crossroads*. 22.
62. Vanlandingham, P. A., & Ceresa, B. P. (2009). Rab7 Regulates Late Endocytic Trafficking Downstream of Multivesicular Body Biogenesis and Cargo Sequestration. *Journal of Biological Chemistry*, *284*(18), 12110–12124.  
<https://doi.org/10.1074/jbc.M809277200>
63. White, J., Johannes, L., Mallard, F., Girod, A., Grill, S., Reinsch, S., Keller, P., Tzschaschel, B., Echard, A., Goud, B., & Stelzer, E. H. K. (1999). Rab6 Coordinates a Novel Golgi to ER Retrograde Transport Pathway in Live Cells. *Journal of Cell Biology*, *147*(4), 743–760. <https://doi.org/10.1083/jcb.147.4.743>
64. Grigoriev, I., Splinter, D., Keijzer, N., Wulf, P. S., Demmers, J., Ohtsuka, T., Modesti, M., Maly, I. V., Grosveld, F., Hoogenraad, C. C., & Akhmanova, A. (2007). Rab6 Regulates Transport and Targeting of Exocytotic Carriers. *Developmental Cell*, *13*(2), 305–314. <https://doi.org/10.1016/j.devcel.2007.06.010>

65. Sala, K., Corbetta, A., Minici, C., Tonoli, D., Murray, D. H., Cammarota, E., Ribolla, L., Ramella, M., Fesce, R., Mazza, D., Degano, M., & de Curtis, I. (2019). The ERC1 scaffold protein implicated in cell motility drives the assembly of a liquid phase. *Scientific Reports*, *9*(1), 13530. <https://doi.org/10.1038/s41598-019-49630-y>
66. Sun, L., & Carpenter, G. (1998). Epidermal growth factor activation of NF- $\kappa$ B is mediated through I $\kappa$ B $\alpha$  degradation and intracellular free calcium. *Oncogene*, *16*, 2095–2102. <https://doi.org/10.1038/sj.onc.1201731>
67. Israel, A. (2010). The IKK Complex, a Central Regulator of NF- $\kappa$ B Activation. *Cold Spring Harbor Perspectives in Biology*, *2*(3), a000158–a000158. <https://doi.org/10.1101/cshperspect.a000158>
68. Kawai, T., & Akira, S. (2007). Signaling to NF- $\kappa$ B by Toll-like receptors. *Trends in Molecular Medicine*, *13*(11), 460–469. <https://doi.org/10.1016/j.molmed.2007.09.002>
69. Lee, K.-W., Lee, Y., Kim, D.-S., & Kwon, H.-J. (2006). Direct role of NF- $\kappa$ B activation in Toll-like receptor-triggered HLA-DRA expression. *European Journal of Immunology*, *36*(5), 1254–1266. <https://doi.org/10.1002/eji.200535577>
70. Liu, T., Zhang, L., Joo, D., & Sun, S.-C. (2017). NF- $\kappa$ B signaling in inflammation. *Signal Transduction and Targeted Therapy*, *2*(1), 17023. <https://doi.org/10.1038/sigtrans.2017.23>

71. Sigala, J. L. D., Bottero, V., Young, D. B., Shevchenko, A., Mercurio, F., & Verma, I. M. (2004). Activation of Transcription Factor NF- $\kappa$ B Requires ELKS, an I $\kappa$ B Kinase Regulatory Subunit. *Science*, *304*(5679), 1963–1967.  
<https://doi.org/10.1126/science.1098387>
72. Wu, Z.-H., Wong, E. T., Shi, Y., Niu, J., Chen, Z., Miyamoto, S., & Tergaonkar, V. (2010). ATM- and NEMO-Dependent ELKS Ubiquitination Coordinates TAK1-Mediated IKK Activation in Response to Genotoxic Stress. *Molecular Cell*, *40*(1), 75–86. <https://doi.org/10.1016/j.molcel.2010.09.010>
73. Ahmad, F. B., & Anderson, R. N. (2021). The Leading Causes of Death in the US for 2020. *JAMA Network*, *325*(18), 1829–1830.  
<https://doi.org/10.1001/jama.2021.5469>
74. Temmam, S., Vongphayloth, K., Baquero, E., Munier, S., Bonomi, M., Regnault, B., Douangboubpha, B., Karami, Y., Chrétien, D., Sanamxay, D., Xayaphet, V., Paphaphanh, P., Lacoste, V., Somlor, S., Lakeomany, K., Phommavanh, N., Pérot, P., Dehan, O., Amara, F., ... Eloit, M. (2022). Bat coronaviruses related to SARS-CoV-2 and infectious for human cells. *Nature*, *604*(7905), 330–336.  
<https://doi.org/10.1038/s41586-022-04532-4>
75. Naqvi, A. A. T., Fatima, K., Mohammad, T., Fatima, U., Singh, I. K., Singh, A., Atif, S. M., Hariprasad, G., Hasan, G. M., & Hassan, Md. I. (2020). Insights into SARS-CoV-2 genome, structure, evolution, pathogenesis and therapies: Structural genomics approach. *Biochimica et Biophysica Acta (BBA) - Molecular Basis of Disease*, *1866*(10), 165878. <https://doi.org/10.1016/j.bbadis.2020.165878>

76. Shemesh, M., Aktepe, T. E., Deerain, J. M., McAuley, J. L., Audsley, M. D., David, C. T., Purcell, D. F. J., Urin, V., Hartmann, R., Moseley, G. W., Mackenzie, J. M., Schreiber, G., & Harari, D. (2021). SARS-CoV-2 suppresses IFN $\beta$  production mediated by NSP1, 5, 6, 15, ORF6 and ORF7b but does not suppress the effects of added interferon. *PLOS Pathogens*, *17*(8), e1009800. <https://doi.org/10.1371/journal.ppat.1009800>
77. Miorin, L., Kehrer, T., Sanchez-Aparicio, M. T., Zhang, K., Cohen, P., Patel, R. S., Cupic, A., Makio, T., Mei, M., Moreno, E., Danziger, O., White, K. M., Rathnasinghe, R., Uccellini, M., Gao, S., Aydililo, T., Mena, I., Yin, X., Martin-Sancho, L., ... García-Sastre, A. (2020). SARS-CoV-2 Orf6 hijacks Nup98 to block STAT nuclear import and antagonize interferon signaling. *Proceedings of the National Academy of Sciences*, *117*(45), 28344–28354. <https://doi.org/10.1073/pnas.2016650117>
78. Zhang, Y., Chen, Y., Li, Y., Huang, F., Luo, B., Yuan, Y., Xia, B., Ma, X., Yang, T., Yu, F., Liu, J., Liu, B., Song, Z., Chen, J., Yan, S., Wu, L., Pan, T., Zhang, X., Li, R., ... Zhang, H. (2021). The ORF8 protein of SARS-CoV-2 mediates immune evasion through down-regulating MHC-I. *Proceedings of the National Academy of Sciences*, *118*(23), e2024202118. <https://doi.org/10.1073/pnas.2024202118>
79. Yang, J., Petitjean, S. J. L., Koehler, M., Zhang, Q., Dumitru, A. C., Chen, W., Derclaye, S., Vincent, S. P., Soumillon, P., & Alsteens, D. (2020). Molecular interaction and inhibition of SARS-CoV-2 binding to the ACE2 receptor. *Nature Communications*, *11*(1), 4541. <https://doi.org/10.1038/s41467-020-18319-6>



80. Hoffmann, M., Kleine-Weber, H., Schroeder, S., Krüger, N., Herrler, T., Erichsen, S., Schiergens, T. S., Herrler, G., Wu, N.-H., Nitsche, A., Müller, M. A., Drosten, C., & Pöhlmann, S. (2020). SARS-CoV-2 Cell Entry Depends on ACE2 and TMPRSS2 and Is Blocked by a Clinically Proven Protease Inhibitor. *Cell*, *181*(2), 271-280.e8. <https://doi.org/10.1016/j.cell.2020.02.052>
81. Shang, J., Wan, Y., Luo, C., Ye, G., Geng, Q., Auerbach, A., & Li, F. (2020). Cell entry mechanisms of SARS-CoV-2. *Proceedings of the National Academy of Sciences*, *117*(21), 11727–11734. <https://doi.org/10.1073/pnas.2003138117>
82. Zhao, M.-M., Yang, W.-L., Yang, F.-Y., Zhang, L., Huang, W.-J., Hou, W., Fan, C.-F., Jin, R.-H., Feng, Y.-M., Wang, Y.-C., & Yang, J.-K. (2021). Cathepsin L plays a key role in SARS-CoV-2 infection in humans and humanized mice and is a promising target for new drug development. *Signal Transduction and Targeted Therapy*, *6*(1), 134. <https://doi.org/10.1038/s41392-021-00558-8>
83. Bayati, A., Kumar, R., Francis, V., & McPherson, P. S. (2021). SARS-CoV-2 infects cells after viral entry via clathrin-mediated endocytosis. *Journal of Biological Chemistry*, *296*, 100306. <https://doi.org/10.1016/j.jbc.2021.100306>
84. Chang, T., Yang, J., Deng, H., Chen, D., Yang, X., & Tang, Z.-H. (2022). Depletion and Dysfunction of Dendritic Cells: Understanding SARS-CoV-2 Infection. *Frontiers in Immunology*, *13*, 843342. <https://doi.org/10.3389/fimmu.2022.843342>

85. Song, X., Hu, W., Yu, H., Zhao, L., Zhao, Y., Zhao, X., Xue, H.-H., & Zhao, Y. (2020). Little to no expression of angiotensin-converting enzyme-2 on most human peripheral blood immune cells but highly expressed on tissue macrophages. *Cytometry Part A*, 2020, 1–10. <https://doi.org/10.1002/cyto.a.24285>
86. Kvedaraite, E., Hertwig, L., Sinha, I., Ponzetta, A., Hed Myrberg, I., Lourda, M., Dzidic, M., Akber, M., Klingström, J., Folkesson, E., Muvva, J. R., Chen, P., Gredmark-Russ, S., Brighenti, S., Norrby-Teglund, A., Eriksson, L. I., Rooyackers, O., Aleman, S., Strålin, K., ... Unge, C. (2021). Major alterations in the mononuclear phagocyte landscape associated with COVID-19 severity. *Proceedings of the National Academy of Sciences*, 118(6), e2018587118. <https://doi.org/10.1073/pnas.2018587118>
87. Yang, D., Chu, H., Hou, Y., Chai, Y., Shuai, H., Lee, A. C.-Y., Zhang, X., Wang, Y., Hu, B., Huang, X., Yuen, T. T.-T., Cai, J.-P., Zhou, J., Yuan, S., Zhang, A. J., Chan, J. F.-W., & Yuen, K.-Y. (2020). Attenuated Interferon and Proinflammatory Response in SARS-CoV-2–Infected Human Dendritic Cells Is Associated With Viral Antagonism of STAT1 Phosphorylation. *The Journal of Infectious Diseases*, 222(5), 734–745. <https://doi.org/10.1093/infdis/jiaa356>
88. Khan, S., Shafiei, M. S., Longoria, C., Schoggins, J. W., Savani, R. C., & Zaki, H. (2021). SARS-CoV-2 spike protein induces inflammation via TLR2-dependent activation of the NF- $\kappa$ B pathway. *ELife*, 10, e68563. <https://doi.org/10.7554/eLife.68563>

89. Zhao, Y., Kuang, M., Li, J., Zhu, L., Jia, Z., Guo, X., Hu, Y., Kong, J., Yin, H., Wang, X., & You, F. (2021). SARS-CoV-2 spike protein interacts with and activates TLR41. *Cell Research*, *31*(7), 818–820. <https://doi.org/10.1038/s41422-021-00495-9>
90. Shirato, K., & Kizaki, T. (2021). SARS-CoV-2 spike protein S1 subunit induces pro-inflammatory responses via toll-like receptor 4 signaling in murine and human macrophages. *Heliyon*, *7*(2), e06187. <https://doi.org/10.1016/j.heliyon.2021.e06187>
91. van der Donk, L. E. H., Eder, J., van Hamme, J. L., Brouwer, P. J. M., Brinkkemper, M., van Nuenen, A. C., van Gils, M. J., Sanders, R. W., Kootstra, N. A., Bermejo-Jambrina, M., & Geijtenbeek, T. B. H. (2022). SARS-CoV-2 infection activates dendritic cells via cytosolic receptors rather than extracellular TLRs. *European Journal of Immunology*, *52*(4), 646–655. <https://doi.org/10.1002/eji.202149656>
92. Delamarre, L., Pack, M., Chang, H., Mellman, I., & Trombetta, E. S. (2005). Differential Lysosomal Proteolysis in Antigen-Presenting Cells Determines Antigen Fate. *Science*, *307*(5715), 1630–1634. <https://doi.org/10.1126/science.1108003>
93. Erwig, L.-P., McPhillips, K. A., Wynes, M. W., Ivetic, A., Ridley, A. J., & Henson, P. M. (2006). Differential regulation of phagosome maturation in macrophages and dendritic cells mediated by Rho GTPases and ezrin–radixin–moesin (ERM)

proteins. *Proceedings of the National Academy of Sciences*, 103(34), 12825–12830. <https://doi.org/10.1073/pnas.0605331103>

94. Lv, J., Wang, Z., Qu, Y., Zhu, H., Zhu, Q., Tong, W., Bao, L., Lv, Q., Cong, J., Li, D., Deng, W., Yu, P., Song, J., Tong, W.-M., Liu, J., Liu, Y., Qin, C., & Huang, B. (2021). Distinct uptake, amplification, and release of SARS-CoV-2 by M1 and M2 alveolar macrophages. *Cell Discovery*, 7(1), 24. <https://doi.org/10.1038/s41421-021-00258-1>
95. Shang, C., Zhuang, X., Zhang, H., Li, Y., Zhu, Y., Lu, J., Ge, C., Cong, J., Li, T., Tian, M., Jin, N., & Li, X. (2021). Inhibitors of endosomal acidification suppress SARS-CoV-2 replication and relieve viral pneumonia in hACE2 transgenic mice. *Virology Journal*, 18(1), 46. <https://doi.org/10.1186/s12985-021-01515-1>
96. Khan, Md. A.-A.-K., & Islam, A. B. M. Md. K. (2021). SARS-CoV-2 Proteins Exploit Host's Genetic and Epigenetic Mediators for the Annexation of Key Host Signaling Pathways. *Frontiers in Molecular Biosciences*, 7, 598583. <https://doi.org/10.3389/fmolb.2020.598583>
97. Josset, L., Menachery, V. D., Gralinski, L. E., Agnihothram, S., Sova, P., Carter, V. S., Yount, B. L., Graham, R. L., Baric, R. S., & Katze, M. G. (2013). Cell Host Response to Infection with Novel Human Coronavirus EMC Predicts Potential Antivirals and Important Differences with SARS Coronavirus. *MBio*, 4(3), e00165-13. <https://doi.org/10.1128/mBio.00165-13>

98. Menachery, V. D., Schäfer, A., Burnum-Johnson, K. E., Mitchell, H. D., Einfeld, A. J., Walters, K. B., Nicora, C. D., Purvine, S. O., Casey, C. P., Monroe, M. E., Weitz, K. K., Stratton, K. G., Webb-Robertson, B.-J. M., Gralinski, L. E., Metz, T. O., Smith, R. D., Waters, K. M., Sims, A. C., Kawaoka, Y., & Baric, R. S. (2018). MERS-CoV and H5N1 influenza virus antagonize antigen presentation by altering the epigenetic landscape. *Proceedings of the National Academy of Sciences*, *115*(5). <https://doi.org/10.1073/pnas.1706928115>
99. Wilk, A. J., Rustagi, A., Zhao, N. Q., Roque, J., Martínez-Colón, G. J., McKechnie, J. L., Ivison, G. T., Ranganath, T., Vergara, R., Hollis, T., Simpson, L. J., Grant, P., Subramanian, A., Rogers, A. J., & Blish, C. A. (2020). A single-cell atlas of the peripheral immune response in patients with severe COVID-19. *Nature Medicine*, *26*(7), 1070–1076. <https://doi.org/10.1038/s41591-020-0944-y>
100. Munnur, D., Teo, Q., Eggermont, D., Lee, H. H. Y., They, F., Ho, J., van Leur, S. W., Ng, W. W. S., Siu, L. Y. L., Beling, A., Ploegh, H., Pinto-Fernandez, A., Damianou, A., Kessler, B., Impens, F., Mok, C. K. P., & Sanyal, S. (2021). Altered ISGylation drives aberrant macrophage-dependent immune responses during SARS-CoV-2 infection. *Nature Immunology*, *22*(11), 1416–1427. <https://doi.org/10.1038/s41590-021-01035-8>
101. Saichi, M., Ladjemi, M. Z., Korniotis, S., Rousseau, C., Ait Hamou, Z., Massenet-Regad, L., Amblard, E., Noel, F., Marie, Y., Bouteiller, D., Medvedovic, J., Pène, F., & Soumelis, V. (2021). Single-cell RNA sequencing of blood antigen-presenting cells in severe COVID-19 reveals multi-process defects in antiviral

immunity. *Nature Cell Biology*, 23(5), 538–551. <https://doi.org/10.1038/s41556-021-00681-2>

102. Yoo, J.-S., Sasaki, M., Cho, S. X., Kasuga, Y., Zhu, B., Ouda, R., Orba, Y., de Figueiredo, P., Sawa, H., & Kobayashi, K. S. (2021). SARS-CoV-2 inhibits induction of the MHC class I pathway by targeting the STAT1-IRF1-NLRC5 axis. *Nature Communications*, 12(1), 6602. <https://doi.org/10.1038/s41467-021-26910-8>
103. Dirk, B. S., Pawlak, E. N., Johnson, A. L., Van Nynatten, L. R., Jacob, R. A., Heit, B., & Dikeakos, J. D. (2016). HIV-1 Nef sequesters MHC-I intracellularly by targeting early stages of endocytosis and recycling. *Scientific Reports*, 6(1), 37021. <https://doi.org/10.1038/srep37021>
104. El Baba, R., & Herbein, G. (2020). Management of epigenomic networks entailed in coronavirus infections and COVID-19. *Clinical Epigenetics*, 12(1), 118. <https://doi.org/10.1186/s13148-020-00912-7>
105. Gordon, D. E., Jang, G. M., Bouhaddou, M., Xu, J., Obernier, K., White, K. M., O'Meara, M. J., Rezelj, V. V., Guo, J. Z., Swaney, D. L., Tummino, T. A., Hüttenhain, R., Kaake, R. M., Richards, A. L., Tutuncuoglu, B., Foussard, H., Batra, J., Haas, K., Modak, M., ... Krogan, N. J. (2020). A SARS-CoV-2 protein interaction map reveals targets for drug repurposing. *Nature*, 583(7816), 459–468. <https://doi.org/10.1038/s41586-020-2286-9>

106. Roe, M. K., Junod, N. A., Young, A. R., Beachboard, D. C., & Stobart, C. C. (2021). Targeting novel structural and functional features of coronavirus protease nsp5 (3CLpro, Mpro) in the age of COVID-19. *Journal of General Virology*, *102*(3). <https://doi.org/10.1099/jgv.0.001558>
107. Bensussen, A., Álvarez-Buylla, E. R., & Díaz, J. (2021). SARS-CoV-2 Nsp5 Protein Causes Acute Lung Inflammation, A Dynamical Mathematical Model. *Frontiers in Systems Biology*, *1*, 764155. <https://doi.org/10.3389/fsysb.2021.764155>
108. Drayman, N., DeMarco, J. K., Jones, K. A., Azizi, S.-A., Froggatt, H. M., Tan, K., Maltseva, N. I., Chen, S., Nicolaescu, V., Dvorkin, S., Furlong, K., Kathayat, R. S., Firpo, M. R., Mastrodomenico, V., Bruce, E. A., Schmidt, M. M., Jedrzejczak, R., Muñoz-Alía, M. Á., Schuster, B., ... Tay, S. (2021). Masitinib is a broad coronavirus 3CL inhibitor that blocks replication of SARS-CoV-2. *Science*, *373*(6557), 931–936. <https://doi.org/10.1126/science.abg5827>
109. Milligan, J. C., Zeisner, T. U., Papageorgiou, G., Joshi, D., Soudy, C., Ulferts, R., Wu, M., Lim, C. T., Tan, K. W., Weissmann, F., Canal, B., Fujisawa, R., Deegan, T., Nagaraj, H., Bineva-Todd, G., Basier, C., Curran, J. F., Howell, M., Beale, R., ... Diffley, J. F. X. (2021). Identifying SARS-CoV-2 antiviral compounds by screening for small molecule inhibitors of Nsp5 main protease. *Biochemical Journal*, *478*(13), 2499–2515. <https://doi.org/10.1042/BCJ20210197>
110. Scott, B. M., Lacasse, V., Blom, D. G., Tonner, P. D., & Blom, N. S. (2022). Predicted coronavirus Nsp5 protease cleavage sites in the human proteome. *BMC Genomic Data*, *23*(1), 25. <https://doi.org/10.1186/s12863-022-01044-y>

111. Fung, S.-Y., Siu, K.-L., Lin, H., Yeung, M. L., & Jin, D.-Y. (2021). SARS-CoV-2 main protease suppresses type I interferon production by preventing nuclear translocation of phosphorylated IRF3. *International Journal of Biological Sciences*, 17(6), 1547–1554. <https://doi.org/10.7150/ijbs.59943>
112. Korcsmaros, T. (2021). SARS-CoV-2 Causes a Different Cytokine Response Compared to Other Cytokine Storm-Causing Respiratory Viruses in Severely Ill Patients. *Frontiers in Immunology*, 12(629193), 11.
113. Li, W., Qiao, J., You, Q., Zong, S., Peng, Q., Liu, Y., Hu, S., Liu, W., Li, S., Shu, X., & Sun, B. (2021). SARS-CoV-2 Nsp5 Activates NF- $\kappa$ B Pathway by Upregulating SUMOylation of MAVS. *Frontiers in Immunology*, 12, 750969. <https://doi.org/10.3389/fimmu.2021.750969>
114. Schneider, C. A., Rasband, W. S., & Eliceiri, K. W. (2012). NIH Image to ImageJ: 25 years of image analysis. *Nature Methods*, 9(7), 671–675. <https://doi.org/10.1038/nmeth.2089>
115. Rueden, C. T., Schindelin, J., Hiner, M. C., DeZonia, B. E., Walter, A. E., Arena, E. T., & Eliceiri, K. W. (2017). ImageJ2: ImageJ for the next generation of scientific image data. *BMC Bioinformatics*, 18(1), 529. <https://doi.org/10.1186/s12859-017-1934-z>
116. Lac, A., Lam, A. L., & Heit, B. (2022). Optimizing Long-Term Live Cell Imaging. In *Fluorescent Microscopy* (Vol. 2440, pp. 57–73). Methods in Molecular Biology. [https://link.springer.com/protocol/10.1007/978-1-0716-2051-9\\_3](https://link.springer.com/protocol/10.1007/978-1-0716-2051-9_3)



117. Tamura, K., Stecher, G., & Kumar, S. (2021). MEGA11: Molecular Evolutionary Genetics Analysis Version 11. *Molecular Biology and Evolution*, *38*(7), 3022–3027. <https://doi.org/10.1093/molbev/msab120>
118. Balleza, E., Kim, J. M., & Cluzel, P. (2018). Systematic characterization of maturation time of fluorescent proteins in living cells. *Nature Methods*, *15*(1), 47–51. <https://doi.org/10.1038/nmeth.4509>
119. Los, G. V., Encell, L. P., McDougall, M. G., Hartzell, D. D., Karassina, N., Zimprich, C., Wood, M. G., Learish, R., Ohana, R. F., Urh, M., Simpson, D., Mendez, J., Zimmerman, K., Otto, P., Vidugiris, G., Zhu, J., Darzins, A., Klaubert, D. H., Bulleit, R. F., & Wood, K. V. (2008). HaloTag: A Novel Protein Labeling Technology for Cell Imaging and Protein Analysis. *ACS Chemical Biology*, *3*(6), 373–382. <https://doi.org/10.1021/cb800025k>
120. Santerre, M., Arjona, S. P., Allen, C. N., Shcherbik, N., & Sawaya, B. E. (2021). Why do SARS-CoV-2 NSPs rush to the ER? *Journal of Neurology*, *268*(6), 2013–2022. <https://doi.org/10.1007/s00415-020-10197-8>
121. Zhang, J., Cruz-cosme, R., Zhuang, M.-W., Liu, D., Liu, Y., Teng, S., Wang, P.-H., & Tang, Q. (2020). A systemic and molecular study of subcellular localization of SARS-CoV-2 proteins. *Signal Transduction and Targeted Therapy*, *5*(1), 269. <https://doi.org/10.1038/s41392-020-00372-8>
122. Li, J., Guo, C., Rood, C., & Zhang, J. (2021). A C terminus–dependent conformational change is required for HDAC3 activation by nuclear receptor

corepressors. *Journal of Biological Chemistry*, 297(4), 101192.

<https://doi.org/10.1016/j.jbc.2021.101192>

123. Paroni, G., Mizzau, M., Henderson, C., Del Sal, G., Schneider, C., & Brancolini, C. (2004). Caspase-dependent Regulation of Histone Deacetylase 4 Nuclear-Cytoplasmic Shuttling Promotes Apoptosis. *Molecular Biology of the Cell*, 15(6), 2804–2818. <https://doi.org/10.1091/mbc.e03-08-0624>
124. Irving, A. T., Ahn, M., Goh, G., Anderson, D. E., & Wang, L.-F. (2021). Lessons from the host defences of bats, a unique viral reservoir. *Nature*, 589(7842), 363–370. <https://doi.org/10.1038/s41586-020-03128-0>
125. Nyitrai, H., Wang, S. S. H., & Kaeser, P. S. (2020). ELKS1 Captures Rab6-Marked Vesicular Cargo in Presynaptic Nerve Terminals. *Cell Reports*, 31(10), 107712. <https://doi.org/10.1016/j.celrep.2020.107712>
126. Niles, M. A., Gogesch, P., Kronhart, S., Ortega Iannazzo, S., Kochs, G., Waibler, Z., & Anzaghe, M. (2021). Macrophages and Dendritic Cells Are Not the Major Source of Pro-Inflammatory Cytokines Upon SARS-CoV-2 Infection. *Frontiers in Immunology*, 12, 647824. <https://doi.org/10.3389/fimmu.2021.647824>
127. Gil-Etayo, F. J., Suárez-Fernández, P., Cabrera-Marante, O., Arroyo, D., Garcinuño, S., Naranjo, L., Pleguezuelo, D. E., Allende, L. M., Mancebo, E., Lalueza, A., Díaz-Simón, R., Paz-Artal, E., & Serrano, A. (2021). T-Helper Cell Subset Response Is a Determining Factor in COVID-19 Progression. *Frontiers in*

*Cellular and Infection Microbiology*, 11, 624483.

<https://doi.org/10.3389/fcimb.2021.624483>

128. Pavel, A. B., Glickman, J. W., Michels, J. R., Kim-Schulze, S., Miller, R. L., & Guttman-Yassky, E. (2021). Th2/Th1 Cytokine Imbalance Is Associated With Higher COVID-19 Risk Mortality. *Frontiers in Genetics*, 12, 706902.  
<https://doi.org/10.3389/fgene.2021.706902>
129. Montazersaheb, S., Hosseiniyan Khatibi, S. M., Hejazi, M. S., Tarhriz, V., Farjami, A., Ghasemian Sorbeni, F., Farahzadi, R., & Ghasemnejad, T. (2022). COVID-19 infection: An overview on cytokine storm and related interventions. *Virology Journal*, 19(1), 92. <https://doi.org/10.1186/s12985-022-01814-1>
130. Arshad, N., Laurent-Rolle, M., Ahmed, W. S., Hsu, J. C.-C., Mitchell, S. M., Pawlak, J., Sengupta, D., Biswas, K. H., & Cresswell, P. (2022). SARS-CoV-2 accessory proteins ORF7a and ORF3a use distinct mechanisms to downregulate MHC-I surface expression [Preprint]. *Immunology*.  
<https://doi.org/10.1101/2022.05.17.492198>
131. Neumann, J., Eis-Hübinger, A. M., & Koch, N. (2003). Herpes Simplex Virus Type 1 Targets the MHC Class II Processing Pathway for Immune Evasion. *The Journal of Immunology*, 171(6), 3075–3083.  
<https://doi.org/10.4049/jimmunol.171.6.3075>
132. Temme, S., Eis-Hübinger, A. M., McLellan, A. D., & Koch, N. (2010). The Herpes Simplex Virus-1 Encoded Glycoprotein B Diverts HLA-DR into the Exosome

Pathway. *The Journal of Immunology*, 184(1), 236–243.

<https://doi.org/10.4049/jimmunol.0902192>

133. Gogoi, M., Ravikumar, V., Dixit, N. M., & Chakravorty, D. (2018). Salmonella escapes antigen presentation through K63 ubiquitination mediated endosomal proteolysis of MHC II via modulation of endosomal acidification in dendritic cells. *Pathogens and Disease*, 76(2). <https://doi.org/10.1093/femspd/ftx125>
134. Lapaque, N., Hutchinson, J. L., Jones, D. C., Méresse, S., Holden, D. W., Trowsdale, J., & Kelly, A. P. (2009). Salmonella regulates polyubiquitination and surface expression of MHC class II antigens. *Proceedings of the National Academy of Sciences*, 106(33), 14052–14057.
135. Kwan, W. C., McMaster, W. R., Wong, N., & Reiner, N. E. (1992). Inhibition of expression of major histocompatibility complex class II molecules in macrophages infected with *Leishmania donovani* occurs at the level of gene transcription via a cyclic AMP-independent mechanism. *Infection and Immunity*, 60(5), 2115–2120. <https://doi.org/10.1128/iai.60.5.2115-2120.1992>
136. Li, D., Qian, L., Chen, C., Shi, M., Yu, M., Hu, M., Song, L., Shen, B., & Guo, N. (2009). Down-Regulation of MHC Class II Expression through Inhibition of CIITA Transcription by Lytic Transactivator Zta during Epstein-Barr Virus Reactivation. *The Journal of Immunology*, 182(4), 1799–1809. <https://doi.org/10.4049/jimmunol.0802686>

137. Chiu, I., Davis, D. M., & Strominger, J. L. (1999). Trafficking of spontaneously endocytosed MHC proteins. *Proceedings of the National Academy of Sciences*, *96*(24), 13944–13949. <https://doi.org/10.1073/pnas.96.24.13944>
138. Kitamura, H., Morikawa, H., Kamon, H., Iguchi, M., Hojyo, S., Fukada, T., Yamashita, S., Kaisho, T., Akira, S., Murakami, M., & Hirano, T. (2006). Toll-like receptor-mediated regulation of zinc homeostasis influences dendritic cell function. *Nature Immunology*, *7*(9), 971–977. <https://doi.org/10.1038/ni1373>
139. Ong, Goldenberg, Hansen, & Mattes. (1999). Cell surface expression and metabolism of major histocompatibility complex class II invariant chain (CD74) by diverse cell lines: CD74 metabolism. *Immunology*, *98*(2), 296–302. <https://doi.org/10.1046/j.1365-2567.1999.00868.x>
140. Furuta, K., Walseng, E., & Roche, P. A. (2013). Internalizing MHC class II-peptide complexes are ubiquitinated in early endosomes and targeted for lysosomal degradation. *Proceedings of the National Academy of Sciences*, *110*(50), 20188–20193. <https://doi.org/10.1073/pnas.1312994110>
141. Liu, Z., & Roche, P. A. (2015). Macropinocytosis in phagocytes: Regulation of MHC class-II-restricted antigen presentation in dendritic cells. *Frontiers in Physiology*, *6*. <https://doi.org/10.3389/fphys.2015.00001>
142. Masaki, K., Hiraki, Y., Onishi, H., Satoh, Y., Roche, P. A., Tanaka, S., & Furuta, K. (2020). Ligation of MHC Class II Induces PKC-Dependent Clathrin-Mediated

Endocytosis of MHC Class II. *Cells*, 9(8), 1810.

<https://doi.org/10.3390/cells9081810>

143. Wang, K., Peterson, P. A., & Karlsson, L. (1997). Decreased Endosomal Delivery of Major Histocompatibility Complex Class II-invariant Chain Complexes in Dynamin-deficient Cells. *Journal of Biological Chemistry*, 272(27), 17055–17060. <https://doi.org/10.1074/jbc.272.27.17055>
144. Acharya, D., Li, X. R. (Lisa), Heineman, R. E.-S., & Harrison, R. E. (2020). Complement Receptor-Mediated Phagocytosis Induces Proinflammatory Cytokine Production in Murine Macrophages. *Frontiers in Immunology*, 10, 3049. <https://doi.org/10.3389/fimmu.2019.03049>
145. Sánchez-Mejorada, G., & Rosales, C. (1998). Fc $\gamma$  Receptor-mediated Mitogen-activated Protein Kinase Activation in Monocytes Is Independent of Ras. *Journal of Biological Chemistry*, 273(42), 27610–27619. <https://doi.org/10.1074/jbc.273.42.27610>
146. Alonso, A., Bayón, Y., Renedo, M., & Crespo, M. S. (2000). Stimulation of Fc $\gamma$ R receptors induces monocyte chemoattractant protein-1 in the human monocytic cell line THP-1 by a mechanism involving I $\kappa$ B- $\alpha$  degradation and formation of p50/p65 NF- $\kappa$ B/Rel complexes. *International Immunology*, 12(4), 547–554. <https://doi.org/10.1093/intimm/12.4.547>
147. Hang, D. T. T., Song, J.-Y., Kim, M.-Y., Park, J.-W., & Shin, Y.-K. (2011). Involvement of NF- $\kappa$ B in changes of IFN- $\gamma$ -induced CIITA/MHC-II and iNOS

- expression by influenza virus in macrophages. *Molecular Immunology*, 48(9–10), 1253–1262. <https://doi.org/10.1016/j.molimm.2011.03.010>
148. Liu, F., Dowling, M., Yang, X.-J., & Kao, G. D. (2004). Caspase-mediated Specific Cleavage of Human Histone Deacetylase 4. *Journal of Biological Chemistry*, 279(33), 34537–34546. <https://doi.org/10.1074/jbc.M402475200>
149. Colombo, R., Boggio, R., Seiser, C., Draetta, G. F., & Chiocca, S. (2002). The adenovirus protein Gam1 interferes with sumoylation of histone deacetylase 1. *EMBO Reports*, 3(11), 1062–1068. <https://doi.org/10.1093/embo-reports/kvf213>
150. David, G., Neptune, M. A., & DePinho, R. A. (2002). SUMO-1 Modification of Histone Deacetylase 1 (HDAC1) Modulates Its Biological Activities. *Journal of Biological Chemistry*, 277(26), 23658–23658. <https://doi.org/10.1074/jbc.M203690200>
151. Kirsh, O., Seeler, J.-S., Pichler, A., & Gast, A. (2002). The SUMO E3 ligase RanBP2 promotes modification of the HDAC4 deacetylase. *EMBO Journal*, 21(11), 2682–2691. <https://doi.org/10.1093/emboj/21.11.2682>
152. Menachery, V. D., Eisfeld, A. J., Schäfer, A., Josset, L., Sims, A. C., Proll, S., Fan, S., Li, C., Neumann, G., Tilton, S. C., Chang, J., Gralinski, L. E., Long, C., Green, R., Williams, C. M., Weiss, J., Matzke, M. M., Webb-Robertson, B.-J., Schepmoes, A. A., ... Baric, R. S. (2014). Pathogenic Influenza Viruses and Coronaviruses Utilize Similar and Contrasting Approaches To Control Interferon-

Stimulated Gene Responses. *MBio*, 5(3), e01174-14.

<https://doi.org/10.1128/mBio.01174-14>

153. Masternak, K., Peyraud, N., Krawczyk, M., Barras, E., & Reith, W. (2003). Chromatin remodeling and extragenic transcription at the MHC class II locus control region. *Nature Immunology*, 4(2), 132–137. <https://doi.org/10.1038/ni883>
154. Keeton, R., Tincho, M. B., Ngomti, A., Baguma, R., Benede, N., Suzuki, A., Khan, K., Cele, S., Bernstein, M., Karim, F., Madzorera, S. V., Moyo-Gwete, T., Mennen, M., Skelem, S., Adriaanse, M., Mutithu, D., Aremu, O., Stek, C., du Bruyn, E., ... Riou, C. (2022). T cell responses to SARS-CoV-2 spike cross-recognize Omicron. *Nature*, 603(7901), 488–492. <https://doi.org/10.1038/s41586-022-04460-3>
155. Shipkova, M., & Wieland, E. (2012). Surface markers of lymphocyte activation and markers of cell proliferation. *Clinica Chimica Acta*, 413(17–18), 1338–1349. <https://doi.org/10.1016/j.cca.2011.11.006>
156. Tao, W., Rubart, M., Ryan, J., Xiao, X., Qiao, C., Hato, T., Davidson, M. W., Dunn, K. W., & Day, R. N. (2015). A practical method for monitoring FRET-based biosensors in living animals using two-photon microscopy. *American Journal of Physiology-Cell Physiology*, 309(11), C724–C735. <https://doi.org/10.1152/ajpcell.00182.2015>
157. Chung, H., He, S., Nasreen, S., Sundaram, M. E., Buchan, S. A., Wilson, S. E., Chen, B., Calzavara, A., Fell, D. B., Austin, P. C., Wilson, K., Schwartz, K. L.,



- Brown, K. A., Gubbay, J. B., Basta, N. E., Mahmud, S. M., Righolt, C. H., Svenson, L. W., MacDonald, S. E., ... Kwong, J. C. (2021). Effectiveness of BNT162b2 and mRNA-1273 covid-19 vaccines against symptomatic SARS-CoV-2 infection and severe covid-19 outcomes in Ontario, Canada: Test negative design study. *BMJ*, n1943. <https://doi.org/10.1136/bmj.n1943>
158. Polack, F. P., Thomas, S. J., Kitchin, N., Absalon, J., Gurtman, A., Lockhart, S., Perez, J. L., Pérez Marc, G., Moreira, E. D., Zerbini, C., Bailey, R., Swanson, K. A., Roychoudhury, S., Koury, K., Li, P., Kalina, W. V., Cooper, D., Frenck, R. W., Hammitt, L. L., ... Gruber, W. C. (2020). Safety and Efficacy of the BNT162b2 mRNA Covid-19 Vaccine. *New England Journal of Medicine*, 383(27), 2603–2615. <https://doi.org/10.1056/NEJMoa2034577>
159. Florindo, H. F., Kleiner, R., Vaskovich-Koubi, D., Acúrcio, R. C., Carreira, B., Yeini, E., Tiram, G., Liubomirski, Y., & Satchi-Fainaro, R. (2020). Immune-mediated approaches against COVID-19. *Nature Nanotechnology*, 15(8), 630–645. <https://doi.org/10.1038/s41565-020-0732-3>
160. Nemet, I., Kliker, L., Lustig, Y., Zuckerman, N., Erster, O., Cohen, C., Kreiss, Y., Alroy-Preis, S., Regev-Yochay, G., Mendelson, E., & Mandelboim, M. (2022). Third BNT162b2 Vaccination Neutralization of SARS-CoV-2 Omicron Infection. *New England Journal of Medicine*, 386(5), 492–494. <https://doi.org/10.1056/NEJMc2119358>
161. Hammond, J., Leister-Tebbe, H., Gardner, A., Abreu, P., Bao, W., Wisemandle, W., Baniecki, M., Hendrick, V. M., Damle, B., Simón-Campos, A., Pypstra, R., &

- Rusnak, J. M. (2022). Oral Nirmatrelvir for High-Risk, Nonhospitalized Adults with Covid-19. *New England Journal of Medicine*, 386(15), 1397–1408.  
<https://doi.org/10.1056/NEJMoa2118542>
162. Wen, W., Chen, C., Tang, J., Wang, C., Zhou, M., Cheng, Y., Zhou, X., Wu, Q., Zhang, X., Feng, Z., Wang, M., & Mao, Q. (2022). Efficacy and safety of three new oral antiviral treatment (molnupiravir, fluvoxamine and Paxlovid) for COVID-19 : a meta-analysis. *Annals of Medicine*, 54(1), 516–523.  
<https://doi.org/10.1080/07853890.2022.2034936>
163. Que, Y., Zhang, X.-L., Liu, Z.-X., Zhao, J.-J., Pan, Q.-Z., Wen, X.-Z., Xiao, W., Xu, B.-S., Hong, D.-C., Guo, T.-H., Shen, L.-J., Fan, W.-J., Chen, H.-Y., Weng, D.-S., Xu, H.-R., Zhou, P.-H., Zhang, Y.-Z., Niu, X.-H., & Zhang, X. (2021). Frequent amplification of HDAC genes and efficacy of HDAC inhibitor chidamide and PD-1 blockade combination in soft tissue sarcoma. *Journal for ImmunoTherapy of Cancer*, 9(2), e001696. <https://doi.org/10.1136/jitc-2020-001696>
164. Cycon, K. A., Mulvaney, K., Rimsza, L. M., Persky, D., & Murphy, S. P. (2013). Histone deacetylase inhibitors activate CIITA and MHC class II antigen expression in diffuse large B-cell lymphoma. *Immunology*, 140(2), 259–272.  
<https://doi.org/10.1111/imm.12136>
165. Woods, D. M., Woan, K., Cheng, F., Wang, H., Perez-Villarroel, P., Lee, C., Lienlaf, M., Atadja, P., Seto, E., Weber, J., Sotomayor, E. M., & Villagra, A. (2013). The antimelanoma activity of the histone deacetylase inhibitor

panobinostat (LBH589) is mediated by direct tumor cytotoxicity and increased tumor immunogenicity. *Melanoma Research*, 23(5), 341–348.

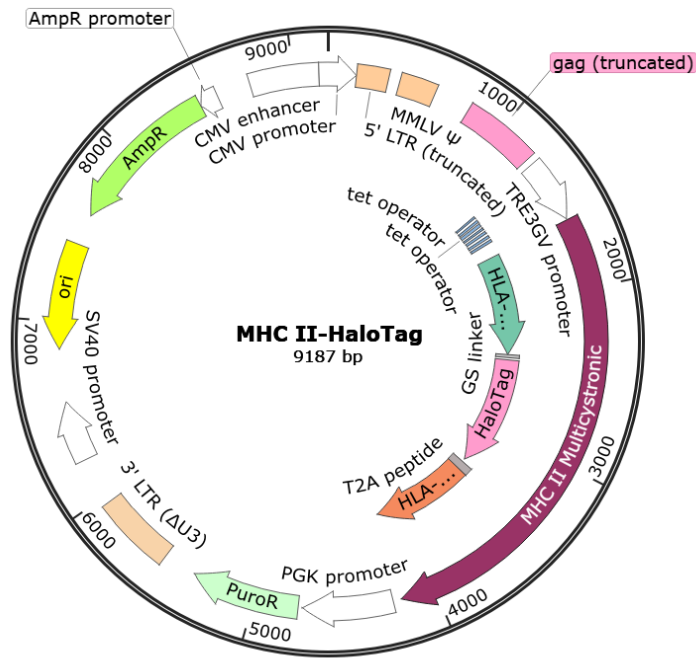
<https://doi.org/10.1097/CMR.0b013e328364c0ed>

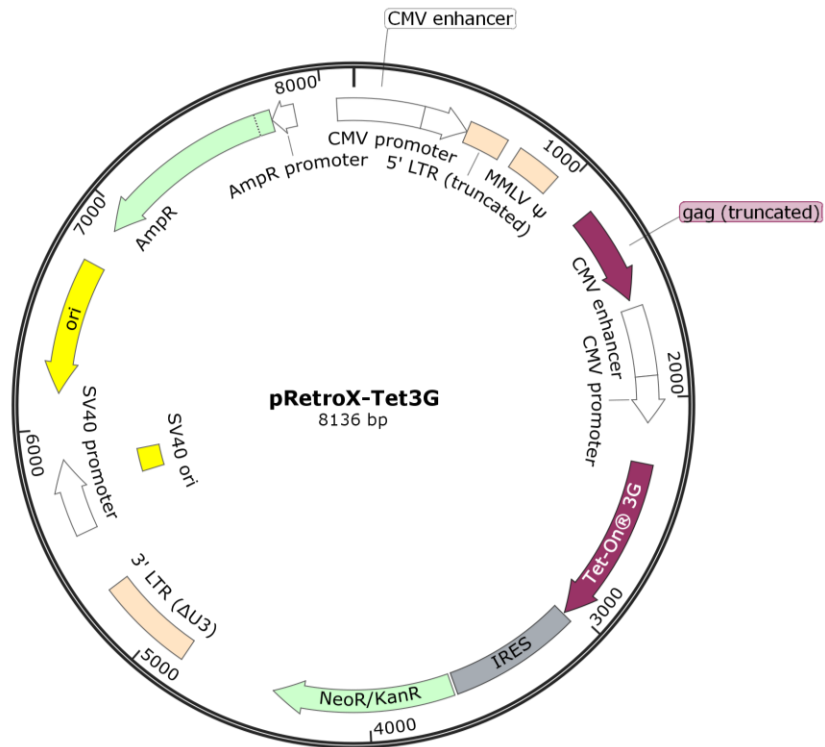
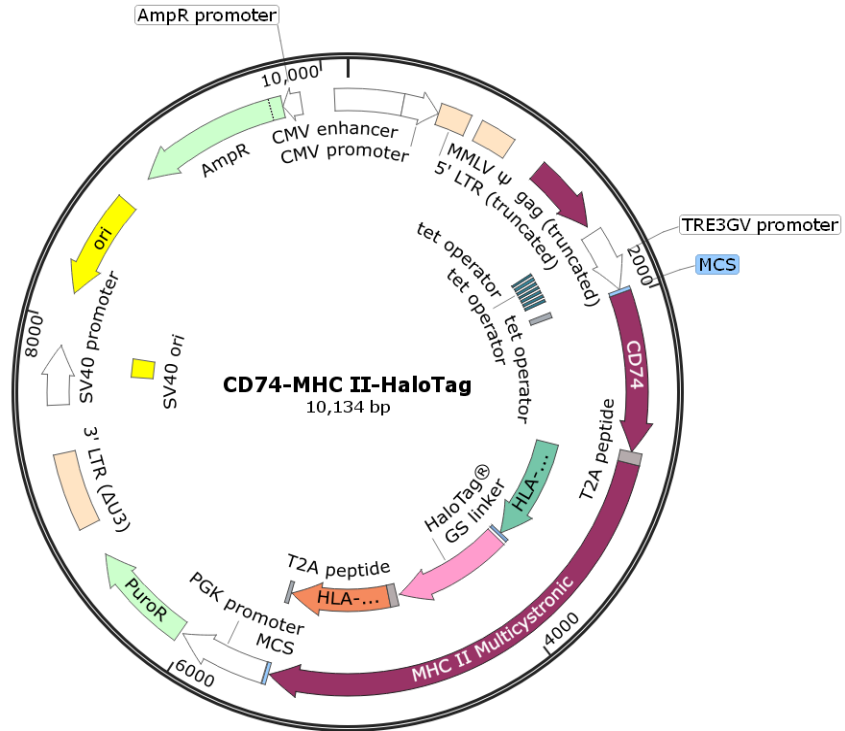
166. Ripamonti, C., Spadotto, V., Pozzi, P., Stevenazzi, A., Vergani, B., Marchini, M., Sandrone, G., Bonetti, E., Mazzarella, L., Minucci, S., Steinkühler, C., & Fossati, G. (2022). HDAC Inhibition as Potential Therapeutic Strategy to Restore the Deregulated Immune Response in Severe COVID-19. *Frontiers in Immunology*, 13, 841716. <https://doi.org/10.3389/fimmu.2022.841716>
167. P, K. M., Sivashanmugam, K., Kandasamy, M., Subbiah, R., & Ravikumar, V. (2021). Repurposing of histone deacetylase inhibitors: A promising strategy to combat pulmonary fibrosis promoted by TGF- $\beta$  signalling in COVID-19 survivors. *Life Sciences*, 266, 118883. <https://doi.org/10.1016/j.lfs.2020.118883>
168. Shweta, S., & Krishna K, S. (2020). Valproic Acid in Prevention and Treatment of COVID-19. *International Journal of Respiratory and Pulmonary Medicine*, 7(3). <https://doi.org/10.23937/2378-3516/1410138>

## Appendices

### Appendix A. Vector maps of MHC II-HaloTag constructs used in this study.

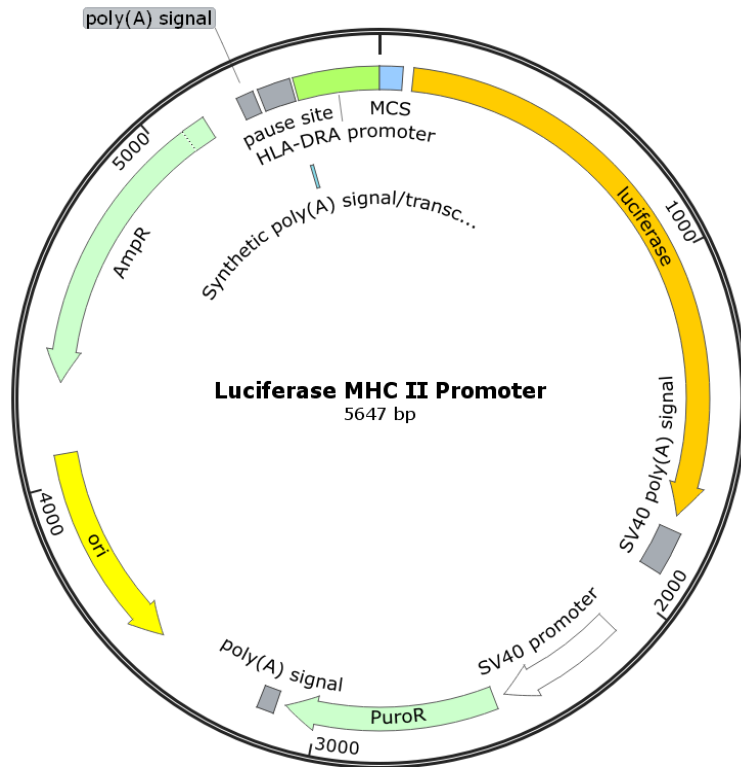
Maps prepared in SnapGene.

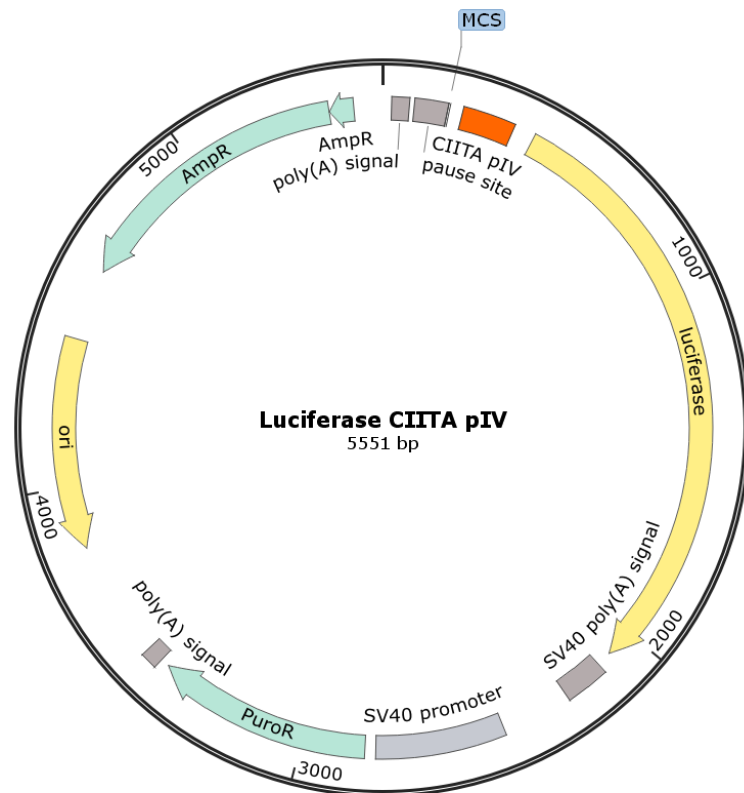
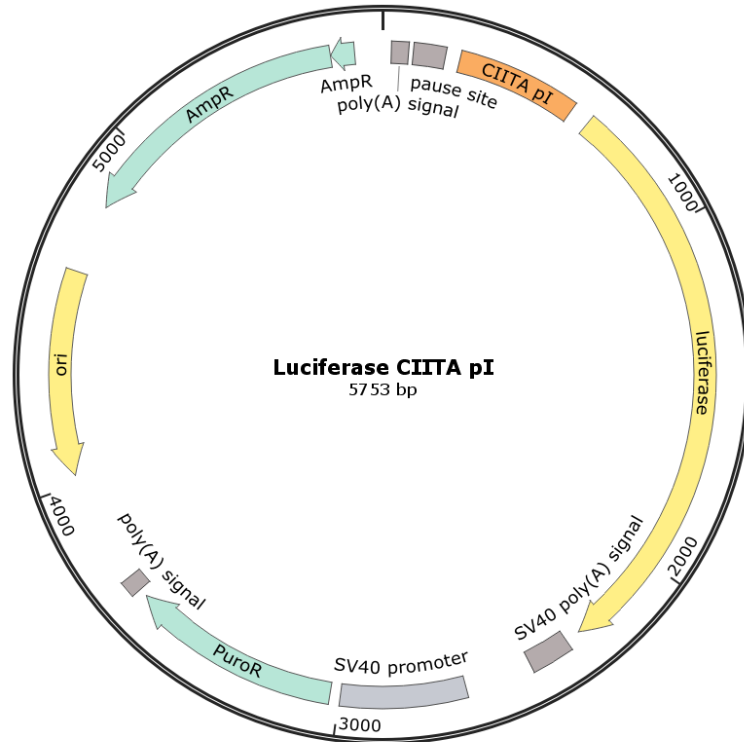


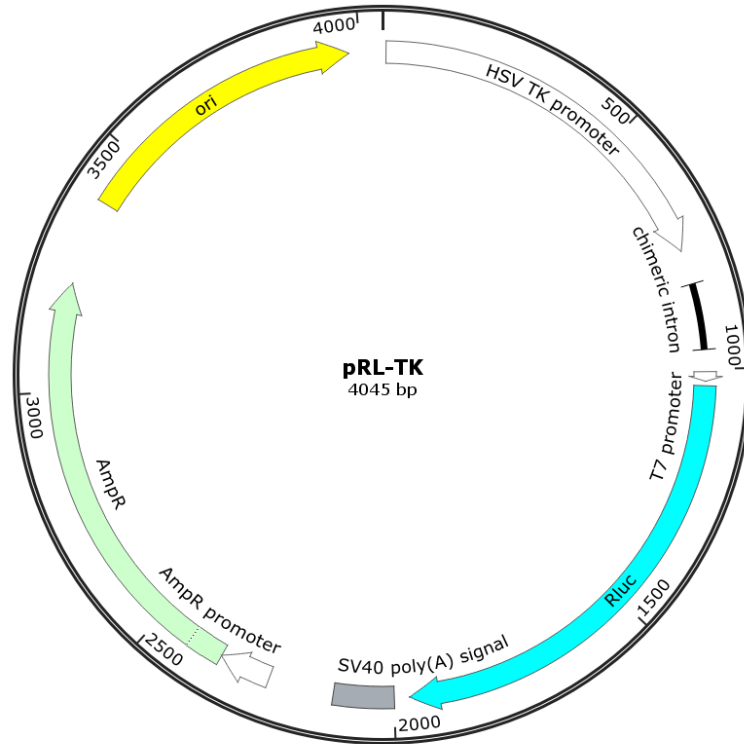


**Appendix B. Vector maps of luciferase reporter constructs used in this study.**

Maps prepared in SnapGene.



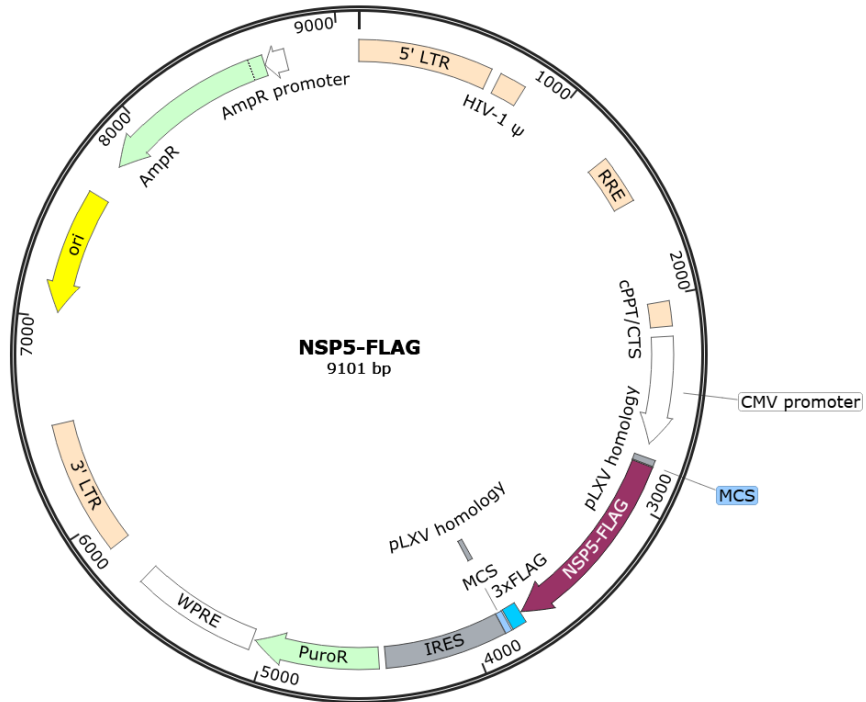


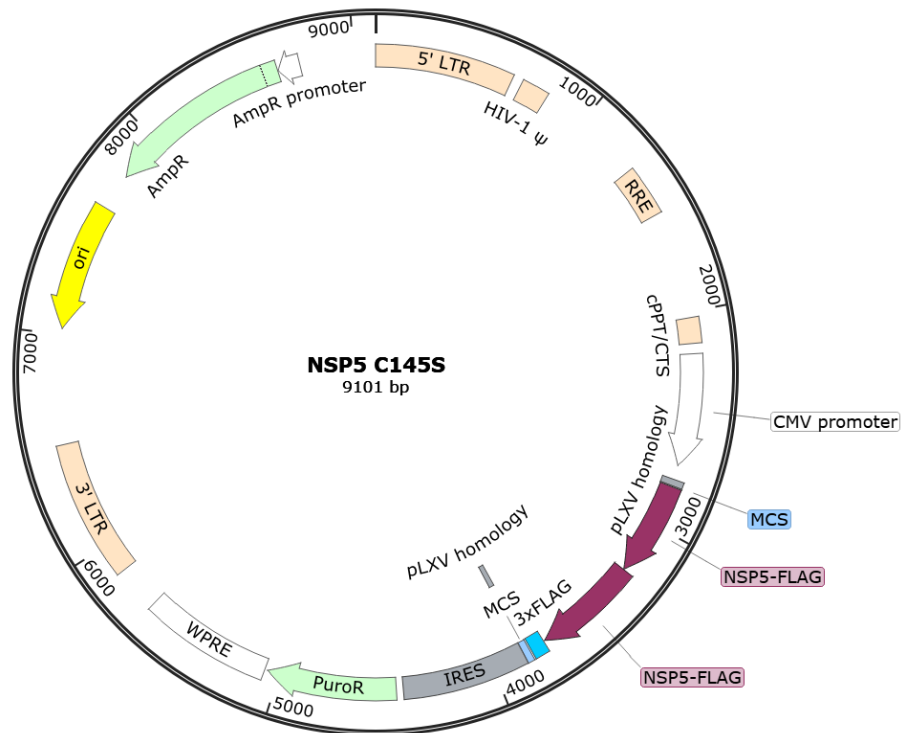
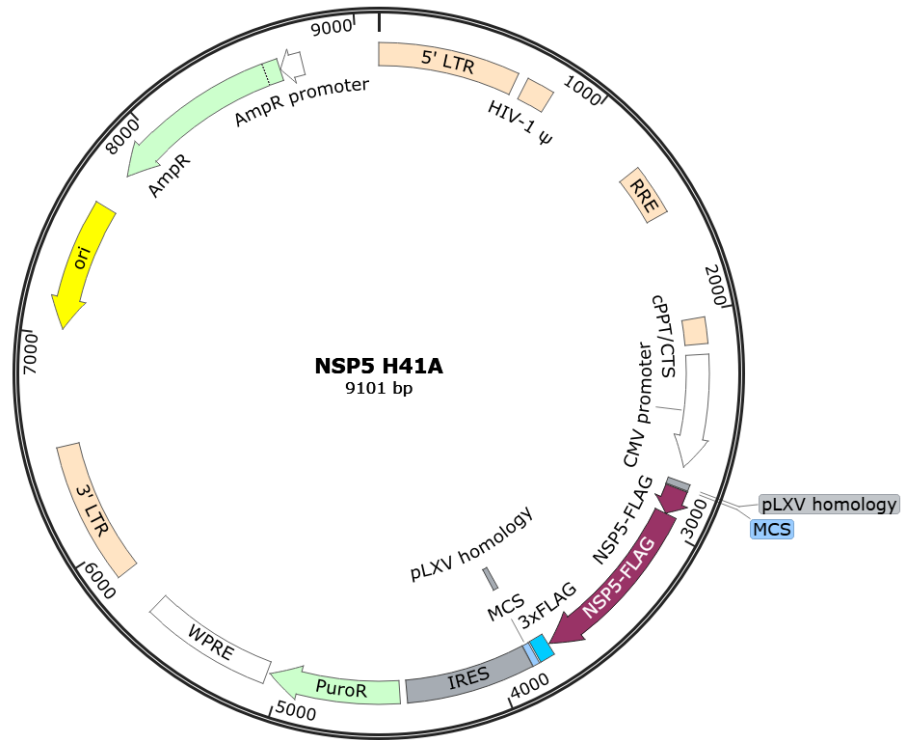


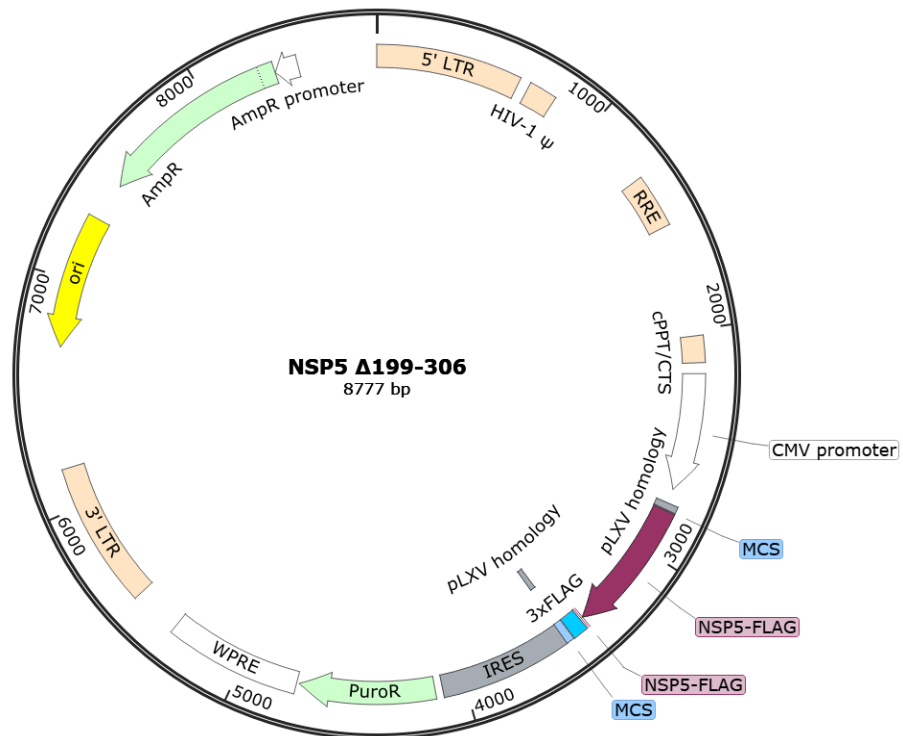
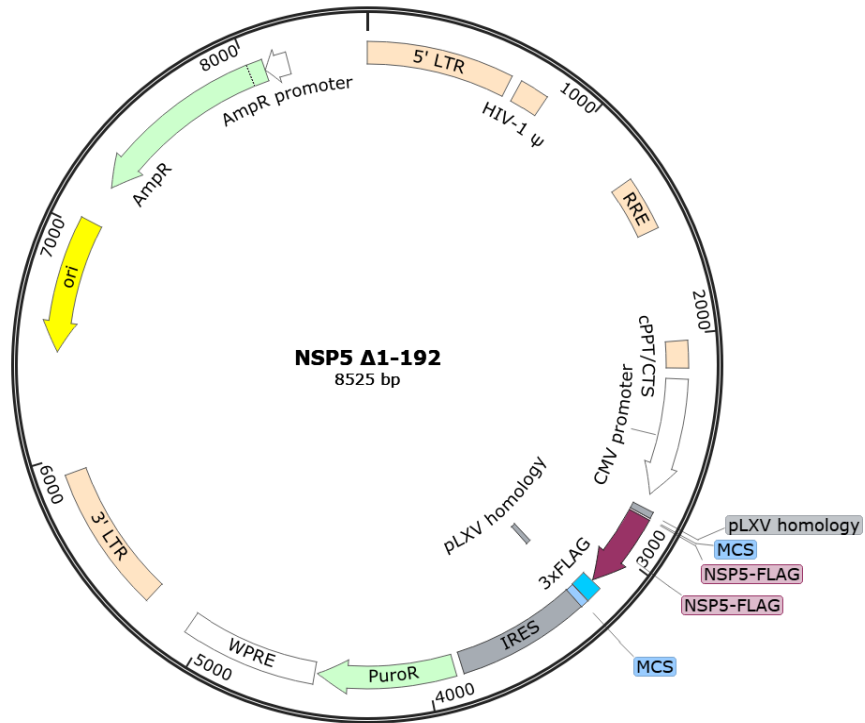


## Appendix C. Vector maps of NSP5 lentiviral vectors used in this study.

Maps prepared in SnapGene.







## Curriculum Vitae

**Name:** Alex Lac

**Post-secondary Education and Degrees:** The University of Western Ontario  
London, Ontario, Canada  
2015-2020 B.M.Sc (Hons.) Microbiology and Immunology

The University of Western Ontario  
London, Ontario, Canada  
2020-2022 M.Sc. (expected) Microbiology and Immunology

**Honours and Awards:** The University of Western Ontario  
Western Four-Year Continuing Admission Scholarship  
2015-2020

The University of Western Ontario  
Dean's Honour List  
2015-2016, 2016-2017, 2017-2018, 2019-2020

Canadian Institutes of Health Research (CIHR)  
Frederick Banting and Charles Best Canada Graduate Scholarship  
2021-2022

Department of Microbiology and Immunology  
Dr. RGE Murray Graduate Student Seminar Award  
2022

Department of Microbiology and Immunology  
Dr. Frederick W. Luney Graduate Travel Award  
2022

Canadian Society for Immunology (CSI)  
Poster Award  
2022

**Related Work Experience** Teaching Assistant – Biology of Infection and Immunity 2500A  
The University of Western Ontario  
2021-2022

**Publications:**  
**Lac, A, Lam, A.L., and B. Heit (2022).** Optimizing Long-Term Live Cell Imaging. *Methods in Molecular Biology*. 2440:57-73.